Geologic Characterization and Production Potential of the Mancos B Interval, Eastern Uinta Basin, Utah

Prepared for Utah School and Institutional Trust Lands Administration

(Photo: Mancos B outcrop, Prairie Canyon, Colorado)

by Ryan Gall (UGS), Lauren Birgenheier (University of Utah), and
Tyler Wiseman (SITLA)

June 2020

Utah Geological Survey
a division of
Utah Department of Natural Resources

DATA PRIVACY STATEMENT

Data included in this report was donated from the KGH Operating Company and Robert L. Bayless, Producer LLC. Each company has agreed to release their data to the Utah Geological Survey (UGS), the State of Utah School and Institutional Trust Lands Administration (SITLA), and to each other. This document shall remain a SITLA-internal document until confidentiality agreements are released. A redacted version of the document will be provided for distribution at the discretion of SITLA.

EXECUTIVE SUMMARY

The Mancos B interval is prospective for liquid production in the eastern Uinta Basin of Utah where promising reservoir and seal potential is widespread. Our study suggests that areas of the northeastern Uinta Basin are the most prospective for Mancos B liquid targets and that some areas of the southeastern Uinta Basin are also prospective for exploration. The liquid potential of the Mancos B is largely reliant on quality reservoir packages, the presence of high-quality source rock in the lower Mancos Shale, and a stratigraphic seal or structural trap.

Throughout the 60+ year history of drilling the Mancos B, operators have used novel techniques in conjunction with increased reservoir knowledge to produce from new areas and bolster production in known oil and gas fields. Air drilling allowed the first successful Mancos B completions in the water-sensitive formation in 1959, and production was significantly increased with casing and targeted perforation zones in the following decades. The advent of directional drilling has allowed for highly targeted wells in conventional play areas, and horizontal drilling has shown recent success following more unconventional play models. Akin to early Mancos B operators, current and future Mancos B operators will benefit from increased geological understanding and improved drilling and completion techniques to enhance hydrocarbon recovery.

Mancos B reservoir packages can be mapped throughout the eastern Uinta Basin, which is promising for exploration prospects in Utah. As a result of a complex depositional setting, Mancos B reservoir packages vary vertically in their stratigraphic location and exhibit prominent lateral lithologic changes at local and regional scales. Thus, the success of future exploration wells will rely on a localized understanding of the Mancos B depositional environment, reservoir characteristics, and local structure. Completion methods will need to be fine-tuned to account for clay-rich reservoirs and mobile authigenic clays.

Many of the most successful Mancos B oil wells to date are located on Banta Ridge, a northeast-southwest structural trend on the northwestern flank of the Douglas Creek Arch. Most Banta Ridge wells are in Colorado, although the structural trend extends into Utah where several wells have produced economic quantities of oil. Banta Ridge and other oil-producing areas on the Douglas Creek Arch are approached by operators with a conventional play model. In this model, hydrocarbons migrated from downdip locations lower in the stratigraphy and became trapped in Mancos B sandstone reservoirs by sealing extensional faults on the structural high of the Douglas Creek Arch. Recently, KGH Operating has tested an unconventional play model

with horizontal wells in the relatively laterally continuous Mancos B reservoir interval located north of the Banta Ridge (Colorado) and in the SITLA Bonanza Block of northeastern Uinta Basin (Utah). Oil production from these wells provides evidence for stratigraphically trapped liquids in some Mancos B reservoirs. Further, the wells demonstrate that an unconventional drilling approach may be applicable to this play especially in locations with limited structure.

Historical exploration/production activity shows highly variable well results, even at local scales. This compartmentalization of hydrocarbons is one of the most significant factors impeding predictive development of the Mancos B. The cause of compartmentalization varies by region. Near the Douglas Creek Arch, we interpret the structural location and related faults to be a dominant factor; in the Uinta Basin, where faults are less common, we attribute compartmentalization to a combination of variable lithological characteristics, burial history, structure, and diagenetic alteration. Water production has hindered economic returns in some horizontal Mancos B wells, similar to other horizontal wells in the lower Mancos Shale. We speculate that some of the high water production is related to clay-bound formation water that was not expelled during burial and hydrocarbon generation; however, the anomalously high water production in some wells may be associated with other yet to be determined factors. Localized understanding of the reservoir quality, clay mineralogy, and the use of clay-appropriate completion techniques may help mitigate water production in future wells.

CONTENTS

FIGURES

TABLES

APPENDICES

INTRODUCTION

The Mancos B is a 200–800 ft thick heterolithic reservoir-bearing unit located in northeastern Utah and northwestern Colorado. With a long history of gas production and recent oil production on and near the Douglas Creek Arch in Colorado, the eastern Uinta Basin of Utah is a prospective area for Mancos B exploration. Over the last two decades, the Mancos B has produced approximately 2 million barrels of oil from vertical, directional, and a limited number of horizontal wells mostly located near the Douglas Creek Arch near the Utah-Colorado border. Building off of play concepts and the success in Colorado, a small number of Utah wells (8 vertical, 1 horizontal) have recently proven the liquid potential of the Mancos B in the eastern Uinta Basin, although further study is required to better define prospective Mancos B locales and enhance hydrocarbon recovery.

The Mancos B is composed of interbedded sandstone and mudstone encased entirely in the 2000+ ft thick mudstone-dominated Cretaceous Mancos Shale. Formally defined as part of the Prairie Canyon Member, the Mancos B interval exists between the central Uinta Basin of Utah and extends to the Piceance Basin of Colorado (Cole and others, 1997; figure 1). Deposited in an offshore location of the Cretaceous Interior Seaway, the depositional environment of the Mancos B sandstone reservoir packages is unusual and has been widely debated (e.g., Kopper, 1962; Cole and Young, 1991; Cole and others, 1997; Hampson and others, 1999; Buatois and others, 2019). The offshore depositional setting and enigmatic structural history have complicated the predictive assessment of oil and gas bearing units of the Mancos B, although pervasively charged reservoirs, primarily on Douglas Creek Arch and Piceance Basin of Colorado, have been producing oil and gas since the 1950s.

Technological advances have greatly increased operator success drilling and producing from the tight clay-rich Mancos B reservoirs over the last 60+ years. The advent of air drilling, casing and perforating, and directional and horizontal wells in conjunction with better defined reservoirs have all improved hydrocarbon recovery. The main production concerns facing the Mancos B in Utah are the distribution of reservoir facies, compartmentalization of hydrocarbons, and clay content that can impact drilling, completions, and recovery. The role and importance of structural trapping to well success is also not well understood and debated.

Herein, we address production variables and provide an updated characterization of the Mancos B reservoir in Utah. We utilized new cores from the northeastern Uinta Basin, legacy cores from the southeastern Uinta Basin, well log data, and production data to assess potential reservoir facies and the hydrocarbon-bearing Mancos B intervals in Utah. Further, we provide a more thorough understanding of the depositional setting that impacts the distribution of reservoir facies, especially in less explored areas in the southeastern Uinta Basin.

Objective

The objective of this report is to provide a detailed geological characterization and evaluation of the Mancos B interval in the eastern Uinta Basin of Utah for SITLA. This report focuses on liquid production potential and synthesizes information from core, well logs, and production data in an effort to increase future production success of the Mancos B in Utah.

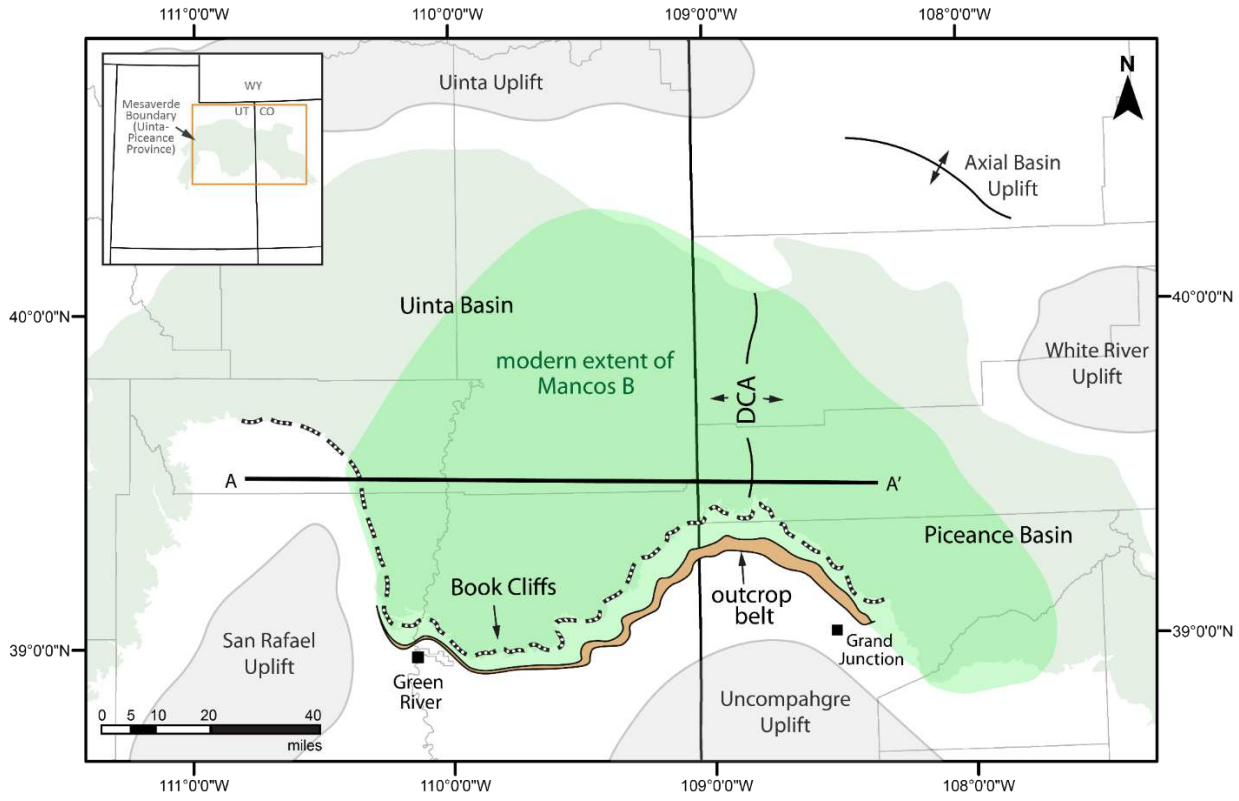

Figure 1. *Modern extent of rock genetically related to the Mancos B interval (Prairie Canyon Member) and regional uplifts and basins. DCA = Douglas Creek Arch. See figure 6 for A-A′ cross section. Mancos B extent modified from Cole and others (1997). Mesaverde boundary modified from U.S. Geological Survey Digital Data Series DDS-69-B.*

Tasks

1) Literature review and outcrop study.
2) Collect available data.
    a. Well logs, production data, geochemical data, reservoir quality analyses, source rock analyses.
    b. Create spatial databases for analysis in Petra and ArcGIS.
3) Assess available data and identify integral data gaps and areas of focus.
4) Perform detailed geologic descriptions of slabbed cores and meet with industry professionals.
    a. Bonanza State 20-15H core: travel to Billings, Montana, to meet with KGH Operating Company and describe core at Hohn Engineering, PLLC.
    b. Weaver Ridge 13-16 core: travel to Denver, Colorado, to meet with Robert L. Bayless, Producer LLC, and describe core at Triple O Slabbing.
    c. Crooked Canyon Unit 10-10-14-23, Trapp Springs Unit 1-25-14-23, Main Canyon State 8-2-15-22 cores: travel to Lakewood, Colorado, to describe core at USGS Core Repository and discuss with Anschutz Operating Company.
5) Draft core descriptions and build integrated core log plates.
6) Create new data (petrographic thin sections, x-ray diffraction (XRD) analyses, SEM and EDS analyses).
7) Perform regional analysis of data. Create new subsurface maps and cross sections.
8) Synthesize data and write final report. Summarize the petroleum potential of the Mancos B in Utah.

"MANCOS B" DEFINITION

"Mancos B" is a widely used industry name for the productive sandstone reservoir packages located in the Prairie Canyon Member of the Mancos Shale Formation (figure 2). Herein, we use "Mancos B interval" and "Mancos B" to refer to the interval within the Prairie Canyon Member that has production potential and define it as the area between the base of the stratigraphically lowest sandstone-dominated reservoir package and the top of the stratigraphically highest sandstone-dominated reservoir package in the Prairie Canyon Member. In some oil and gas fields of northwestern Colorado, the "Mancos A" is recognized as a separate reservoir overlying the Mancos B; however, Mancos A log markers are not regionally extensive in Utah and thus the Mancos A and its stratigraphic equivalents are included within the Mancos B of this study.

STUDY AREA

This study focuses on the Mancos B interval in the eastern Uinta Basin of Utah and includes the broader modern extent of the Mancos B interval in the Uinta-Piceance Province (figure 3). This area includes the Douglas Creek Arch and Piceance Basin of western Colorado

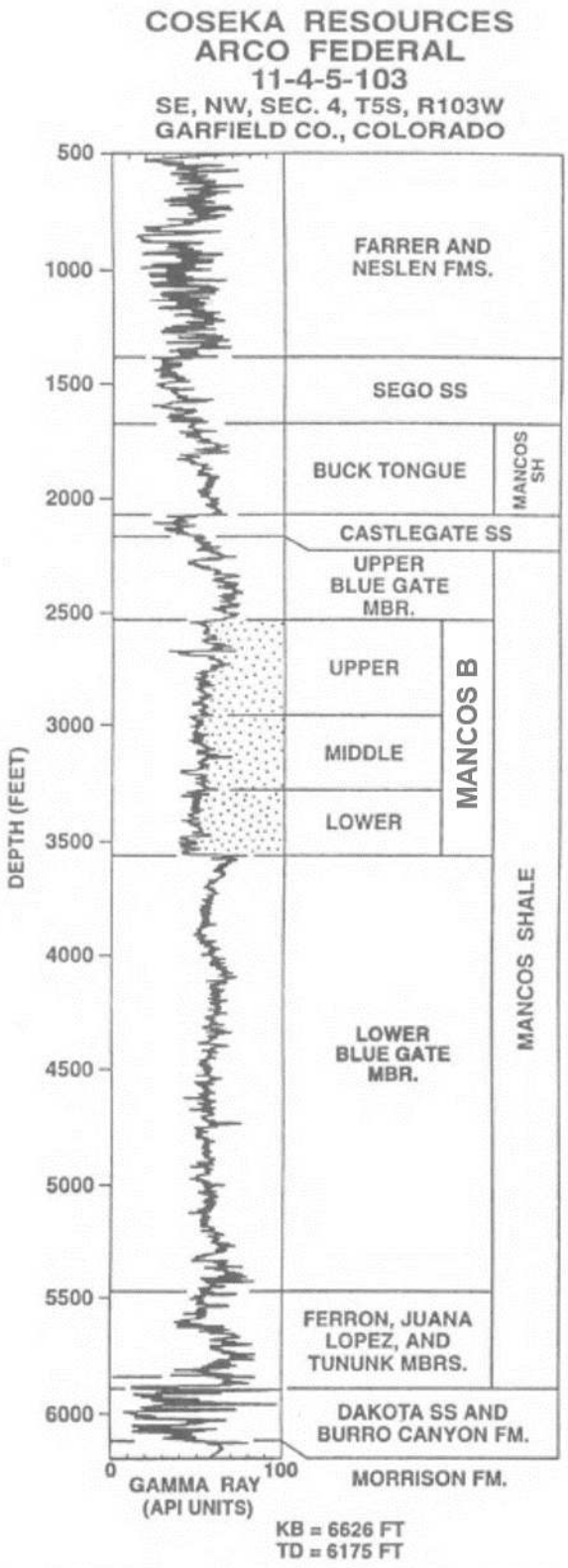

Figure 2. *Type log showing log definition of the Mancos B (Prairie Canyon Member) with the Cretaceous stratigraphy of the Uinta-Piceance Province. Modified from Cole and others (1997).*

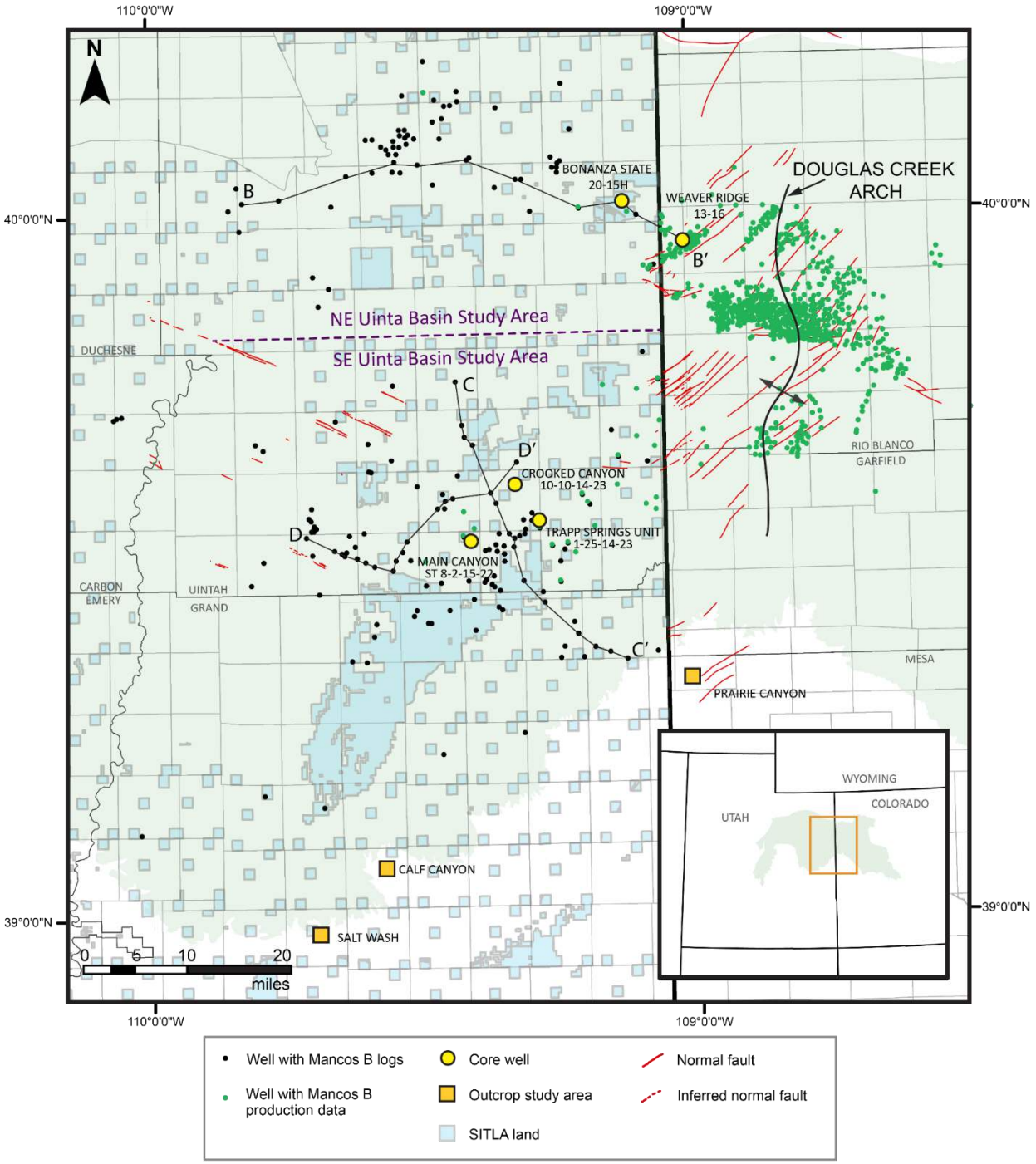

Figure 3. *Mancos B data used in this study with major structural features. Fault data collected from Sprinkel (2011) and Stoeser and others (2005).*

and extends from outcrops exposed along the Book Cliffs in the south to the Uinta and Axial uplifts in the north (figure 1).

The eastern Uinta Basin focus area is divided into two separate study areas due to regional variations in depositional environment, structural setting, and data availability: 1) the southeastern Uinta Basin on the Tavaputs Plateau which includes the SITLA Holliday and Seep Ridge blocks; and 2) the northeastern Uinta Basin which includes the SITLA Bonanza block and the Banta Ridge trend near the western flank of the Douglas Creek Arch (figure 3).

DATASETS AND METHODS

This report synthesizes a variety of datasets from core, well logs, and production reports. Five wells with core totaling 855 ft from the eastern Uinta Basin were examined (figure 3; tables 1 and 2). Two cores are from the northeastern Uinta Basin: 1) Bonanza State 20-15H, collected from the SITLA Bonanza Block, Utah, in 2017 by KGH Operating Company (KGH); and 2) Weaver Ridge 13-16, cored by Robert L. Bayless, LLC, in 2014. Three wells contain multiple sections of core from the southeastern Uinta Basin, all collected by Coseka Resources (U.S.A.) (Coseka) in the early 1980s: (1) Crooked Canyon Unit 10-10-14-23; (2) Trapp Springs Unit 1-25-14-23; and (3) Main Canyon State 8-2-15-22.

We described each core at the centimeter to decimeter scale with attention to lithology, sedimentary structures, and ichnology. Twelve 20- to 40-µm-thick petrographic thin sections were used in petrographic analyses at the Reservoirs Research Group (L. Birgenheier) lab at the University of Utah (appendix A); six thin section billets were polished and used in scanning electron microscopy (SEM) and energy dispersive X-ray spectroscopy (EDS) analyses with the FEI Quanta 600 at the Nanofab lab at the University of Utah (appendix B). Seven x-ray diffraction (XRD) samples were analyzed at the Utah Core Research Center and eight XRD samples were assessed by Core Laboratories in Houston, TX (appendix C). Data donated by KGH and Robert L. Bayless, Producer LLC (Bayless) or acquired from the U.S. Geological Survey includes additional XRD data (appendix C), conventional core analyses (appendix D), and source rock analyses (appendix E).

Geophysical logs from 205 wells in the Uinta Basin were used to map the Mancos B in the subsurface (appendix F). Production data from 721 wells were acquired from the Colorado Oil and Gas Conservation Commission (COGCC) and the Utah Division of Oil, Gas and Mining (DOGM) (appendix G). Due to inconsistent and missing data, pre-1984 production data in Utah and pre-1999 production data in Colorado are not assessed in this report.

The “Mancos B” designation was not historically used by all operators to report drilling and perforation targets. In order to attain a complete dataset of all Mancos B wells, we used well logs and perforation data acquired from DOGM to identify wells that have produced or tested the Mancos B interval in Utah. Wells that have comingled Mancos B production data or tested the Mancos B in conjunction with other formations are not assessed in this report though are provided in appendix H.

Table 1. Core details

Well Name	API	Date Collected	Total Core	Stratigraphy Captured	UTM E (NAD83)	UTM N (NAD83)
Bonanza State 20-15H	4304755745	Aug 2017	330.3′	239′ Lower McB 91′ LBGM	658559	4431331
Weaver Ridge 13-16	0510311782	Oct-Nov 2010	40.5′	40.4′ Lower McB 0.1′ LBGM	669905	4425167
Crooked Canyon Unit 10-10-14-23	4304730708	May-Jul 1980	*169.5′	91′ UBGM 26′ Upper McB 52.5′ Lower McB	643626	4386488
Trapp Springs Unit 1-25-14-23	4304730975	May-Jun 1981	148.1′	2.5′ UBGM 145.6′ Upper McB 11.5′ Middle McB	647235	4380875
Main Canyon State 8-2-15-22	4304731135	Jul-Aug 1981	236.1′	58.3′ Upper McB 117.4′ Middle McB 60.4′ Lower McB	636174	4377877

**Only Mancos B portion of Crooked Canyon Unit 10-10-14-23 assessed in this study; Upper Blue Gate Member excluded from description and analysis.*

Table 2. Core sampling data

Well Name	API	XRD	CCA	Petrography	SEM	EDS	SRA
Bonanza State 20-15H	4304755745	12	200	12	6	6	25
Weaver Ridge 13-16	0510311782	5	47		2		
Crooked Canyon Unit 10-10-14-23	4304730708	5	13				4
Trapp Springs Unit 1-25-14-23	4304730975	5					5
Main Canyon State 8-2-15-22	4304731135	5	19				5

Number of individual samples analyzed by core. XRD = X-ray diffraction (mineralogy), CCA = conventional core analyses (porosity and permeability), SEM = scanning electron microscopy (nano-scale imaging), EDS = energy dispersive X-ray spectroscopy (elemental mapping on SEM), SRA= source rock analyses.

SUMMARY OF PREVIOUS STUDIES

The Mancos B was first recorded as a 100- to 400-ft-thick interval of interbedded sandstone and shale contained within the Mancos Shale of northwestern Colorado by Kopper (1962). Kellogg (1977) refined geophysical log boundaries of the Mancos B and was the first to publish a regional subsurface map of the Mancos B in the Uinta and Piceance basins.

Witherbee and others (1983) used eight Mancos B cores from the Douglas Creek Arch and Uinta Basin to characterize three sandstone lithofacies relevant to natural gas production, focusing on the reservoir and geochemical properties. Cole and Young (1991) extended the stratigraphic range of the Mancos B to include 1200 ft of interbedded and interlaminated sandstone and siltstone and completed a thorough outcrop-based study of mudstone and sandstone facies in Prairie Canyon, Colorado. Cole and others (1997) formally defined the Mancos B interval as the Prairie Canyon Member of the Mancos Shale, based on unique reservoir and lithological properties relative to other members of the Mancos Shale.

Cole and Young (1991) and Cole and others (1997) provide detailed depositional models for prodeltaic plume deposition and offshore current reworking of the Mancos B. Hampson and others (1999, 2001) reinterpreted the depositional setting as tidally influenced shoreface. Additional early interpretations are provided by Kopper (1962), Newman (1985), Noe (1993), Taylor and Lovell (1995), Kellogg (1997), and Johnson (2003). Recent studies by Pattison (2005a,b), Pattison and others (2007), Hampson (2010, 2016), and Buatois and others (2019) have converged on a turbidity current driven depositional model in which updip channelized deposits delivered sediment to downdip, offshore prodeltaic lobes or fans. Well studied outcrop channel-fill packages of south-central and western Uinta Basin (e.g., the Woodside Interval and Hatch Mesa Sandstone) are interpreted as roughly time-equivalent to the Mancos B reservoir interval in this study and are discussed in Fouch and others (1983), Chan and others (1991), Swift and others (1987), Taylor and Lovell (1995), and Eide and others (2015).

Structure and paleogeographic evolution of the eastern Uinta Basin study area and Douglas Creek Arch are discussed in Osmond (1965), Kopper (1962), Stone (1986), Franczyk and others (1992), White and others (2002), and Bader and others (2009). Thermal maturity and burial of the Mancos Shale are discussed in Nuccio and Roberts (2003), Zhang and others (2009), Quick and Ressetar (2012), and Hobbs and others (2015). Diagenetic alteration of the upper Mancos is studied in Nadeau and Reynolds (1981), Taylor and Gawthorpe (2003), Taylor and Machent (2010), and Taylor and MacQuaker (2014). Depositional models for the lower Mancos below the Mancos B are published in Birgenheier and others (2017) and DeReuil and Birgenheier (2019).

Large-scale studies of the petroleum potential of Mancos Shale reservoirs have been completed by Kirshbaum (2003), Schamel (2006), and Ressetar and Birgenheier (2015). Early best production practices in the Piceance Basin are discussed in McLennan and others (1983) and the first horizontal completion recommendation is included in Middlebrook and others (1993). Longman and Koepsell (2005) characterize subsurface Mancos B and hydrocarbon trends via FMI logs. Coryell and McCarthy (2014) discuss the development of the Mancos B in its most successful field to date, Banta Ridge on the Utah-Colorado border. Recent work by DeReuil and others (2019) provided detailed analysis and discussion of geomechanical properties of heterolithic Mancos lithofacies.

GEOLOGIC BACKGROUND

Mancos Shale

The 94 to 80 Ma Cretaceous Mancos Shale was deposited in an epicontinental sea that occupied a large foreland basin in western North America, the Cretaceous Western Interior Seaway (figures 4 and 5). The north-south-trending Western Interior Seaway extended from the Arctic Ocean to the Gulf of Mexico and was bordered by the Cordilleran thrust belt to the west and a stable craton to the east (Livaccari, 1991; DeCelles and others, 1995). Flexural subsidence from crustal loading related to thrusting created the foredeep and was a primary control on sedimentation (Jordan, 1981; Yoshida and others, 1996). In the Utah-Colorado study area, siliciclastic sediment from the Sevier fold and thrust belt was delivered to the basin via fluvial deltaic input, and carbonate accumulated to the east on a sediment-starved shallow ramp (Jordan, 1981; Decelles, 1994).

The Cretaceous stratigraphy of Utah and Colorado has been well studied due to its relevance to hydrocarbon exploration, high-quality exposures in the Book Cliffs along the southern margin of the Uinta Basin, and the resultant scientific value to sedimentary geology (e.g., Hancock and Kauffman, 1979; Fouch and others, 1983; Van Wagoner and others, 1988; Yoshida, 2000). Marginal marine deposits are represented by shoreline and fluvial-deltaic sandstones (e.g., the Ferron Sandstone, Emery Sandstone, Start Point Sandstone, Blackhawk Formation, and Castlegate Sandstone), and the syndepositional downdip mudstone-dominated deposits amalgamated to form the >2000-ft-thick Mancos Shale or a regionally named equivalent (e.g., the Niobrara Formation of eastern Colorado and Kansas; Sonnenberg, 2011). In northeastern Utah, the Mancos conformably overlies the fluvial to shallow marine Dakota Sandstone and is overlain by the fluvial-deltaic Castlegate Sandstone (Molenaar and Cobban, 1991; Miall and Arush, 2001).

First described in southwestern Colorado by Cross and Purington (1899) as “2000 ft of dark shale,” the Mancos has since been divided into lithostratigraphic subdivisions based on unique compositional characteristics (Molenaar and Cobban, 1991, Dyman and others, 1994; Schwans, 1995). In northeastern Utah, these units in ascending stratigraphic order are the Tununk Shale Member, Coon Springs Sandstone, Juana Lopez Member, Lower Blue Gate Member, “Mancos B” or Prairie Canyon Member, and Upper Blue Gate Member (figure 4). The clay-rich and organic-lean Upper Blue Gate and Lower Blue Gate members compose most of the Mancos, which were deposited in a dynamic prodelta and offshore mudbelt environments (Birgenheier and others, 2017). The Mancos B as well as the Juana Lopez Member are unique Mancos packages in which coarser grained sediment and organic matter was delivered into the deeper basin via offshore-directed flows (Pattison, 2005a; Buatois and others, 2019; DeReuil and Birgenheier, 2019).

Mancos B and the Prairie Canyon Member

“Mancos B” is widely used industry nomenclature for the sandstone reservoir packages contained within the Prairie Canyon Member, which is formally defined by Cole and others (1997) as heterolithic interval of interbedded and interlaminated sandstone and quartz-rich

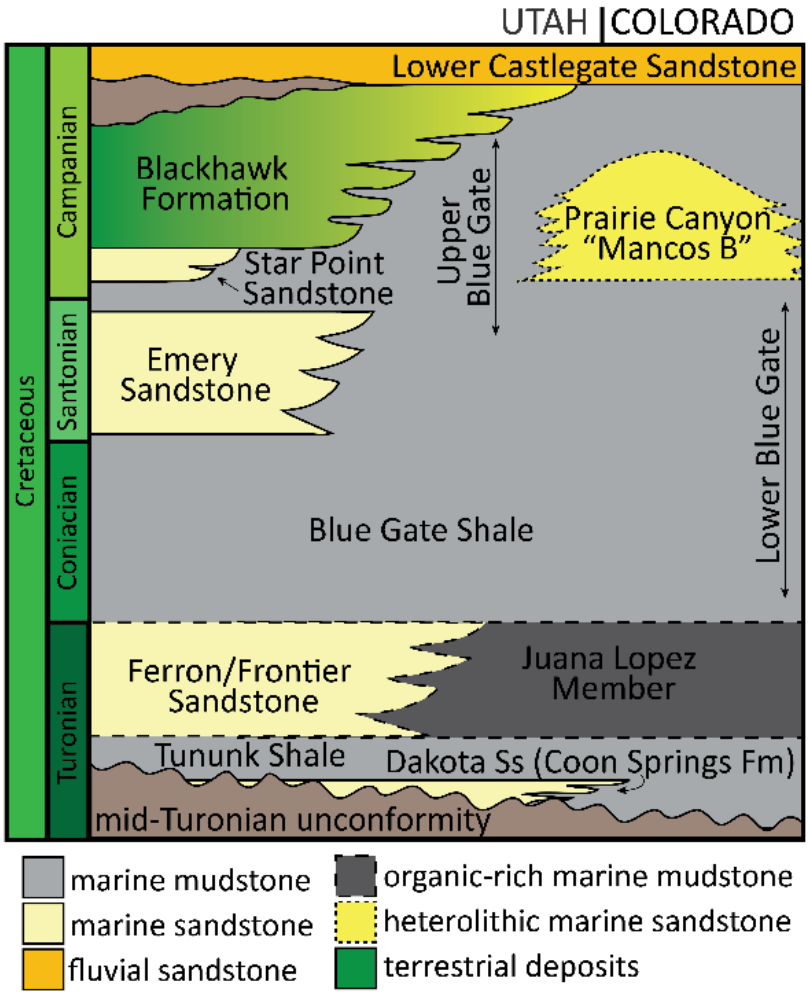

Figure 4. *Cretaceous stratigraphy of the Uinta Basin and western Piceance Basin, Utah and Colorado. Modified from DeReuil and Birgenheier (2019).*

Figure 5. *Paleogeographic reconstruction of the Cretaceous Western Interior Seaway at time of Mancos B deposition. Study area highlighted by orange square. Modified from Blakey (2014).*

mudstone up to 1250 ft thick bounded by the Lower Blue Gate and Upper Blue Gate members (figure 6). Fifty to one-hundred miles east of the time-equivalent shoreline sandstones, the geographically isolated Mancos B exists roughly from central Uinta Basin to the central Piceance Basin. The northern mappable extent of the Mancos B is contained by the Uinta and Axial Uplifts. The southern mappable extent is limited by the erosional outcrop exposure at the base of the Book Cliffs between Thompson Springs, Utah, and Grand Junction, Colorado (figure 1). Biostratigraphic age data suggest the Mancos B was deposited from the latest Santonian to the early-late Campanian (Fouch and others, 1983; Chan and others, 1991; Cole and others, 1997).

The eastern Mancos B consists of interlaminated to interbedded very fine to fine-grained moderately sorted sandstone and silty claystone. The heterolithic lamina and beds are contained in tabular aggradational to coarsening-upwards packages (figure 7a–c). Individual sandstone beds can be up to several ft thick, though are rarely more than 1 ft thick even at the depocenter near the Douglas Creek Arch (Kellogg, 1977). Intercalated mudstones generally range from several inches thick to discontinuous thin drapes. Common sedimentary structures observed in sandstone and mudstone lamina and beds include combined flow ripple lamination, current ripple lamination, lenticular lamination, wavy lamination, flaser bedding, plane parallel lamination, and sole marks (Cole and Young, 1991; Cole and others, 1997; Hampson and others, 1999; Pattison and others, 2007). A highly diverse assemblage of ichnofossils consist of *Chondrites, Paleophyycus, Planolites, Rhyizocrallium, Skolithos, Terebellinia, Ophiomorpha, Teichichnus, Cylindrichnus,* and *Thalassinoides* (Cole and others, 1997; Hampson and others, 1999; Buatois and others, 2019). Bioclasts including pelecypod fragments, fish vertebra, and shark teeth have all been observed in the Mancos B (Cole and others, 1997). Natural fractures are not common in the Mancos B, although Middlebrook and others (1993) note one thin core interval with fractures from the Douglas Creek Arch; fractures are perpendicular to bedding, less than 1.5 inches, and calcite filled (Middlebrook and others, 1993).

In the western part of the Mancos B outcrop belt, large erosionally based channels are observed in outcrop near Nash Wash, Calf Canyon, and Pinto Wash, Utah (figures 1 and 7d). Collectively called the “Pinto Wash Interval” following Cole and Young (1991), individual channels range from 4 to 27 ft thick and are up to 1500 ft wide. In some localities, the channels are stacked into multi-story bodies up to 40 ft thick and may laterally extend over a mile (Hampson and others, 1999). The channels are filled with interlaminated carbonaceous mudstone and very fine to medium-grained sandstone lamina that conform to the base. Paleoflow indicators from the Pinto Wash Interval indicate a dominantly east-southeast directed flow (span 90° to 168°; mean 126°; Cole and others, 1997). Ichnofauna in the Pinto Wash Interval are less diverse and dominated by *Paleophycus* and *Planolites* with minor occurrences of *Rosselia, Rhizocorallium, Terebellinia, Arenicolites,* and *Skolithos* (Hampson and others, 1999; Buatois and others, 2019).

The Mancos B (then referred to as the “’B’ Zone of the Mancos Shale”) was first interpreted by Kopper (1962) to represent nearshore proximal delta deposits. Since, several additional interpretations have been applied to the heterolithic package including prodelta plumes (Cole and Young, 1991), isolated shelf bars attributed to sea-level fall (Cole and others, 1997), and lowstand tidally influenced shoreface deposits (Hampson and others, 1999). Recent detailed sedimentological and ichnological studies have converged on turbidity current-

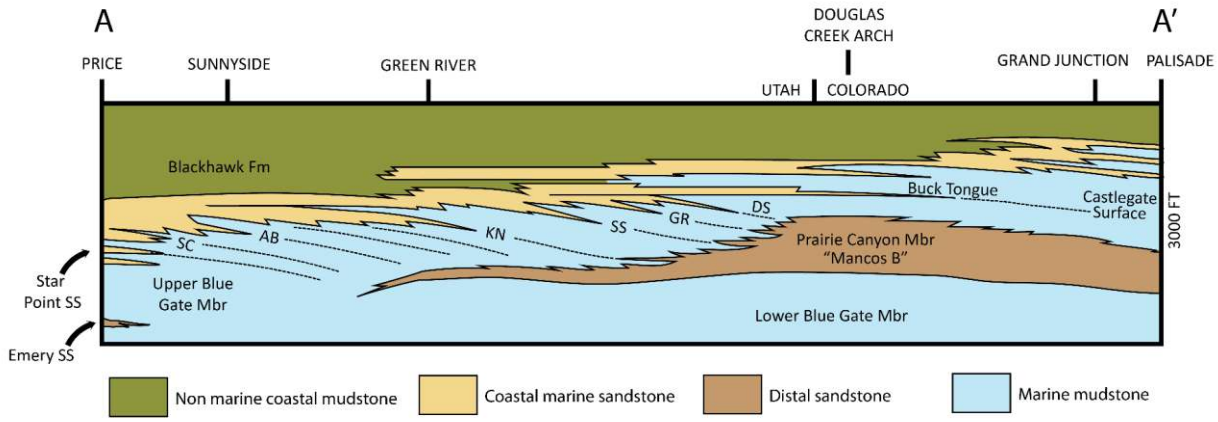

Figure 6. *Cross section illustrating relationship between the Mancos B and the stratigraphy of the Book Cliffs. See figure 1 for A-A' line. Blackhawk Formation abbreviations: SC= Spring Canyon; AB = Aberdeen; KN = Kenilworth; SS = Sunnyside; GR = Grassy; DS = Desert. Modified from Cole and Young (1991).*

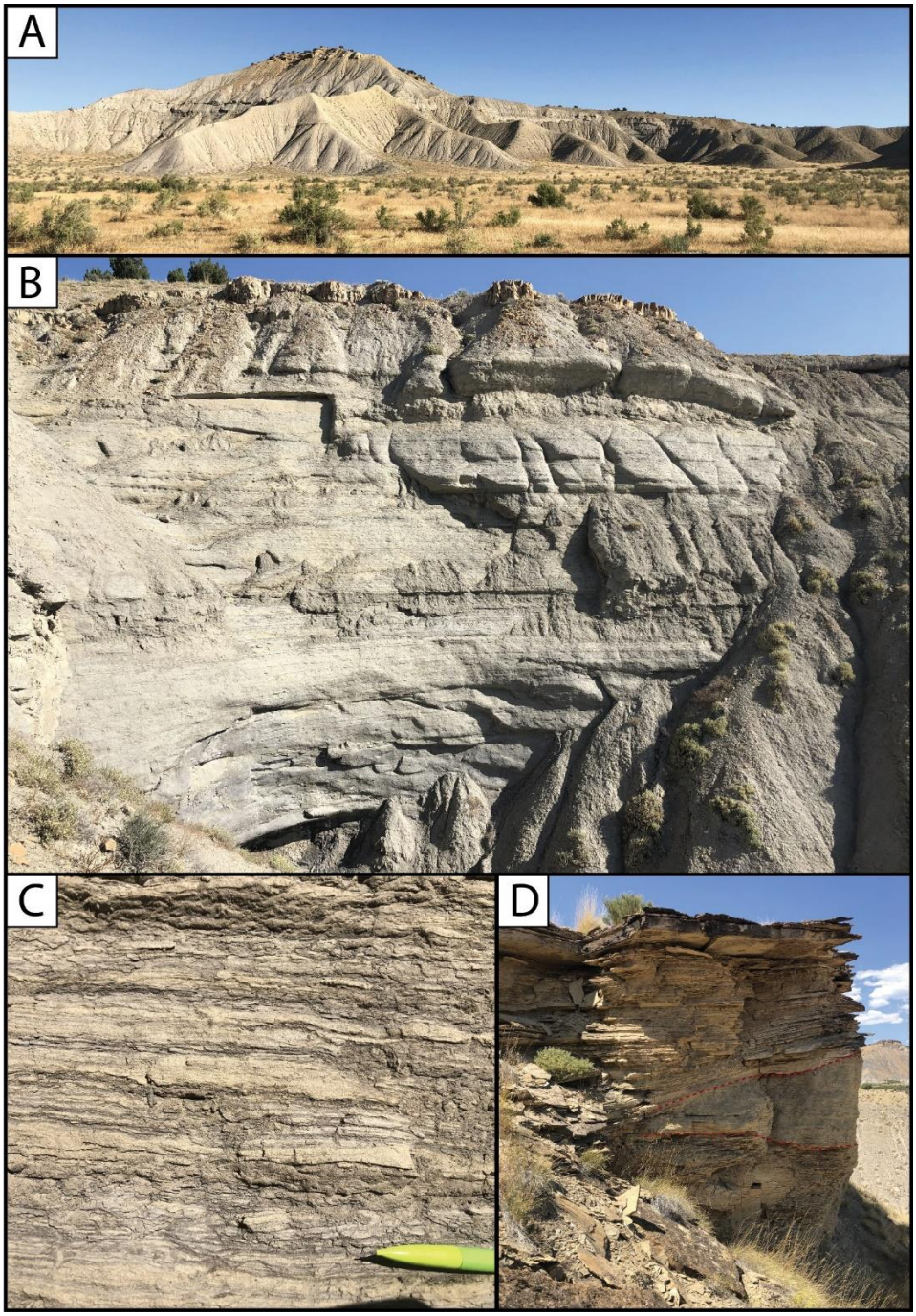

Figure 7. *Mancos B outcrops from the southeastern Uinta Basin. Photos A-C from Prairie Canyon, Colorado. Photo D from Calf Canyon, Utah. A) Typical Mancos B outcrop commonly seen in the southern Book Cliffs; B) An example showing the tabular nature of the interbedded and interlaminated sandstone and mudstone, Mancos B deposits in the eastern study area. Note resistant outcrop capping beds, which are composed of Fe-dolomite; C) Close-up (pencil for scale) lamina-scale alterations between sandstone and mudstone that are typical of Mancos B deposits; D) Channelized heterolithic strata from the Pinta Wash Interval in Calf Canyon (western study area). Significant inclined or channelized erosional surfaces are highlighted by dashed red line.*

influenced shelf environment in which storm- and hyperpycnal-currents delivered relatively coarse sediment sourced from proximal environments to the distal basin via sediment bypass channels (figures 8 and 9; Pattison and others, 2007; Hampson, 2010, 2016; Buatois and others, 2019).

In the subsurface, the base of the Mancos B is defined by an abrupt shift from high to low gamma and low to high resistivity, representing the transition from the clay-rich Lower Blue Gate to sandy Mancos B (figure 2). This shift generally occurs about 2300 ft above the Dakota Sandstone (Cole and others, 1997). The top of the Mancos B is also defined by log shifts from low to high gamma representing a shift is sandstone-claystone ratios, although this pick is more variable in stratigraphic location than the base. Cole and others (1997) place the top of the Prairie Canyon Member consistently 300 to 600 ft below the Castlegate Sandstone in the eastern Uinta Basin, although in most cases the top Mancos B reservoir package is considerably farther below the Castlegate. High-resolution correlation of logs is possible at local scales with a high density of wells; however, regional correlation of geophysical logs involves a degree of interpretation and there is considerable variation among previous workers (e.g., Kellogg, 1977; Cole and Young, 1991*;* Johnson, 2003; Pattison, 2005a; Pattison and others, 2007; Hampson, 2016).

Precise correlation of the isolated Mancos B to the proximal shoreline sandstones is difficult with limited data to constrain depositional timing. It is generally agreed that the majority of the Mancos B and entire Prairie Canyon Member is correlative to the Blackhawk Formation (figure 6). Kellogg (1977) and Cole and Young (1991) correlated the basal Mancos B surface to the Emery sandstone, whereas more recent interpretations correlate the base to stratigraphically higher sandstone packages. Hampson (2010, 2016) and Hettinger and Kirschbaum (2002) correlated the base Mancos B with the Star Point Sandstone, and others contain the Mancos B within the Aberdeen and Kenilworth members of the Blackhawk Formation (Pattison, 2005a; Pattison and others, 2007; Pattison and Hoffman, 2008).

Structural and Burial History

The Mancos B was deposited in a complex foreland basin setting related to the subduction of the Farallon Plate beneath the North American Plate (Livacarri, 1991). Seismic and borehole evidence from northwestern Colorado suggest that east-trending, north-dipping Precambrian faults may have been re-activated during the Late Cretaceous and potentially formed sub-basins in the Western Interior Seaway in which the Mancos B accumulated (Stone, 1986). Further, modeling suggests active forebulge migration in the Late Cretaceous may have played a role in sediment dispersal in the Cretaceous Interior Seaway (White and others, 2002).

Beginning in the Late Cretaceous after Mancos deposition, the Laramide orogeny resulted in a series of smaller contractional uplifts and foreland basins which broke up the larger Sevier foreland basin system (Dickinson and others, 1998; Johnson, 1992; Mederos and others, 2005). The Uinta and Piceance Basins of Utah and Colorado subsided rapidly relative to the surrounding basement uplifts (Narr and Currie, 1982; Franczyk and others, 1992). By 25 Ma, the Uinta and Piceance Basins had filled with 20,000 ft of Paleogene terrestrial and lacustrine sediment, resulting in the maximum burial depth of the base Mancos Formation of 28,000 to 30,000 ft (Nuccio and Roberts, 2003; Hobbs and others, 2015). Isostatic uplift and asymmetrical Neogene erosion immediately followed maximum burial and removed the Mancos and overlying

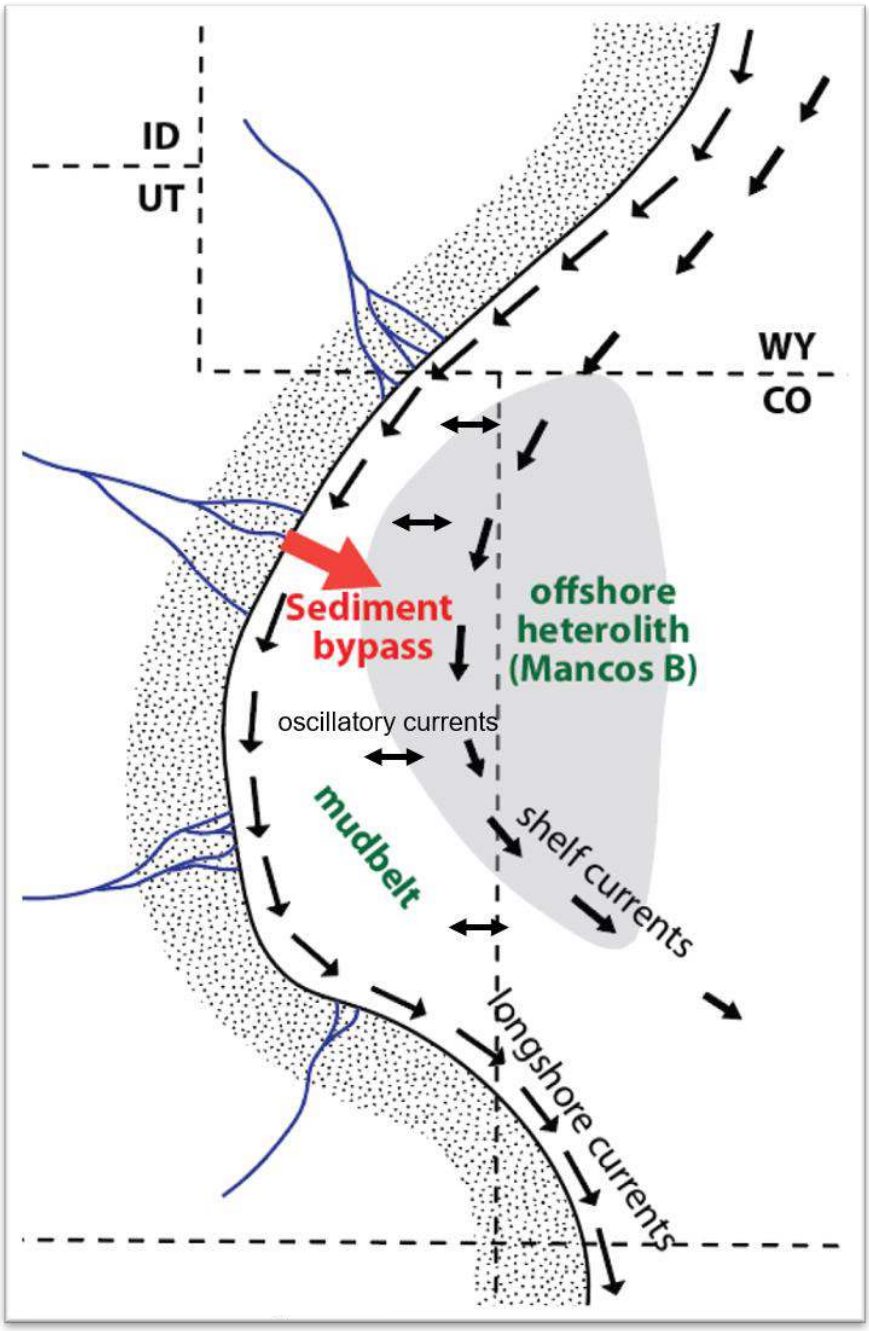

Figure 8. *Interpretation of paleo depositional environment and location of the Mancos B interval. Shoreline position modified from Cole and Young (1991).*

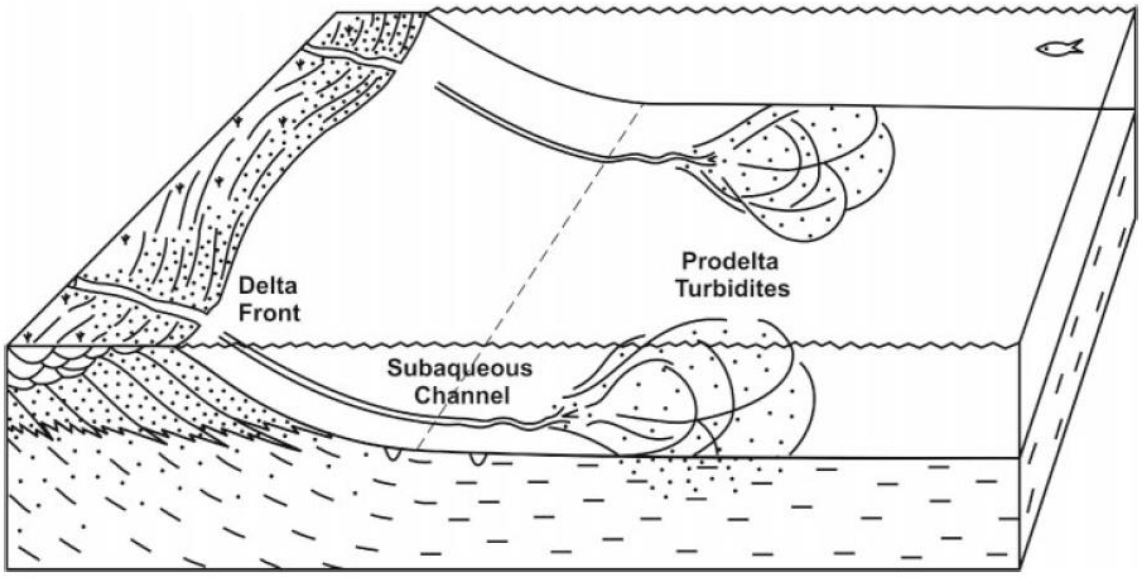

Figure 9. *Box model illustrating depositional environment of the Mancos B from Pattison and others (2007).*

strata south of the Book Cliffs in Utah and Colorado (Francyzyk and others, 1992; Nuccio and Roberts, 2003; Anderson and Harris, 2006). North of the Book Cliffs in the Uinta Basin, over 10,000 ft of overlying Paleogene strata are preserved (Franczyk and others, 1992; Nuccio and Roberts, 2003). Three-dimensional modeling of the Uinta Basin by Hobbs and others (2015) indicates Mancos hydrocarbon generation onset with the Laramide orogeny (~70 Ma) and peak oil generation occurred 55–37 Ma during Eocene burial.

The Douglas Creek Arch is an enigmatic north-south-trending faulted anticline that separates the Uinta and Piceance basins in northwestern Colorado (figure 1; Johnson and Finn, 1986; Bader and others, 2009; Johnson and Finn, 1986*).* The Douglas Creek Arch is characterized by the major east-west-striking, near-vertical Douglas Creek fault which crosscuts the Mancos Shale and overlying Mesaverde group (Johnson and Finn, 1986; Pantea and Schmitt, 1996; Barnum and others, 1997). A series of northeast-southwest-striking, high-angle (60° to vertical) en echelon straight-to-curvilinear normal faults further crosscut Paleogene strata with displacement of up to 1000 ft (Cashion, 1967; Kellogg, 1977; Johnson, 1985; Pantea and Schmitt, 1996; Barnum and others, 1997). Northwest-southeast-trending gilsonite veins are also present in the eastern Uinta Basin, although are likely too high in the stratigraphy to crosscut the Mancos B (Boden and Tripp, 2012).

Surface cross-cutting relationships and subsurface borehole and seismic mapping of faults indicate the Douglas Creek Arch was active during the Laramide orogeny and basement rocks were involved in its development (Johnson and Finn, 1986; Stone, 1986; Johnston and Yin, 2001), and may have been active earlier (Bader and others, 2009). It has been speculated that movement of the Douglas Creek Arch during Mancos B time impacted sedimentation (Cole and others, 1997), although this is still up for debate. In any case, the fault system is likely linked to hydrocarbon migration pathways from source rock to tight sandstone reservoirs like the Mancos B and further responsible for creating local structural traps (Bader and others, 2009).

EXPLORATION AND PRODUCTION HISTORY

Summary

Mancos B wells have had variable production results throughout the >60-year history of drilling in the Uinta-Piceance province. Even adjacent wells have large production discrepancies highlighting variation even at local scales. However, the common thread through the drilling history is that technological advances in conjunction with increased understanding of the reservoir have greatly improved Mancos B well success over time. Operators have known about the pervasively charged Mancos B reservoir on the Douglas Creek Arch since at least the 1940s; however, operators were not able to produce from the water-sensitive formation until 1959 by the use of novel air drilling techniques (Kellogg, 1977). In the mid-late 1960s, the use of casing and targeted perforation zones drastically improved gas recovery from Mancos B reservoirs.

In the mid-2000s, operators began drilling the flanks of the Douglas Creek Arch for oil and gas production. With detailed study of Mancos B reservoir packages and the fault network in the Banta Ridge field, operators began producing substantial quantities of oil from highly targeted vertical and directional wells in a fault-sealed Mancos B reservoir following a

conventional play model (Coryell and McCarthy, 2014). The use of horizontal drilling has further increased Mancos B success. In 2011, the first Mancos B horizontal wells were drilled and show increased hydrocarbon production. Weaver Ridge 13-9H drilled by Bayless targeted the conventionally trapped-hydrocarbons in the Banta Ridge trend and is the highest producing well to date. At the same time, the Meagher 10-1H drilled by KGH successfully tested unconventional play concepts and provided evidence for stratigraphically trapped oil ~2 miles north of Banta Ridge in Colorado near the Utah border. After three additional successful horizontal wells in Colorado, KGH further exemplified unconventional concepts in Utah with the Bonanza State 20-15H horizontal well in the SITLA Bonanza Block in 2016. Conventional and unconventional wells drilled over the last several decades have exhibited variable results and future Mancos B development will rely further on a high-level understanding of reservoir properties and hydrocarbon compartmentalization.

Early History

Drilling in northwestern Colorado dates to the early 1900s, with the first oil discovery in the Rangely field in 1902 (Anderson, 2014) (figure 10). Early wells on the Douglas Creek Arch and Piceance Basin targeted deep oil- and gas-prone formations including the Pennsylvanian Weber Formation, the Jurassic Entrada Sandstone, and the Cretaceous Dakota Formation (Kellogg, 1977). The Douglas Creek Arch yielded relatively shallow gas discoveries in the 1940s and 1950s but recovery from the Mancos B was limited due to formation damage while drilling in the clay-rich formation (Kellogg, 1977). In 1959, air drilling practices allowed the first production from the water-sensitive Mancos B with Continental Oil Company's Douglas Creek Unit #5 well (0510305095) on the Douglas Creek Arch, Rio Blanco County, Colorado (Kopper, 1962; Middlebrook and others, 1993). Active Mancos B development followed with over 40 gas wells drilled by cable tool and air-rotary rigs in Rio Blanco County within three years of the first successful Mancos B well (Kellogg, 1977). The open hole completions of the early gas wells generally yielded less than 300 million cubic ft per day (MCFPD), though increased production rates were achieved in 1966 when Continental Oil Company began casing and perforating new and old Mancos B wells (Kellogg, 1977). The following decades experienced expansion of Mancos B gas production along the crest of the Douglas Creek Arch, and expanded farther to the east and northwest making it a standard gas producing formation in northwest Colorado (Kellogg, 1977; Middlebrook and others, 1993) (figure 11). Perforation zones were identified as the highest porosity and permeability as indicated by density logs, though variable production was observed at local scales (Middlebrook and others, 1993).

Oil from the Mancos B was first produced in 1960 from Continental Oil Company's 36-4 Dragon Trail Unit well located on the down-thrown side of a large fault in the southwestern Dragon Trail field; a second Continental Oil Company well was drilled on the same structure in 1967 and also encountered oil (Kellogg, 1977). From 1960 to 2000, only a small number of wells produced variable amounts of oil from the Douglas Creek Arch, usually in structurally lower positions than gas-only wells. The Piceance Basin continued to produce substantial quantities of gas per economic conditions, though the deep Piceance notably produced almost no oil.

A relatively thick Mancos B reservoir (100–600+ ft) exists in the eastern Uinta Basin of Utah, although early operators did not explore its hydrocarbon potential as thoroughly as the

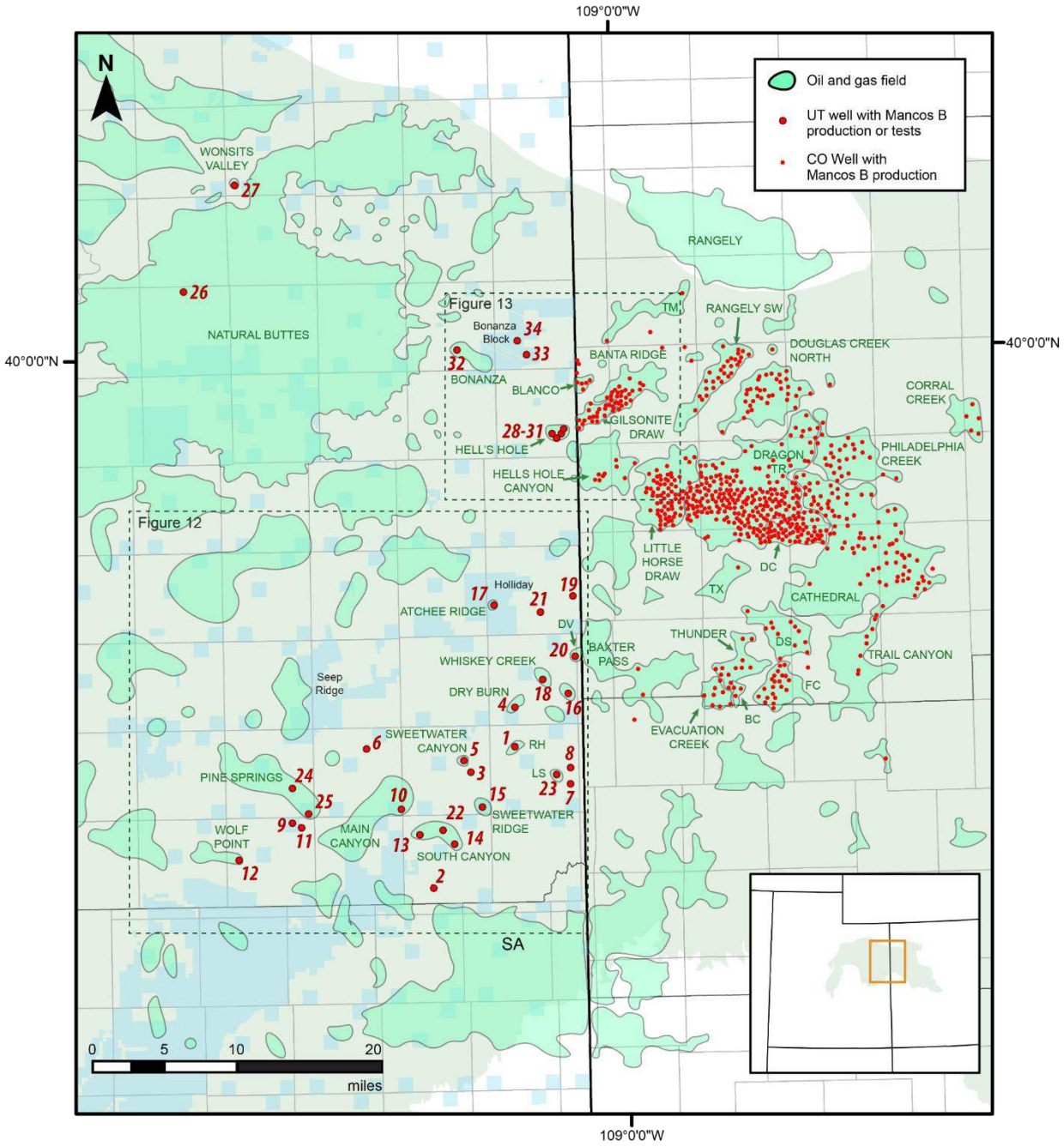

Figure 10. *Oil and gas fields of the study area with all wells that have targeted the Mancos B. The 32 wells in Utah that have tested or produced from the Mancos B correspond to the order they were drilled and are listed in table 4. Oil and gas field abbreviations: BC=Blue Cloud, FC=Foundation Creek, DC=Douglas Creek, DS=Douglas Creek South, DV=Davis Canyon, LS=Lone Spring, RH=Rat Hole Canyon, TM=Taiga Mountain, TX=Texas Mountain.*

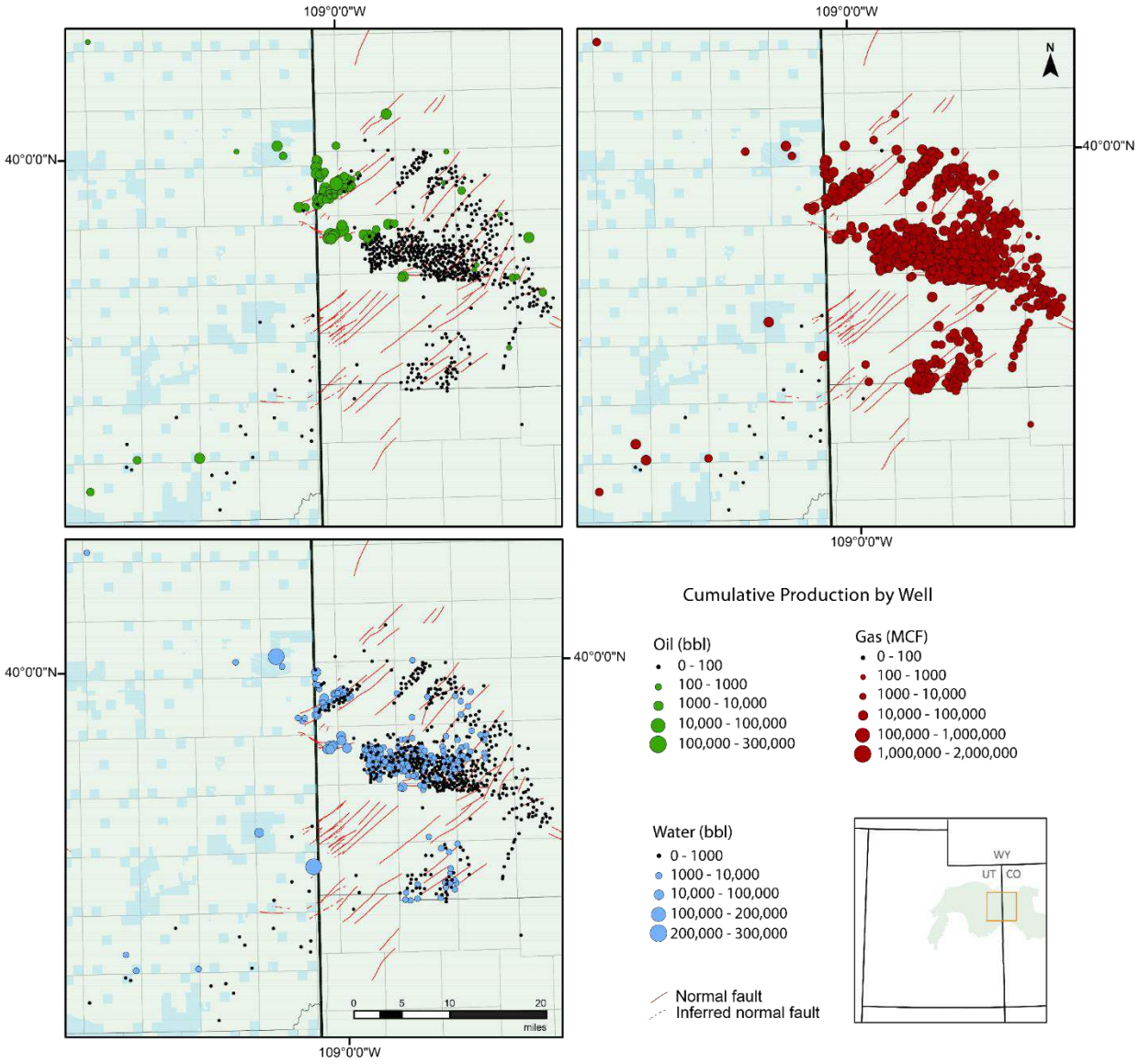

Figure 11. *Oil, gas, and water production from each well that has produced or individually tested the Mancos B in Colorado and Utah. Fault data collected from Sprinkel (2011) and Stoeser and others (2005).*

Douglas Creek Arch and Piceance Basin of western Colorado. Coseka undertook the first natural gas exploration of Utah Mancos B in the late 1970s and early 1980s. Coseka tested multiple zones throughout the Mancos B stratigraphy in 23 wells in the southeastern Uinta Basin from the Wolf Point field (~10 miles southwest of the SITLA Seep Ridge Block) to the Colorado border (figures 10 and 12; tables 3 and 4). Two of the wells have produced oil: 1) Trapp Springs 8-36-14-23 (4304730944), located near Trapp Springs Canyon has produced over 10,000 bbl oil, and 2) Wolf Point Fed 2-18-15-22 (4304731091), located near Winter Ridge, has produced ~1000 bbl oil. The remaining Mancos B test wells were not economic and were plugged and abandoned shortly after drilling (table 2). In 1982, Coseka abandoned Mancos B exploration in Utah.

In 1995–1996, Trinity Petroleum Exploration Inc. tested nine Mancos B wells in the eastern most Uinta Basin (Atchee Ridge, Davis Canyon, and Whiskey Creek fields) (table 4; figure 12). Each of the nine wells failed to produce commercial quantities of hydrocarbons and were either abandoned or later recompleted in the Mesaverde group for gas production, leaving the Mancos B exploration dormant until the 2000s.

Recent History

Beginning in 2003, operators began developing the Banta Ridge area on the western flank of the Douglas Creek Arch in Colorado and into Utah, which has become the most successful Mancos B oil producing area (table 1; figure 13). This area includes the Banta Ridge and Gilsonite Draw fields of Colorado and the Hells Hole field of Utah. Each of these fields is part of the same northeast-southwest-trending structure and together referred to as the 'Banta Ridge trend' in this report (figure 13). The first Mancos B hydrocarbons from the Banta Ridge trend were produced from a recompleted Coseka well (13-16 Federal, 05103088549) in 1982, which originally failed to produce from the Dakota Sandstone in 1980 (Coryell and McCarthy, 2014). Coseka obtained seismic following a northeast structural trend, though only drilled two additional marginal gas wells leaving the field undeveloped. In 2001, operators began systematic gas development in the area by mapping structural traps with legacy seismic data. Through detailed well planning, operators produced minor to moderate quantities of oil from vertical and then directional wells (figures 13 and 14) (Coryell and McCarthy, 2014).

In April 2011, Bayless completed a horizontal Mancos B well (Weaver Ridge 13-9H, 0510311781) in Banta Ridge and produced ~50,000 bbl of oil in its first year (table 5, figures 13 and 14). Bayless drilled several following horizontals on the northern flank of the Banta Ridge trend with relatively high initial production results (figure 15). Simultaneously, KGH was testing more unconventional horizontal concepts several miles north of the main northwest-southeast Banta Ridge structure in an area with few faults. The Meagher 10-1H horizontal well drilled in Blanco field ~2 miles north of the Banta Ridge in July 2011 exemplified unconventional concepts yield increased production from stratigraphically trapped hydrocarbons in the Mancos B (figure 13). Two additional KGH wells in the area north of Blanco field further (Meagher 3-1H and Meagher 3-3H) exhibit unconventional success. All wells show relatively high initial production, and Meagher 3-3H exhibits the highest initial oil production (~13500 bbls in 3 months; figure 15). Decline curves for horizontal wells indicate strongest well performance in the first ~5–15 months (figure 14).

Table 3. Cumulative Mancos B production by state and field.

State / Field	# Wells	Date	Cumulative Production		
			Oil (Mbbl)	Gas (MMCF)	Water (Mbbl)
Colorado (all fields)	*688	1999-2019	1882.31	183823.04	1090.44
Banta Ridge	30	1999-2019	478.73	9251.67	60.09
Gilsonite Draw (western part of Banta Ridge trend)	27	2002-2019	453.63	16039.16	98.91
Blanco	8	2004-2019	200.76	4124.39	23.54
Horizontal wells only (Banta Ridge, Gilsonite Draw, Blanco, wildcat)	7	2011-2019	399.60	3628.27	119.05
Hells Hole Canyon	9	1999-2019	510.67	3829.46	245.13
Lower Horse Draw	71	1999-2019	85.77	30839.77	163.40
Taiga Mountain	6	1999-2019	31.29	288.86	1.22
Utah (all fields)	9	2003-2019	67.10	971.043	270.16
Bonanza Block and Bonanza Field	3	2016-2019	36.59	313.21	250.16
Hells Hole (Utah part of Banta Ridge trend)	3	2003-2019	28.44	121.27	8.19
Pine Springs	2	2003-2019	1.27	477.90	4.42
Wonsits Valley	1	2003-2007	0.80	58.66	7.38

Cumulative oil, gas, and water production by state and field. Field subsets are included for areas that have substantial oil production in Colorado, and all oil-producing fields in Utah. Dates reflect first state recording of production (1999) or the first production from the Mancos B in that field (post-1999). Cumulative gas production for all Colorado fields includes Banta Ridge, Baxter Pass, Blanco, Blue Cloud, Buzzard Creek, Canary, Cathedral, Corral Creek, Douglas Creek, Douglas Creek North, Dragon Trail, Evacuation Creek, Foundation Creek, Gasaway, Gilsonite Draw, Grand Valley, Hells Hole Canyon, Lower Horse Draw, Park Mountain, Philadelphia Creek, Piceance Creek, Rangely Southwest, Rocky Point, Rulison, Sage Brush Hills II, Slater Dome, Soldier Canyon, Taiga Mountain, Texas Mountain, Thunder, Trail Canyon, and Yellow Creek fields (See figure 10 for map). Production data collected and compiled from DOGM and COGCC.

**Twenty wells (all located in Cathedral and Dragon Trail fields) contain comingled production data from Mancos A and B; these mixed wells contribute a total of 3.33 Mbbl, 2343 MMCF, and 1.23 Mbbl water to the cumulative production for Colorado.*

Table 4. Mancos B wells in Utah, pre-2000

*Map ID	API	Well Name	**First Production	Year 1 Oil Production (bbl)	Cumulative Production or Tests (01/01/1984 - 01/01/2020)			
					Months	Oil (bbl)	Gas (MCF)	Water (bbl)
1	4304730325	Rat Hole Cyn Unit 1 7-8-14-25	11/1977	NA	Initial 24 hr test: 0 bbl oil, 157 MCFG, 0 bbl water. No production after 1984 – Dry hole			
2	4304730248	Black Horse 2 1-29-15S-24E	04/1978	NA	Initial 24 hr test: 0 bbl oil, 116 MCFG, 0 bbl water. No production after 1984			
3	4304730332	Sweetwater Cyn 1-L-23	04/1978	NA	Initial 24 hr test: 0.6 bbl oil, 288 MCFG, 0 bbl water. No production after 1984			
4	4304730331	Dry Burn Unit 1 1-29-13S-25E	10/1978	NA	Initial 24 hr test: 0 bbl oil, 204 MCFG, 0 bbl water. No production after 1984 – Dry hole			
5	4304730460	Sweetwater Cyn 1-14-14-24	09/1979	NA	Pre-1984 cumulative: 47 bbl oil, 57 MCF gas, 0 bbl water. No production after 1984			
6	*4304730708	Crooked Cyn 10-10-14-23	07/1980	0	Pre-1984 production: 0 BOPD, 91 MCFGPD, 2-3 BWPD. No production after 1984			
7	4304730597	Rat Hole Unit 3	10/1980	NA	Initial 20 hr test: 0 bbl oil, 190 MCFG, 36 bbl water. No production after 1984			
8	4304730598	Rat Hole Unit 4	10/1980	NA	Initial 6 hr test: 0 bbl oil, 0 MCFG, 0 bbl water. No production after 1984			
9	4304730746	Pine Springs St 11-2-15-22	11/1980	0	Dry hole. No tests.			
10	4304730944	Trapp Springs 8-36-14-23	07/1981	NA	233	10263	96593	1296
11	4304731135	Main Canyon St 8-2-15-22	08/1981	0	Dry hole. No tests.			
12	4304731091	Wolf Point Fed 2-18-15-22	11/1981	NA	80	1808	23877	516
13	4304731104	Black Horse 12-8-15-24	12/1981	NA	Pre-1984 production: 0 BOPD, 109 MCFGPD, 0 BWPD. No production after 1984			
14	4304731045	Black Horse Fed 14-15-15-24	01/1982	NA	Initial 24 hr test: 0 bbl oil, 19 MCFG, 0 bbl water. No production after 1984			
15	4304732593	TPC St 36-14-24 1	05/1995	NA	Dry hole. No tests.			
16	4304732602	Atchee Ridge 24-13-25 1	04/1995	NA	Dry hole. No tests.			
17	4304732660	Seep Canyon St 19-12-25 1	07/1995	NA	No Mancos B production. Recompleted in Mesaverde.			
18	4304732659	Atchee Ridge 15-13-25 1	08/1995	NA	Dry hole. No tests.			
19	4304732605	Evacuation Creek 24-12-25 1	09/1995	NA	Dry hole. No tests.			
20	4304732618	Davis Canyon 12C-13-25-1	04/1996	NA	No Mancos B production. Recompleted in Mesaverde.			
21	4304732587	Dragon Cyn 27-12-25 1	06/1996	NA	Dry hole			
22	4304732592	Black Horse 9-15-24 1	06/1996	NA	Initial 24 hr test: 0 bbl oil, 40 MCFG, 0 bbl water. Shut in.			
23	4304732705	Rat Hole Canyon 23-14-25 1	06/1996	NA	Dry Hole			

**Map ID corresponds to figures 10 and 12. ** Wells completed prior to 1984 lack cumulative production records. Post-1984 data is provided and pre-1984 data is provided if it is available. Production data collected and compiled from DOGM and COGCC.*

Table 5. Horizontal Mancos B wells

API	*Well Name	Operator	First Production	Year 1 Oil Production (bbl)	Cumulative Production (through 12/2019)			
					Months	Oil (bbl)	Gas (MCF)	Water (bbl)
Colorado								
0510311781	Weaver Ridge 13-9H	Bayless	04/2011	49154	102	151751	866824	16702
0510311854	Meagher 10-1H	KGH	07/2011	15331	100	9866	376283	4139
0510311910	Meagher 3-1H	KGH	08/2012	17958	89	31888	434281	4071
0510311932	Weaver Ridge 14-15H	Bayless	09/2013	16692	84	45676	368094	15183
0510311933	Weaver Ridge 23-7H	Bayless	08/2013	16484	74	57711	304889	16452
0510311955	Meagher 14-1H	KGH	11/2013	8109	74	31841	166235	25746
0510312121	Meagher 3-3H	KGH	12/2014	31881	64	70869	1111667	11003
Utah								
4304755745	Bonanza State 20-15H	KGH	02/2018	22468	22	30665	273867	247766

Production data collected and compiled from DOGM and COGCC.

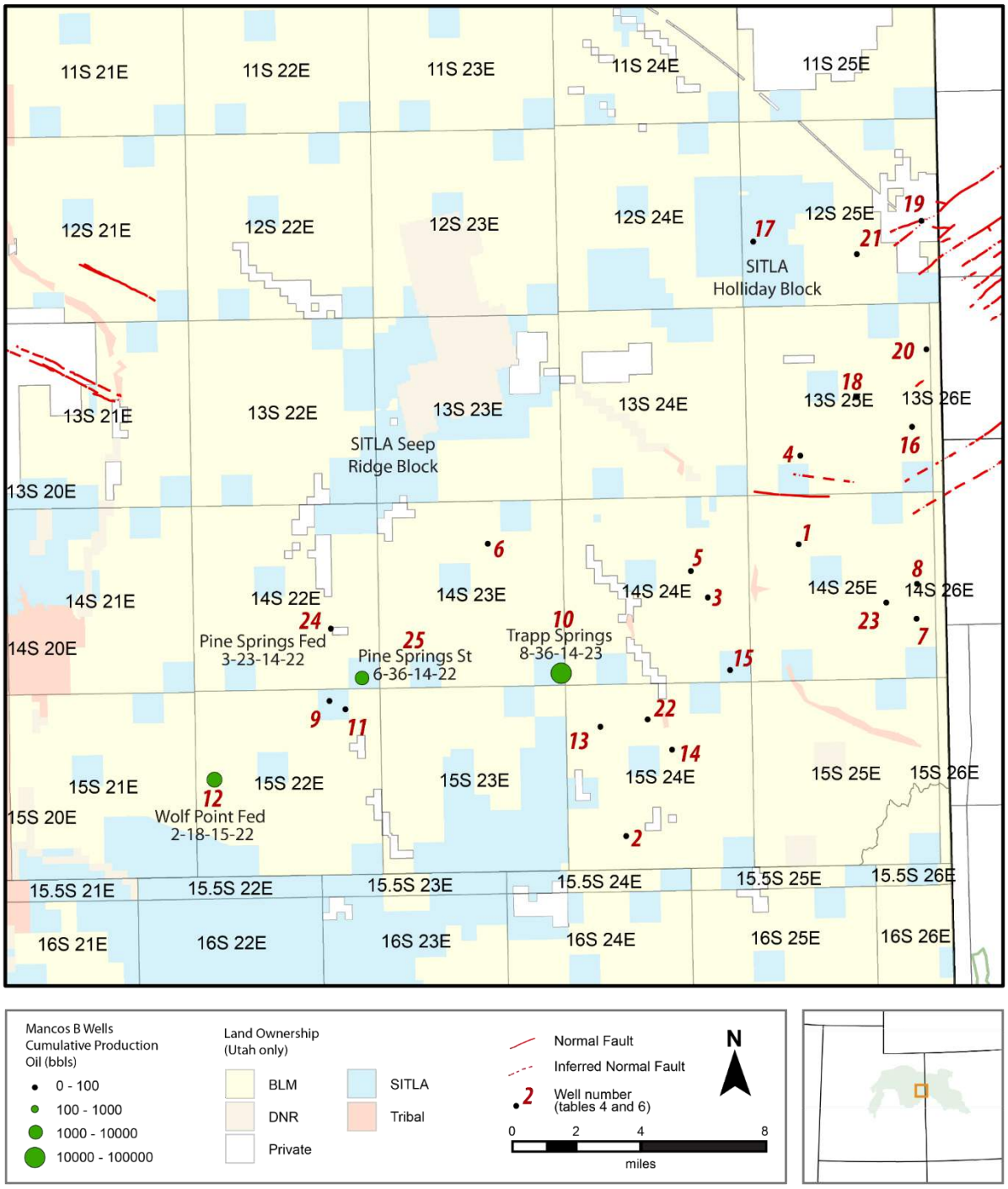

Figure 12. *Cumulative oil production from Mancos B wells in the southeastern Uinta Basin. Wells with oil production (10, 12, 24, and 25) are labeled; other well names and data are found in tables 4 and 6. Fault data collected from Sprinkel (2011) and Stoeser and others (2005).*

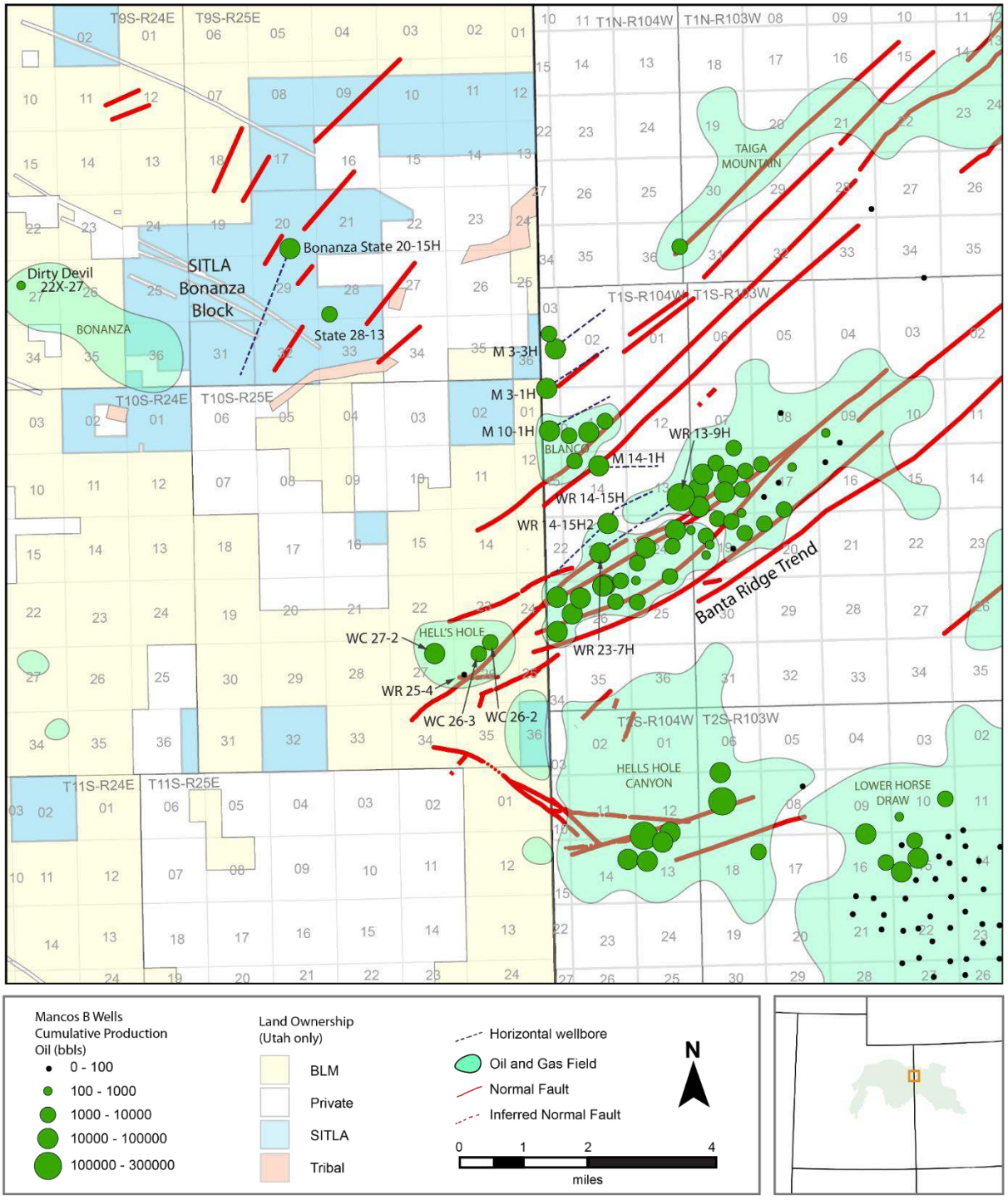

Figure 13. *Cumulative oil production from Mancos B wells, focusing on Banta Ridge and the SITLA Bonanza Block. Common well names are abbreviated as follows: M = Meagher (KGH wells), WC = Weaver Canyon (Bayless wells), WR = Weaver Ridge (Bayless wells). Fault data provided by KGH Operating Company and collected from Stoeser and others (2005), Sprinkel (2011), and Coryell and McCarthy (2014).*

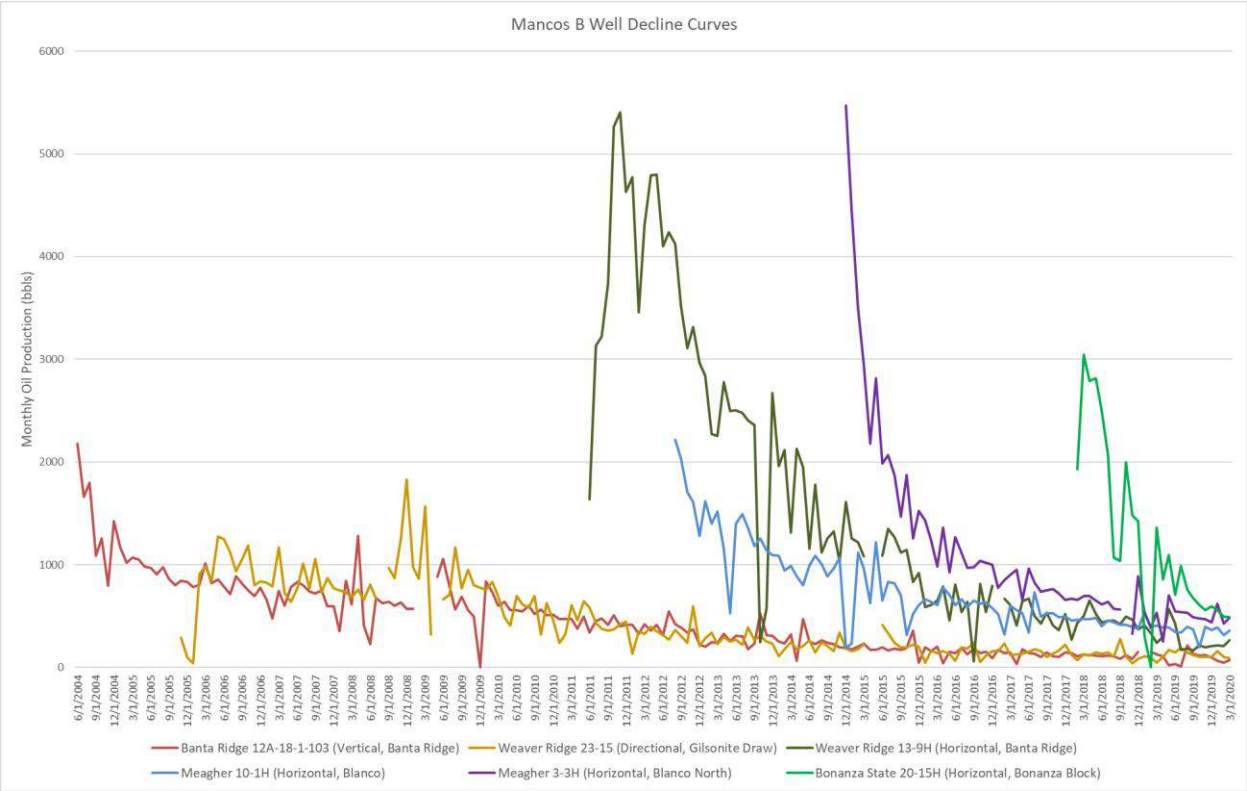

Figure 14. *Monthly production from the highest producing (initial) Mancos B wells. "Weaver Ridge" wells were drilled by Bayless, "Meagher" wells were drilled by KGH.*

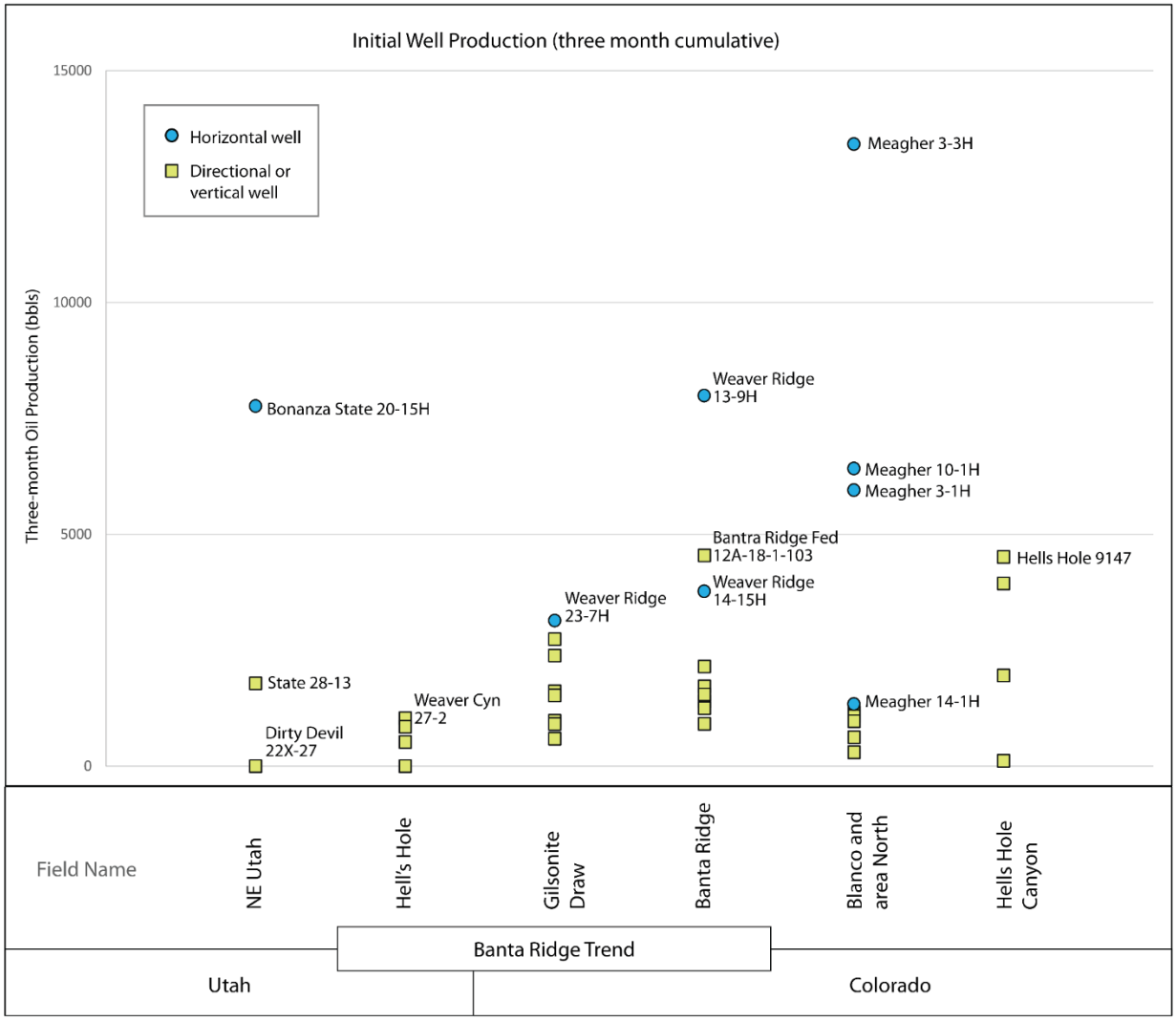

Figure 15. *Initial well production (cumulative oil from first three months) from Mancos B wells, organized by field. "Weaver Ridge" wells were drilled by Bayless, "Meagher" wells were drilled by KGH.*

In Utah, one vertical and three directional gas wells were drilled on the Banta Ridge trend (Hells Hole field) by Bayless with variable production of oil (figures 13 and 15). The best well, Weaver Canyon 27-2 (4304734941) has produced almost 20,000 bbl since 2003, whereas no oil (though substantial gas) has been produced from the neighboring Weaver Canyon 26-5 (4304737473) (table 4; figure 13).

Success on the Banta Ridge trend has been linked to the right combination of structural position, reservoir quality, and favorable gas-to-oil ratios (GOR) (Coryell and McCarthy, 2014), and these attributes are likely important in other producing and prospective fields for liquid production. The Banta Ridge structure is largely defined by a northeast-southwest-trending graben with a series of normal faults and highly variable vertical displacement within the Mancos (Coryell and McCarthy, 2014). These Laramide-age faults are interpreted as the integral hydrocarbon trapping mechanism and thereby are important to identify for successful wells. Generally, the best reservoir unit in Banta Ridge is the lowermost 140–200 ft of the Mancos B, as indicated by low gamma, high porosity, and higher sand-to-shale ratios. Coryell and McCarthy (2014) highlight mixed oil and gas wells are generally poor performers, whereas wells with either a very high or very low GOR can be exceptional performers.

Northwest of Banta Ridge, the SITLA Bonanza Block in Utah has also shown promising oil production from SITLA land. One vertical well (State 28-13) and one horizontal well (Bonanza State 20-15H) have been drilled to date with variable production. State 28-13, drilled by KGH in 2016, has produced >6000 bbl oil from September 2016 to December 2019 and proved the presence of a liquid charged Mancos B reservoir in the SITLA Bonanza Block. The Bonanza State 20-15H horizontal well (~7500 ft vertical depth, 10,460 ft lateral length) was drilled in 2018 by Whiting Oil and Gas (well now operated by KGH), is the only horizontal well to date to target the Mancos B in Utah. As of April 2020, Bonanza State 20-15H has produced over 30,000 bbl oil making it the largest oil producing Mancos B well in Utah, although both Bonanza Block wells were shut-in in April 2020 due to the oil market crash related to the COVID-19 pandemic (table 6). Similar to KGH's Meagher wells in Colorado, the Bonanza Block wells were drilled in a location without a large or extensive northeast-southwest fault network. This suggests the trapping of liquids in the Bonanza Block is not confined to regionally limited faulted blocks and may be pervasively charged. In other words, the Bonanza Block and Meagher wells may behave more like an unconventional reservoir play. This contrasts with previous geologic models for Mancos B production that relied on a structural trap. It is worth noting that even if the area is pervasively charged, the variable production suggests changing GOR throughout the reservoir.

In the structurally deeper northern Uinta Basin, two gas wells have tested the Mancos B (figures 10, 11; table 6). El Paso Production Oil and Gas Company completed the Pawwinnee 3-181 (4304734019) in 2002 and produced ~600 bbl oil in its first year. The well was later recompleted in the Mesaverde with comingled production since June 2004. Shenandoah Energy drilled the SU Purdy 14M-30-7-22 (4304734384) in 2003 (and was later produced by QEP Uinta Basin, Inc.) which produced ~500 bbl oil in its first year. With only limited data, it is hypothesized that the area is not a strong contender for substantial oil production. This hypothesis is supported by pressure gradients and the dominance of gas production from other

Table 6. Mancos B wells in Utah, post-2000

*Map ID	API	Well Name	First Production	Year 1 Oil Production (bbl)	Cumulative Production (01/01/1984 – 01/01/2020)			
					Months	Oil (bbl)	Gas (MCF)	Water (bbl)
N Uinta Basin								
26	4304734019	Pawwinnee 3-181	04/2002	621	27	1106	343258	3064
27	4304734384	SU Purdy 14M-30-7-22	09/2003	575	46	796	58664	7381
NE Uinta Basin								
28	4304734941	Weaver Cyn 27-2	09/2003	2910	149	18891	69891	3725
29	4304737472	Weaver Cyn 26-3	08/2006	2058	111	9545	358367	3267
30	4304737473	Weaver Cyn 26-5	08/2006	0	111	0	51383	4466
31	4304739595	Weaver Cyn 26-2	02/2009	1334	91	6752	482406	4194
32	4304734825	Dirty Devil 22X-27	10/2010	246	95	292	58012	3180
33	4304754984	State 28-13	09/2016	4019	42	6557	47000	6451
34	4304755745	Bonanza State 20-15H	02/2018	22468	22	30665	273867	247766
SE Uinta Basin								
24	4304734675	Pine Springs Fed 3-23-14-22	10/2002	0	206	76	224590	1637
25	4304735555	Pine Springs St 6-36-14-22	09/2005	281	170	1194	256187	2782

**Map ID corresponds to figures 10 and 12. Production data collected and compiled from DOGM and COGCC.*

wells in the area (i.e., wells that produce comingled gas from Mancos B and other formations; appendix H).

The southeastern Uinta Basin of Utah has a history of dry wells resulting in few recent Mancos B tests in the region. However, two wells operated by Foundation Energy Management, LLC have successfully produced substantial gas and some oil from the Pine Springs field (table 6; figure 12). The Pine Springs St 6-36-14-22 (4304734675) has produced ~1200 bbl since 2005 and Pine Springs Fed 6-36-14-22 (4304735555) has produced ~75 bbls since 2002 and show liquid potential exists in the southeastern Uinta Basin. Currently, there is not enough data to determine the full oil potential in the immediate area nor in the lesser explored region north and northeast of the Pine Springs field (e.g., SITLA Seep Ridge and Holladay blocks; figure 12). The production differences between the plugged and abandoned wells drilled in the 1980s and the wells drilled early 2000s are likely attributable to modern drilling and production practices, variable compartmentalization of hydrocarbons, and better-defined reservoir targets by operators.

In addition to the wells that have singly targeted the Mancos B reservoirs, 31 wells have tested the Mancos B in comingled oil and gas wells drilled in the early 2000s, mostly in the northern Uinta Basin. As the wells have not differentiated production between Mancos B and other formations (mainly the Dakota Sandstone and the Mesaverde group), they are not assessed for Mancos B potential; however, well data from comingled wells is located in appendix H.

Produced Water

One factor that impacts the economic success of Mancos B (and other portions of the Mancos stratigraphy) is water production. The highest water production is observed in wells targeting oil-rich Mancos B reservoirs, and the amount of water produced per barrel of oil broadly increases east to west from the Piceance Basin to the Uinta Basin. Water is also associated with gas wells, although is less of an impeding factor (e.g., the average well in the Cathedral field produces ~1 bbl water for every 500 MCF gas; table 3; figure 11).

The Mancos Formation as a whole contains substantial formation water (Ressetar and Birgenheier, 2015). We interpret that residual water is largely clay-bound where not expelled during hydrocarbon generation, especially in areas that were less deeply buried such as the Douglas Creek Arch and the margins of the Uinta Basin. SEM analyses (this study) exhibit significant microporosity in clay-rich facies, which can retain significant volumes of water. The potential for clay-bound formation water (as opposed to migrated water in porous reservoirs) is exemplified by the first horizontal gas well drilled in the clay-rich Mancos Formation in the Natural Buttes field: the HCU 1-30F (4304740396) drilled by XTO Energy in 2010 targeted a coarsening upward mudstone package beneath the Mancos B and produced 41 bbl water to every 1 bbl oil and 350 MMCF. The horizontal drilling and fracturing of the mudstone reservoir likely created pathways for pressurized clay-bound water to escape and explains the relatively high water production.

Some wells with sandstone-rich reservoirs have produced anomalous amounts of water, including the Bonanza State 20-15H well in the SITLA Bonanza Block. Water chemistry comparisons of produced water from Bonanza State 20-15H with nearby offset wells do not offer a strong correlation to the overlying Castlegate aquifer nor the Mancos Formation (appendix I). To date, the high water production from the Bonanza State 20-15H remains enigmatic. As clay

content is likely correlative with water production (see Core Analysis, this study), detailed study of minerology combined with reservoir engineering studies (e.g., wettability) and appropriate completion practices will enhance oil recovery from clay-rich portions of the Mancos B.

CORE STUDY

Stratigraphic Context

In the northeastern Uinta Basin study area, we divided the ~350- to 400-ft-thick Mancos B into lower Mancos B and upper Mancos B sections. The lower Mancos B is further divided into the Bonanza, Dirty Devil, and Boomer intervals based on petrophysical variations and drilling targets designated by KGH (figure 16). The southeastern Uinta Basin contains a 350- to 800-ft-thick section of the Mancos B, which we split into three stratigraphic zones: lower Mancos B, middle Mancos B, and the upper Mancos B (figure 16). These zones were picked based on log boundaries that could correlate across the region and are placed generally at the top of coarsening upwards packages. Robust correlation between the northeastern and southeastern Uinta Basin study areas is difficult due to a lack of stratigraphic markers and a large well-data gap between the areas in the east-central Uinta Basin (figure 3).

In the northeastern Uinta Basin, both Weaver Ridge 13-16 and Bonanza State 20-15H cores targeted the lower Mancos B (table 1; figure 16), which contains the main producing Bonanza interval in Banta Ridge. The 40.5 ft Weaver Ridge 13-16 core contains 0.1 ft of the Lower Blue Gate Member and a partial section (40.4 ft) of the lower Mancos B Bonanza section (figure 17). The 330.3 ft Bonanza State 20-15H core contains 91.3 ft from the Lower Blue Gate Member, a complete 139 ft section of the lower Mancos B, and a partial 100 ft section of the upper Mancos B (figure 18).

In the southeastern Uinta Basin, the three legacy cores targeted multiple areas of the Mancos B stratigraphy and some wells contain multiple core intervals. Crooked Canyon Unit 10-10-14-23 contains two core intervals (figures 16 and 19). One interval is 52.5 ft thick and captures the upper portion of the lower Mancos B. The second interval is 117 ft thick and captures 26 ft of the upper Mancos B and 91 ft of the Upper Blue Gate Member (not described as part of this study). Trapp Springs Unit 1-25-14-23 contains one 148.1 ft core segment that captures 145.6 ft of the upper Mancos B and 2.5 ft of the Upper Blue Gate Member (figures 16 and 20). Main Canyon State 2-8-15-22 contains three core segments that capture 60.4 ft of the lower Mancos B, 117.4 ft of the middle Mancos B, and 58.3 ft of the upper Mancos B (figures 16 and 21).

Lithofacies

Eight lithological facies were identified in the five study cores: 1) Laminated to massive mudstone, 2) Heavily bioturbated heterolith, 3) Laminated mudstone with subordinate sandstone, 4) Parallel laminated muddy sandstone, 5) Wavy bedded sandstone and mudstone, 6) Asymmetrical ripple laminated sandstone, 7) Inclined muddy sandstone, and 8) Massive medium-coarse sandstone (table 7; figure 22). Sandstone-rich facies 4–7 are identified as

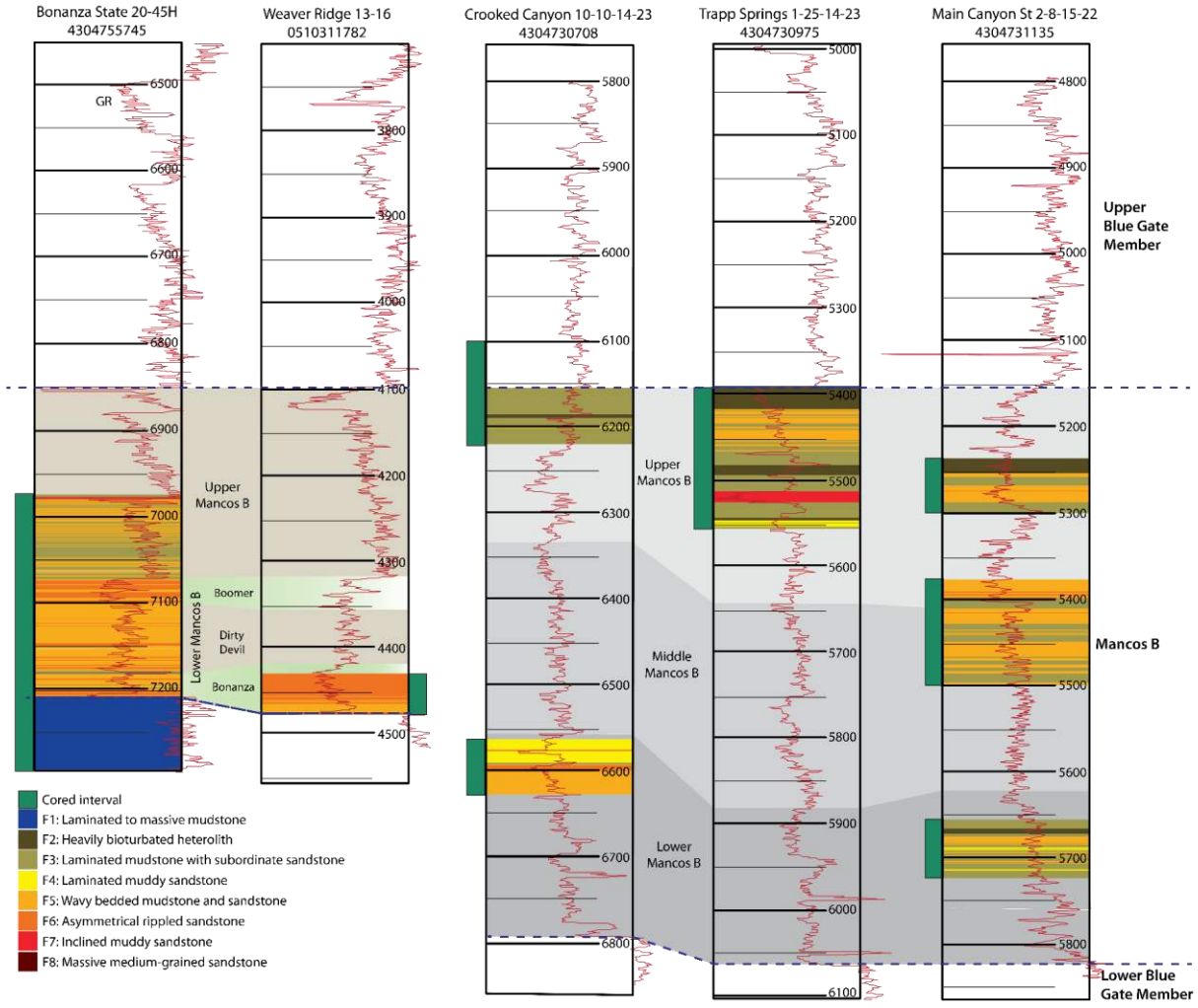

***Figure 16**. Cross section of wells that have cored the Mancos B in the eastern Uinta Basin. Lithofacies observed in core are superimposed with gamma curves. See figure 3 for well locations. See table 7 and figure 21 for lithofacies descriptions.*

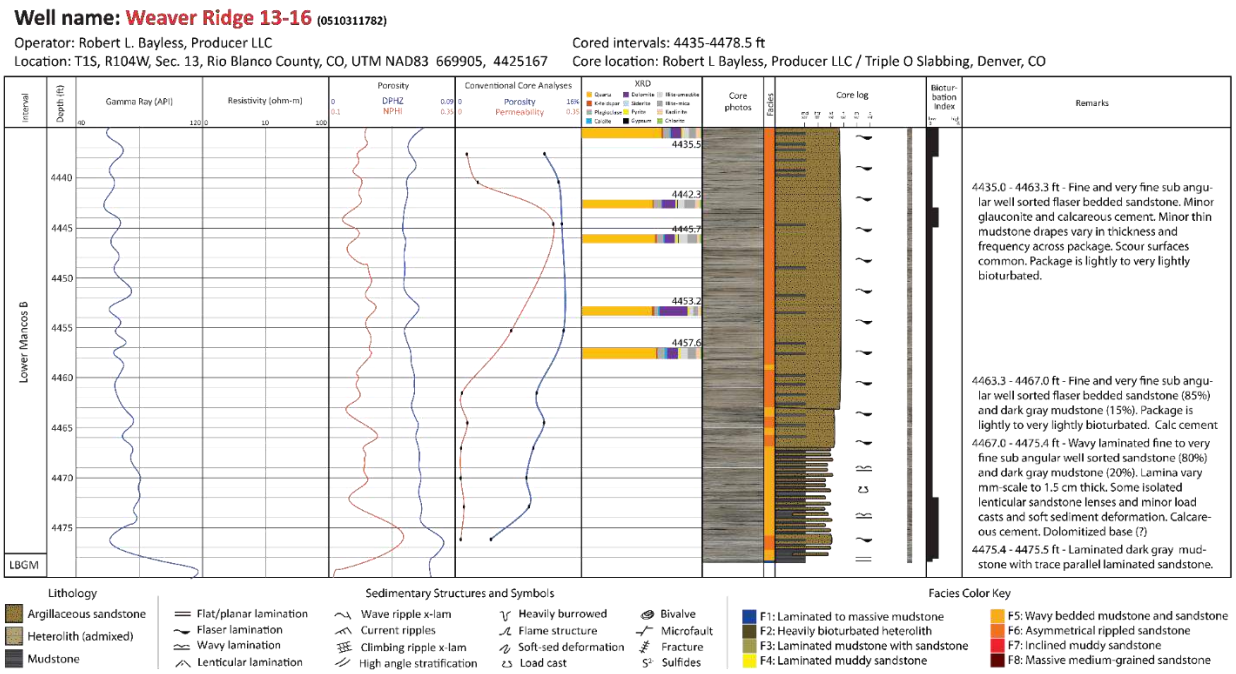

Figure 17. *Core data and description from Weaver Ridge 13-16. LBGM=Lower Blue Gate Member.*

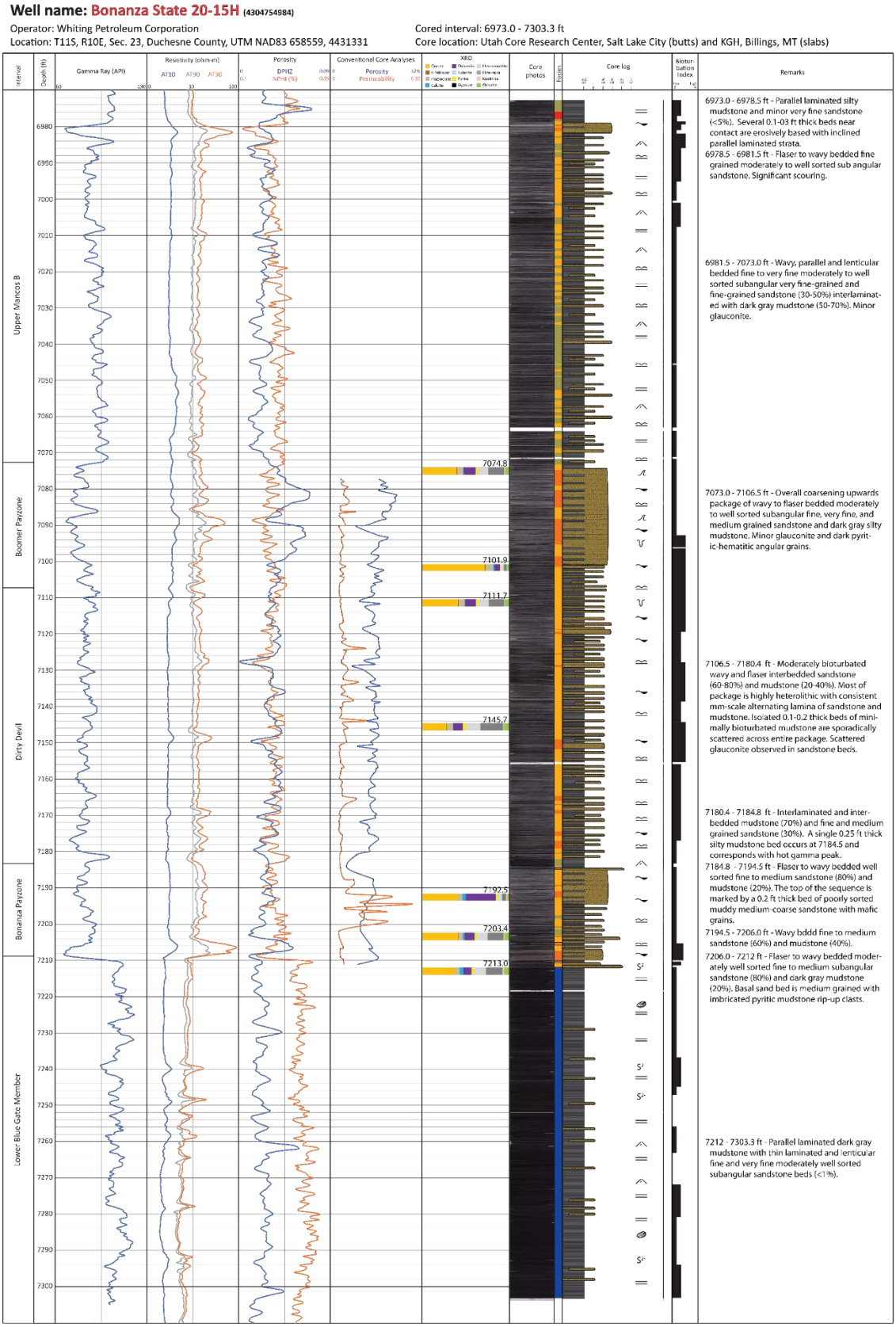

Figure 18. *Core description of Bonanza State 20-15H. See Figure 17 for key to symbols.*

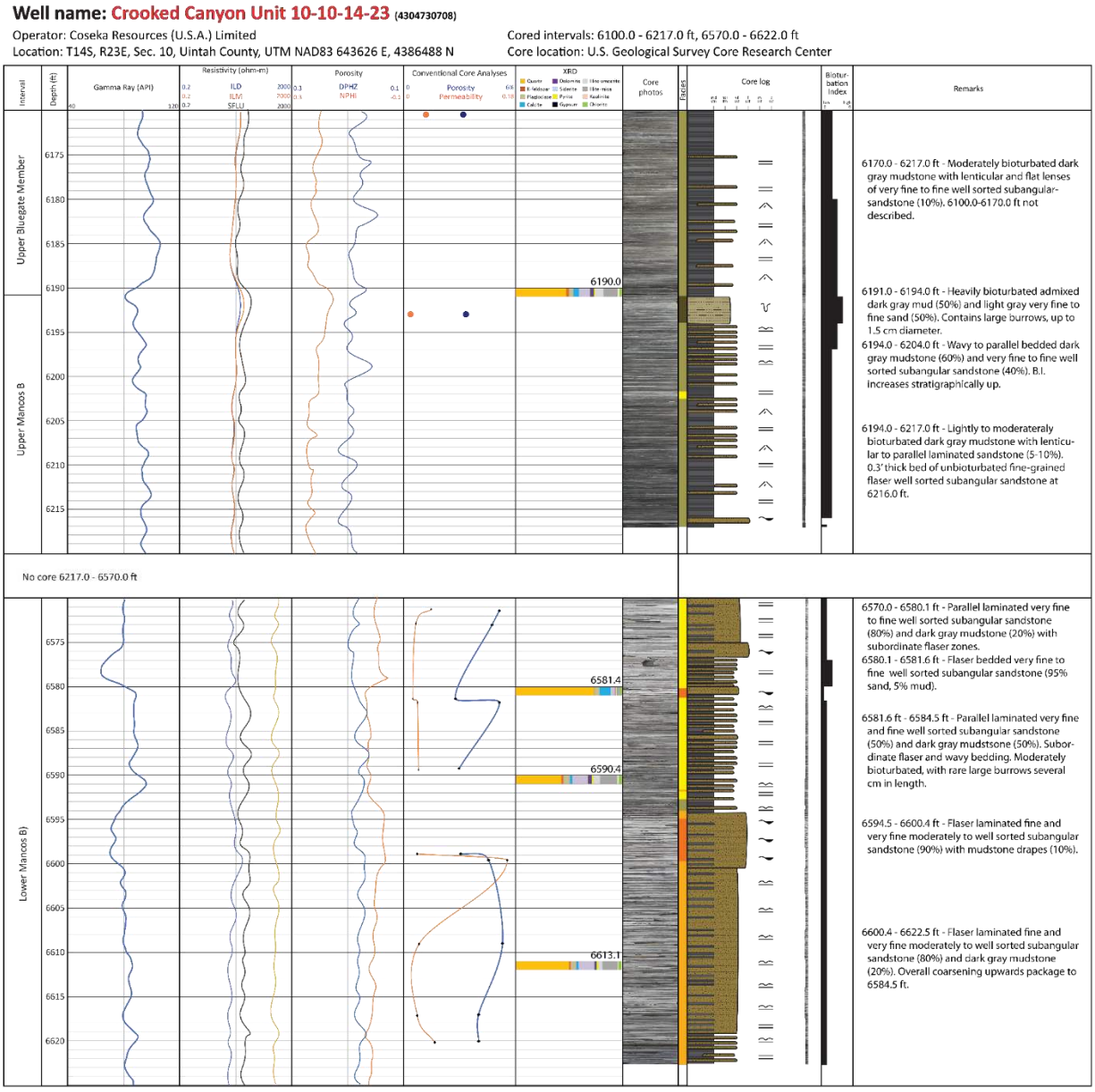

Figure 19. *Core data and description of Crooked Canyon Unit 10-10-1-23. See Figure 17 for key to symbols.*

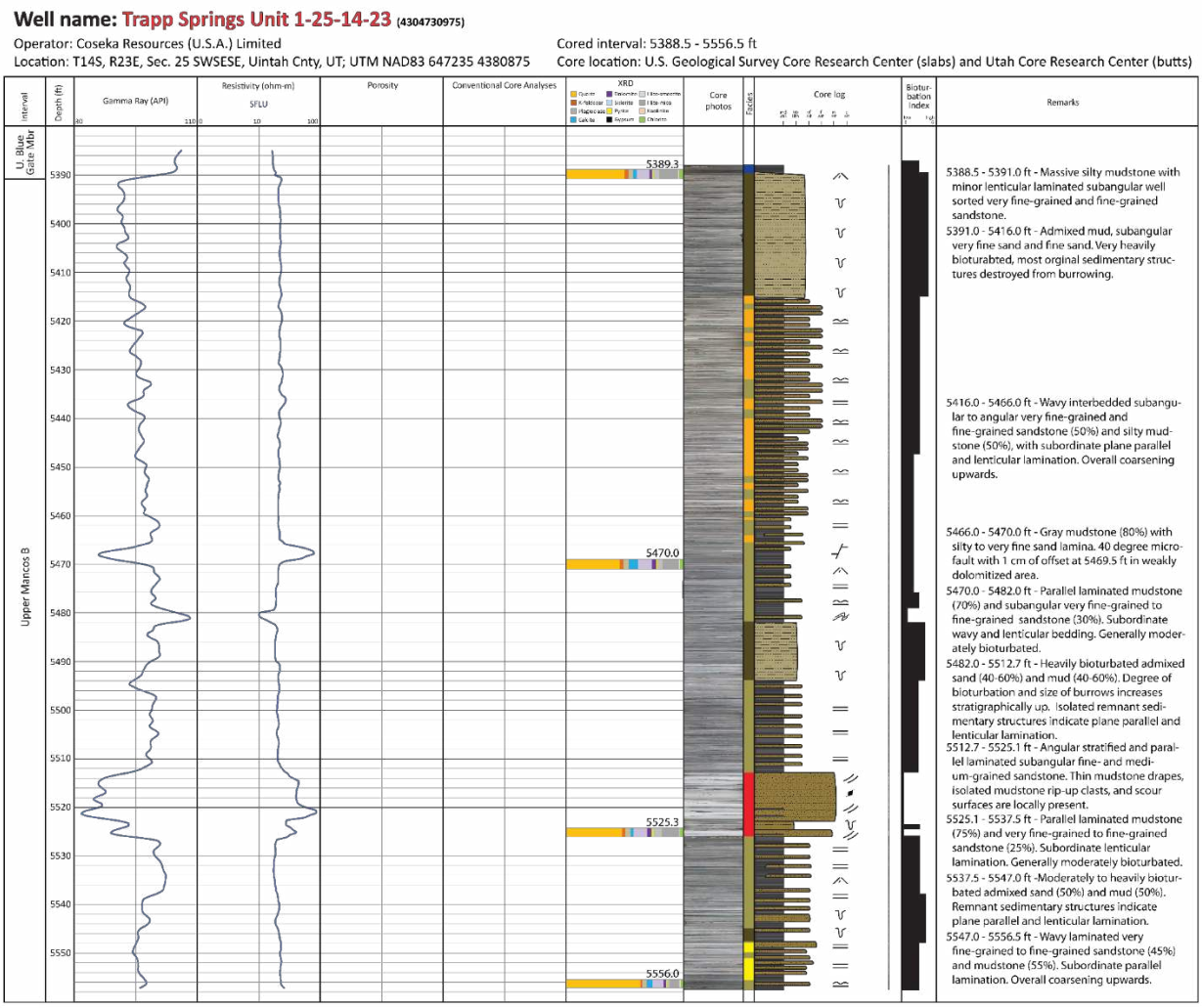

Figure 20. *Core data and description of Trapp Springs Unit 1-25-14-23. See Figure 17 for key to symbols.*

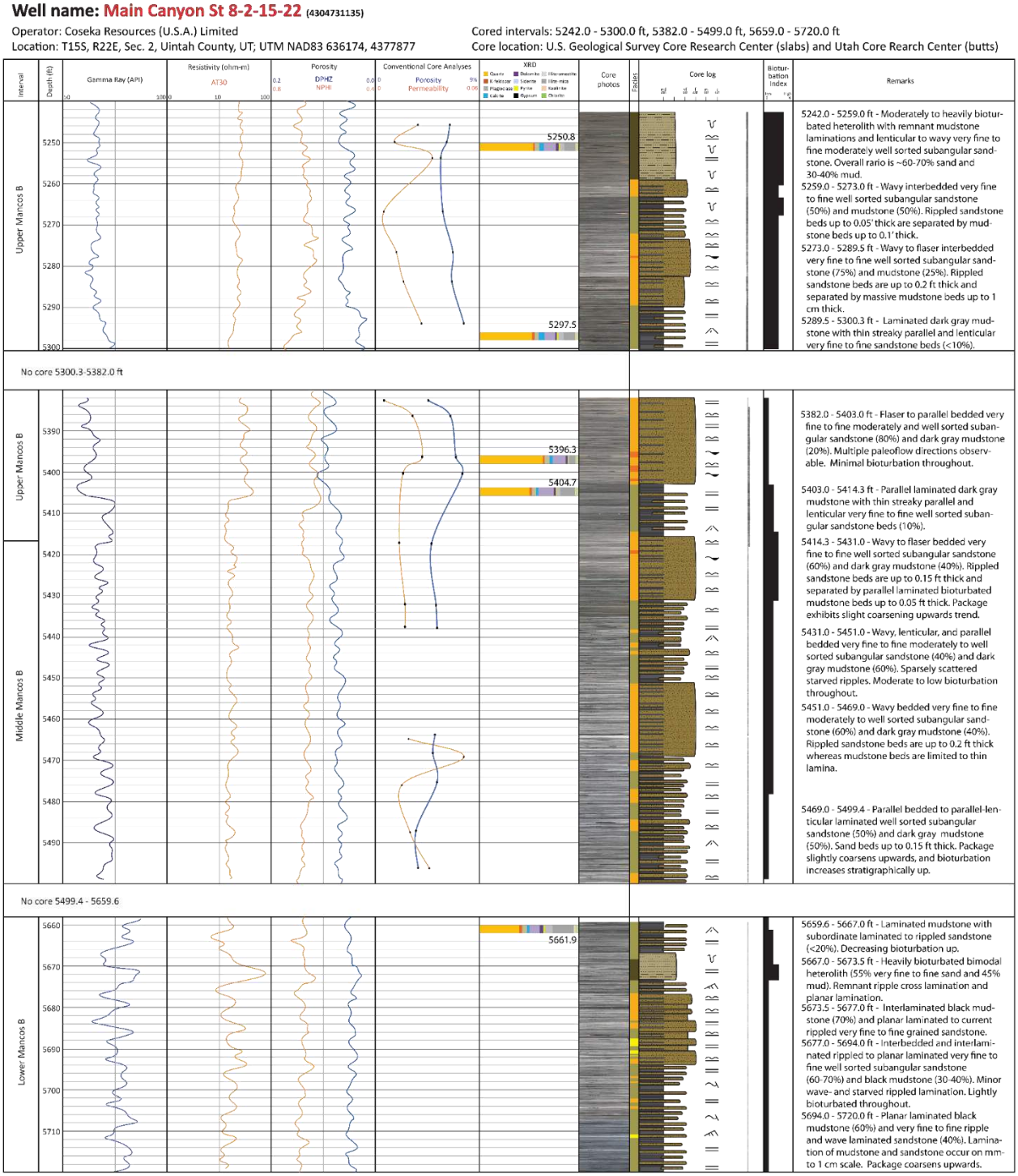

Figure 21. *Core data and description of Main Canyon St 8-2-15-22. See Figure 17 for key to symbols.*

Table 7. Core facies

ID	Lithofacies	Lithology	Sedimentary structures	*B.I.	Other	Interpretation
1	Laminated to massive mudstone	95%+ silty mudstone with minor continuous to lenticular very fine to fine grained argillaceous sandstone lamina	Dominantly plane parallel, very low angle and lenticular lamination. Can appear massive. Rare starved sandstone ripples.	0-3	Occurs in thin beds (<10cm) within Mancos B. Dominant facies of Upper and Lower Blue Gate members	Relatively low energy environment, nearshore mudbelt to distal offshore environment.
2	Heavily bioturbated heterolith	Heavily bioturbated, poorly sorted admixed heterolith composed of clay, silt, and very fine to fine grained sand.	Structures obliterated by bioturbation, remnant plane parallel and ripple lamination rare.	3-5	Gradational contacts, packages are commonly 3-10 ft thick.	Sediment delivery from fluvial and current driven sources. Bioturb-ated in well-oxygenated, relatively low-sediment input environment in distal prodelta turbidite complex above storm wave base.
3	Laminated mudstone with subordinate sandstone	Interlaminated <1-10 mm thick silty mudstone (>50%) and 1-10 mm thick very fine to fine grained argillaceous sandstone (5-50%).	Dominantly plane parallel, very low angle, and lenticular lamination. Starved ripples with unidirectional foresets and asymmetrical and symmetrical crests.	1	Minor organic matter. Commonly drapes and conforms to underlying bed geometry.	Deposited by intermittent fluvially fed hyperpycnal flows below fair weather wave base. Represents on-axis deposition of distal prodelta turbidte complex
4	Parallel laminated muddy sandstone	Interlaminated 1-10 mm thick very fine to fine grained argillaceous sandstone (>50%) and 1-10 mm thick silty mudstone.	Dominantly plane parallel and very low angle lamination. Subordinate starved ripples with unidirectional foresets and asymmetrical crests.	0-1	Sharp basal contacts; gradational upper contact common. Reservoir facies.	Deposited by intermittent fluvially fed hyperpycnal flows below fair weather wave base. Represents on-axis deposition of distal prodelta turbidte complex.
5	Wavy bedded sandstone and mudstone	Interlaminated 3-50 mm thick very fine to medium grained argillaceous sandstone (~50%) and 1-40 mm silty mudstone (~50%).	Dominated by unidirectional foresets with asymmetrical and symmetrical crests. Scours and soft sediment deformation common. Minor parallel lamination, fluid escape structures, wave ripples.	1-3	Abundant coaly and other organic matter preserved in mudstone lamina. Reservoir facies.	Deposited by intermittent fluvially fed hyperpycnal flows commonly reworked by currents above fair weather wave base. Represents near to slightly off axis prodelta turbidite-lobe depocenter.
6	Asymmetrical ripple laminated sandstone	3-50 mm thick very fine to medium grained argillaceous sandstone laminae and beds separated by thin (<5 mm) continuous and discontinuous mudstone drapes.	Dominated by unidirectional foresets with asymmetrical and symmetrical crests. Scours and soft sediment deformation common.	1-2	Sharp flat or irregular basal contact. Reservoir facies.	Deposited by relatively consistent fluvially fed hyperpycnal flows, commonly reworked by currents above fair weather wave base. Represents prodelta turbidite lobe depocenter.
7	Inclined muddy sandstone	40 mm+ packages of 1-10 mm thick inclined fine-grained argillaceous sandstone lamina. Individual laminae are graded.	Inclined curvilinear strata.	0-1	Sharp irregular basal contacts. Only observed in Trap Springs Unit 1-25-14-23. Reservoir facies.	Turbidite channels.
8	Massive medium-coarse sandstone	3-50 mm lamina and beds of medium to coarse grained sandstone. Moderately well sorted. Extensive carbonate cement common.	Massive weakly imbricated sandstone with weakly scoured base and flat, slightly graded top.	0	Sharp base, lightly bioturbated top. Only observed in basal Mancos B, Bonanza State 20-15H.	High energy turbidity flow deposit.

**Bioturbation index (B.I.) following Bann and others (2008). See figure 23 for mineral composition by facies.*

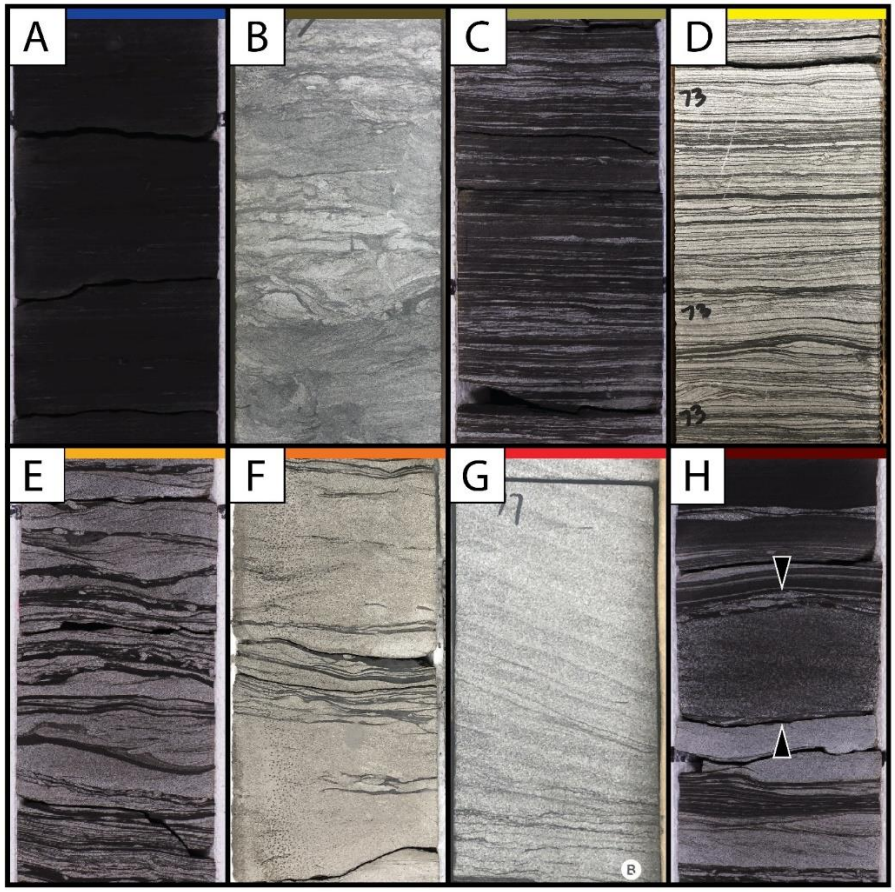

A) Facies 1, laminated to massive mudstone (Bonanza State 20-15H: 7218.8-7219.4 ft).

B) Facies 2, heavily bioturbated heterolith (Trapp Springs Unit 1-25-14-23: 5397.3-5397.9 ft).

C) Facies 3, laminted mudstone with subordinate sandstone (Bonanza State 20-15H: 7041.6-7042.1 ft).

D) Facies 4, parallel laminated muddy sandstone (Crooked Canyon 10-10-14-23: 6573.1- 6573.7 ft).

E) Facies 5, wavy bedded sandstone and mudstone (Bonanza State 20-15H: 7078.9-7079.5 ft).

F) Facies 6, asymmetrical ripple laminated sandstone (Weaver Ridge 13-16: 4455.4-4456.0 ft).

G) Facies 7, Inclined muddy sandstone (Trapp Springs Unit 1-25-14-23 5517.3-5517.9 ft).

H) Facies 8, massive medium-coarse sandstone, upper and lower boundaries marked by arrows (Bonanza State 20-15H: 7184.6-7185.2 ft).

Figure 22. *Core images of core facies. All images are of dry 3-inch-wide core slabs. Color bars correspond to facies designations used in figures 16-21.*

reservoir facies based on relatively high porosity and permeability measurements. Mudstone facies 1–3 and diagenetically altered sandstone facies 8 generally exhibit poor reservoir qualities. Reservoir properties are further discussed below.

Mineralogy

Facies 1–7 contain bimodal grain populations contained within interlaminated to interbedded mudstone and sandstone lithologies. Sandstone grains are subangular to angular, very fine to medium-grained and dominantly consist of quartz grains (40%–75% total composition) (figures 22–27; appendix C). Subordinate fractions of sandstone mineral grains are composed of plagioclase (<10%), potassium feldspar (<5%), dolomite (<1%), and biotite (<1%). Sandstone beds and lamina also contain <30% admixed phyllosilicate minerals, mostly illite, smectite, chlorite, kaolinite, and mica in varying proportions. Sulfides are common (<2%) and most commonly occur as scattered pyrite framboids visible at petrographic scales. Carbonate content varies greatly within and between facies (2%–20% total composition), a result of both detrital grains and diagenetic alteration (discussed further in Diagenetic Features below).

Mudstone beds and lamina consist of >20% clay-sized grains including illite, smectite, chlorite, mica, and kaolinite. Silt-sized and minor larger grains compose up to 65% of mudstone lithologies and are dominated by quartz. Subordinate silt-sized and larger grains consist of plagioclase, potassium feldspar, and carbonate grains. Carbonate composes up to 15% of the composition of mudstone, and dominantly occurs as carbonate grains. Akin to sandstone lithologies, sulfide minerals make up less than 2% of mudstone lithologies, though is commonly observed scattered and clustered near organic material at petrographic and SEM scales. Organic fragments from the micron- to cm-scale are abundantly preserved in mudstone (e.g., figures 24b, 26a, and 27c). Smectite, a detrital swelling clay that can impede drilling and well completions, is present in variable amounts in each core. XRD indicates that smectite composes up to 5% of the bulk mudstone mineralogy in the northeastern Uinta Basin cores and is up to 2.5% of the bulk composition in the southeastern Uinta Basin (appendix C).

Diagenetic Features

Diagenetic alteration can greatly impact reservoir quality by decreasing porosity and permeability, as well as decrease induced fracture potential. Therefore identifying, documenting, and predicting the distribution of diagenetic features in Mancos B sandstone bodies is critical to predicting reservoir quality. This study heavily utilized the two cores from the northeastern Uinta Basin to study these features.

Diagenetic features observed in the Mancos B fit into five general categories: 1) authigenic clay, 2) quartz overgrowth, 3) calcite cement, 4) dolomite replacement, and 5) sulfide precipitation. Overall, the degree of diagenetic alteration and associated reservoir impacts varies substantially both vertically and laterally across the eastern Uinta Basin.

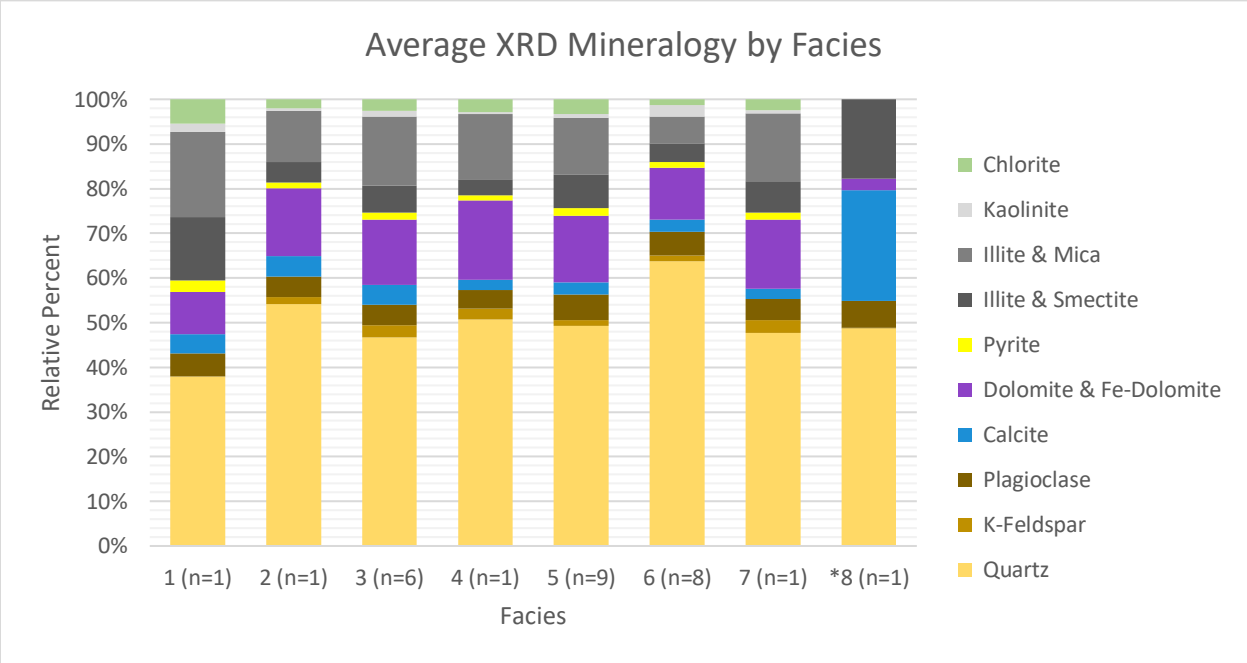

Figure 23. *Mineralogy by facies. *Facies 8 sample does not contain differentiated clay fractions (all clay fractions represented by dark gray).*

Bonanza State 20-15H: Bonanza Zone

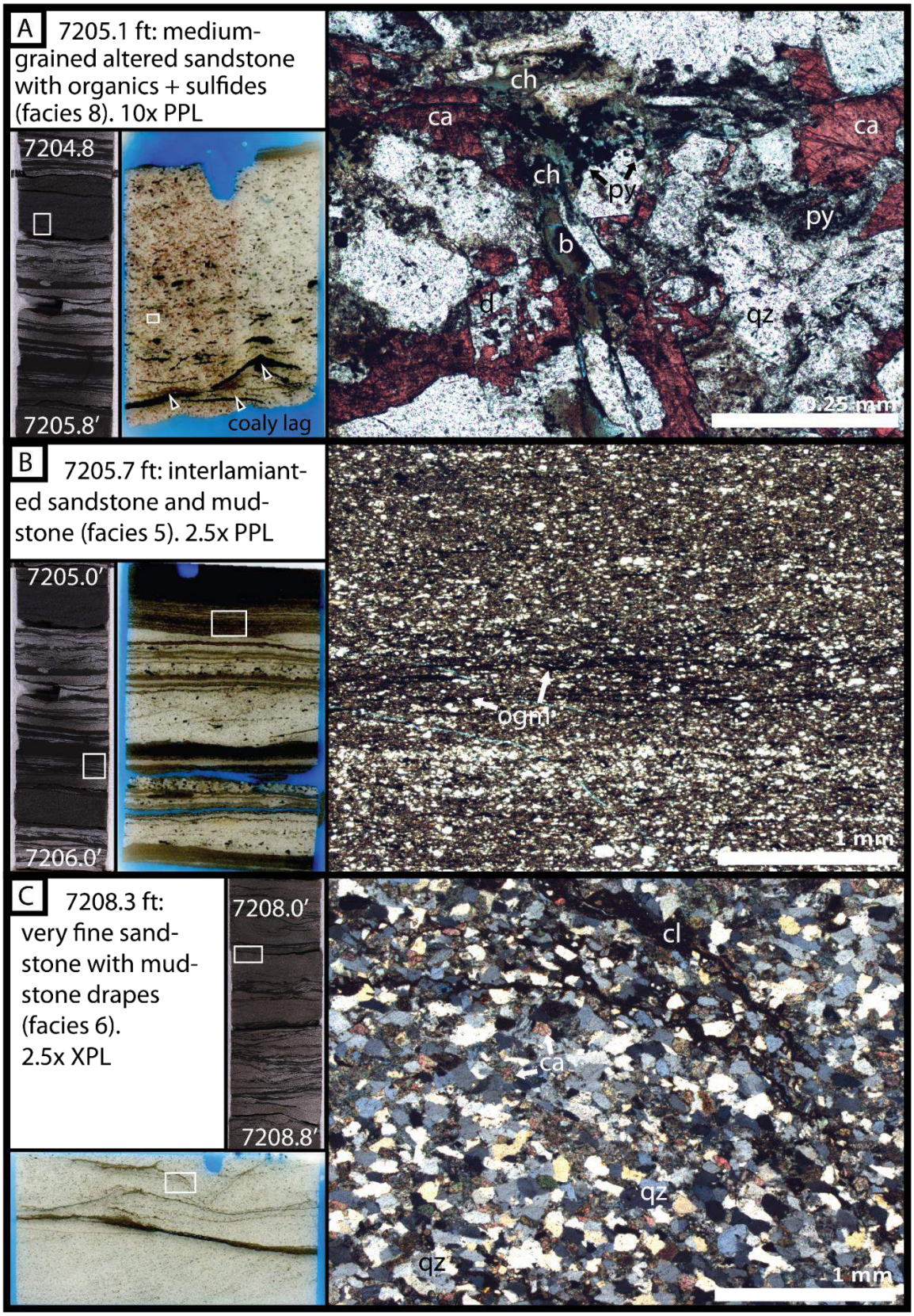

Figure 24. *Core images, thin section scans, and photomicrographs from the Bonanza zone, Bonanza State 20-15H. All core photos are of 3-inch-wide core, and thin sections are 0.75 x 1.25 inches with blue epoxy impregnation. A) Moderately well sorted medium- to coarse-grained sandstone (Facies 8). Thin section scan is ½ stained red for calcite; arrows point to pyrite- and hematite-replaced organic material at base of sandstone bed. Photomicrograph highlights red-stained calcite cement, altered quartz grains, pyrite framboids, and biotite altering to chlorite. B) Interlaminated and well-sorted very fine grained sandstone, fine-grained sandstone, medium-grained sandstone, and mudstone showing significant variation of grain size by laminae. Photomicrograph is of mudstone lamina and color-altered to clearly show organic-rich lamina (black), detrital clay (brown), and silt (gray-white). C) Fine-grained sandstone with thin mudstone drapes. Photomicrograph shows very fine-grained quartz sandstone with irregular mud-rich lamina. Note lack of visible pore space due to calcite (high birefringence, red and green) cement. PPL = plane polarized light, XPL = cross polarized light, b = biotite, ca = calcite, ch = chlorite, cl = clay, d = dolomite, fs = weathered feldspar, py = pyrite, qz = quartz, s = sulfide mineral.*

Bonanza State 20-15H: Dirty Devil and Bonanza Zones

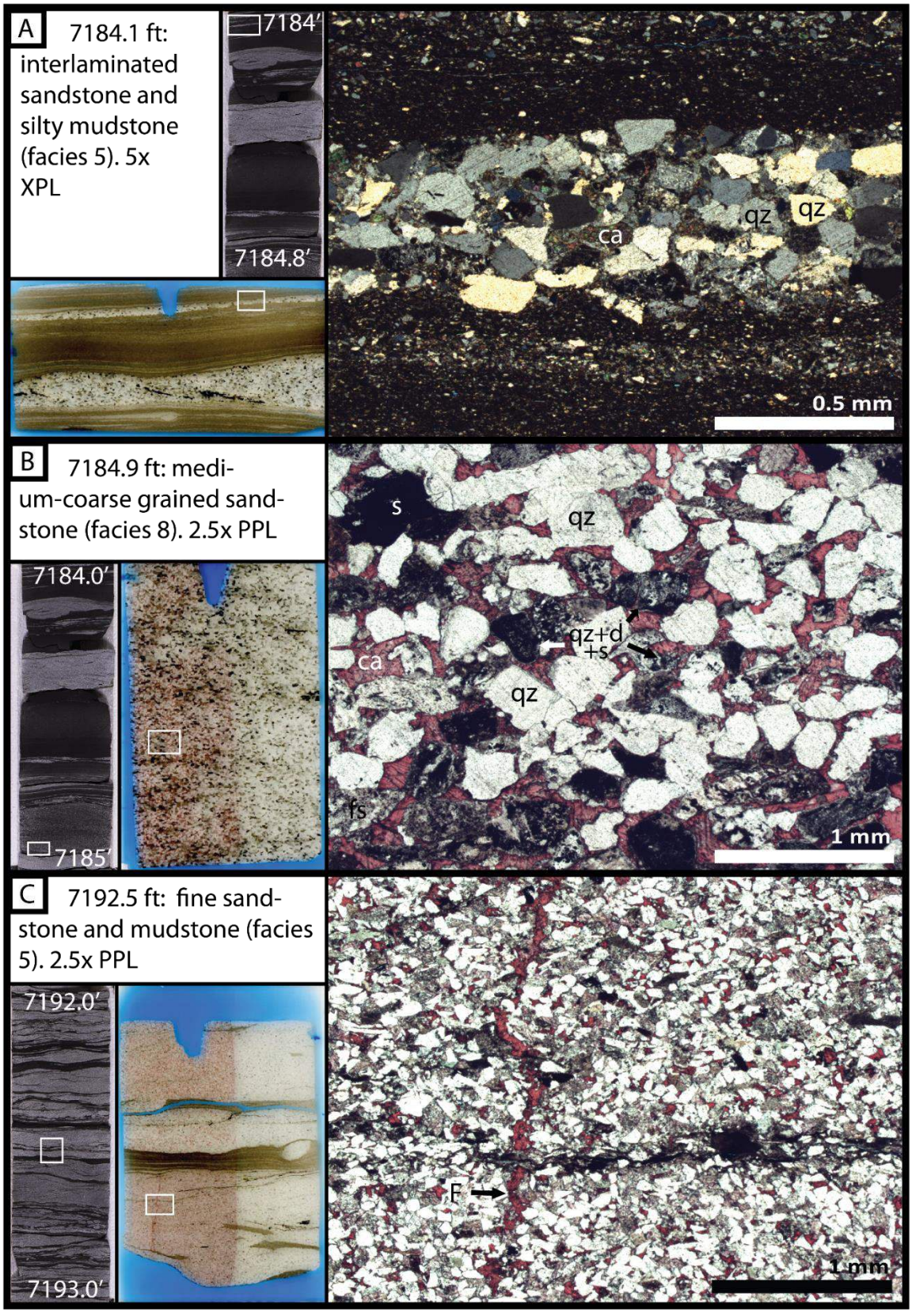

Figure 25. *Core images, thin section scans, and photomicrographs from the Dirty Devil and Bonanza zones, Bonanza State 20-15H. All core photos are of 3-inch-wide core, and thin sections are 0.75 x 1.25 inches with blue epoxy impregnation. A) Interlaminated silty mudstone and very fine to fine-grained sandstone with no visible pore space in the lower Dirty Devil zone. Laminae are moderately to well-sorted with sharp contacts. B) Moderately well sorted medium-grained sandstone which marks the upper boundary of the Bonanza zone. Thin section is ½ stained red for calcite. Photomicrograph highlights abundant red-stained calcite cement and highly altered grains. Grains include feldspar weathering to clay and altered quartz with prominent dolomitization and sulfide (opaque) mineral development. C) Interlaminated and very fine to fine-grained sandstone and mudstone in the Bonanza zone. Thin section is ½ stained red for calcite. Photomicrograph highlights calcite-filled vertical fracture in well-sorted angular to subangular quartz sandstone. PPL = plane polarized light, XPL = cross polarized light, ca = calcite, cl = clay, d = dolomite, F = fracture, fs = weathered feldspar, py = pyrite, qz = quartz, s = sulfide mineral.*

Bonanza State 20-15H: Dirty Devil Zone

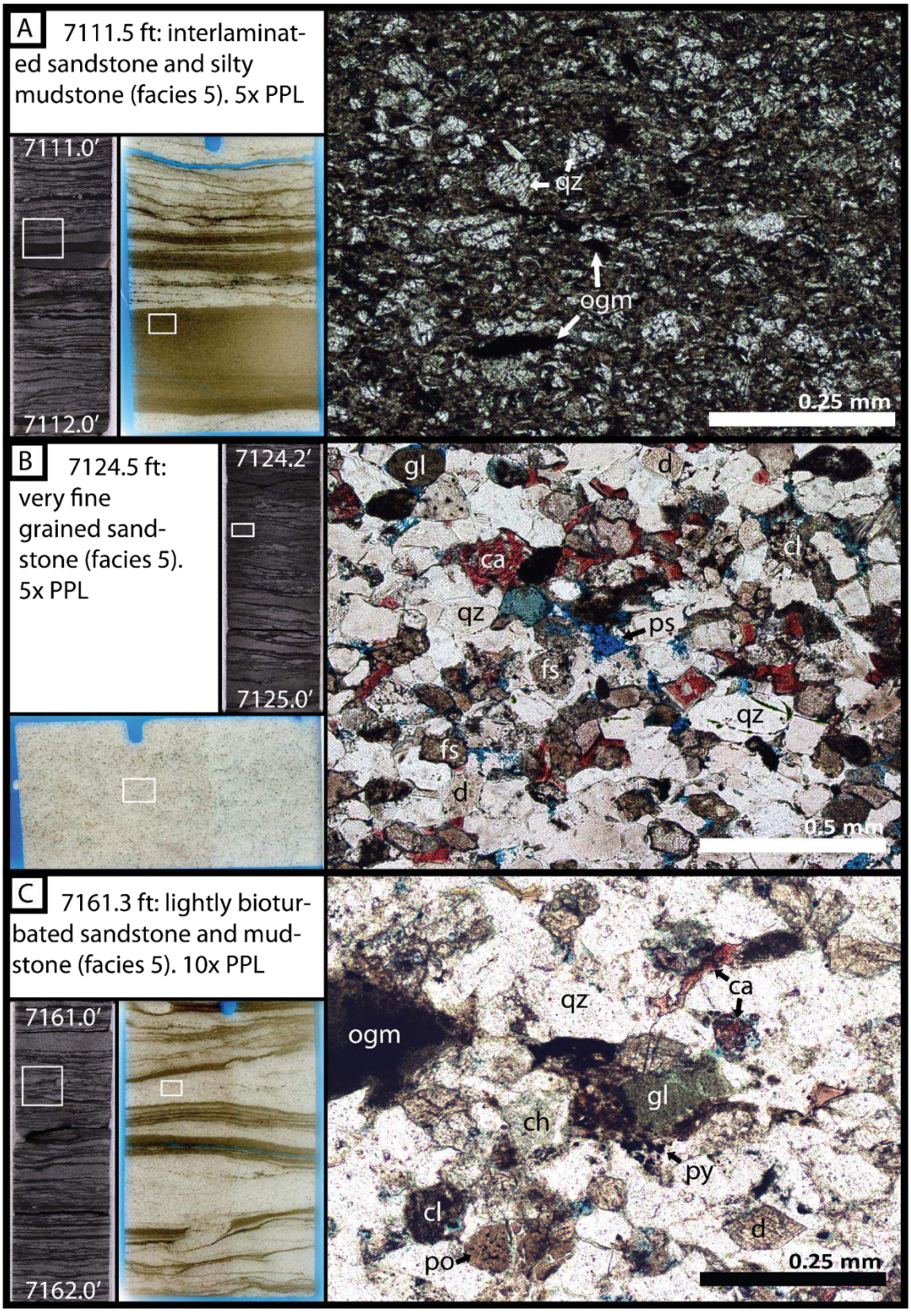

Figure 26. *Core images, thin section scans, and photomicrographs from the Dirty Devil zone, Bonanza State 20-15H. All core photos are of 3-inch-wide core, and thin sections are 0.75 x 1.25 inches with blue epoxy impregnation. A) Interlaminated very fine and fine-grained sandstone and mudstone. Photomicrograph shows poorly sorted mudstone with significant quartz silt and organic matter (black) in clay matrix. B) Very fine grained sandstone. Photomicrograph shows significant interconnected pore space, red-stained calcite cement, abundant altered feldspar grains weathering to clay, and dolomite grains. C) Interlaminated and lightly bioturbated very fine grained sandstone and mudstone. Photomicrograph shows abundant chlorite, glauconite, organic matter, and phosphate-rich organic matter. Authigenic dolomite, quartz overgrowth, and calcite cement all reduce porosity (blue). PPL = plane polarized light, ca = calcite, cl = clay, d = dolomite, fs = weathered feldspar, gl – glauconite, ogm = organic matter, po = phosphate-rich organic matter, ps = pore space, py = pyrite, qz = quartz, s = sulfide mineral.*

Bonanza State 20-15H: Boomer Zone

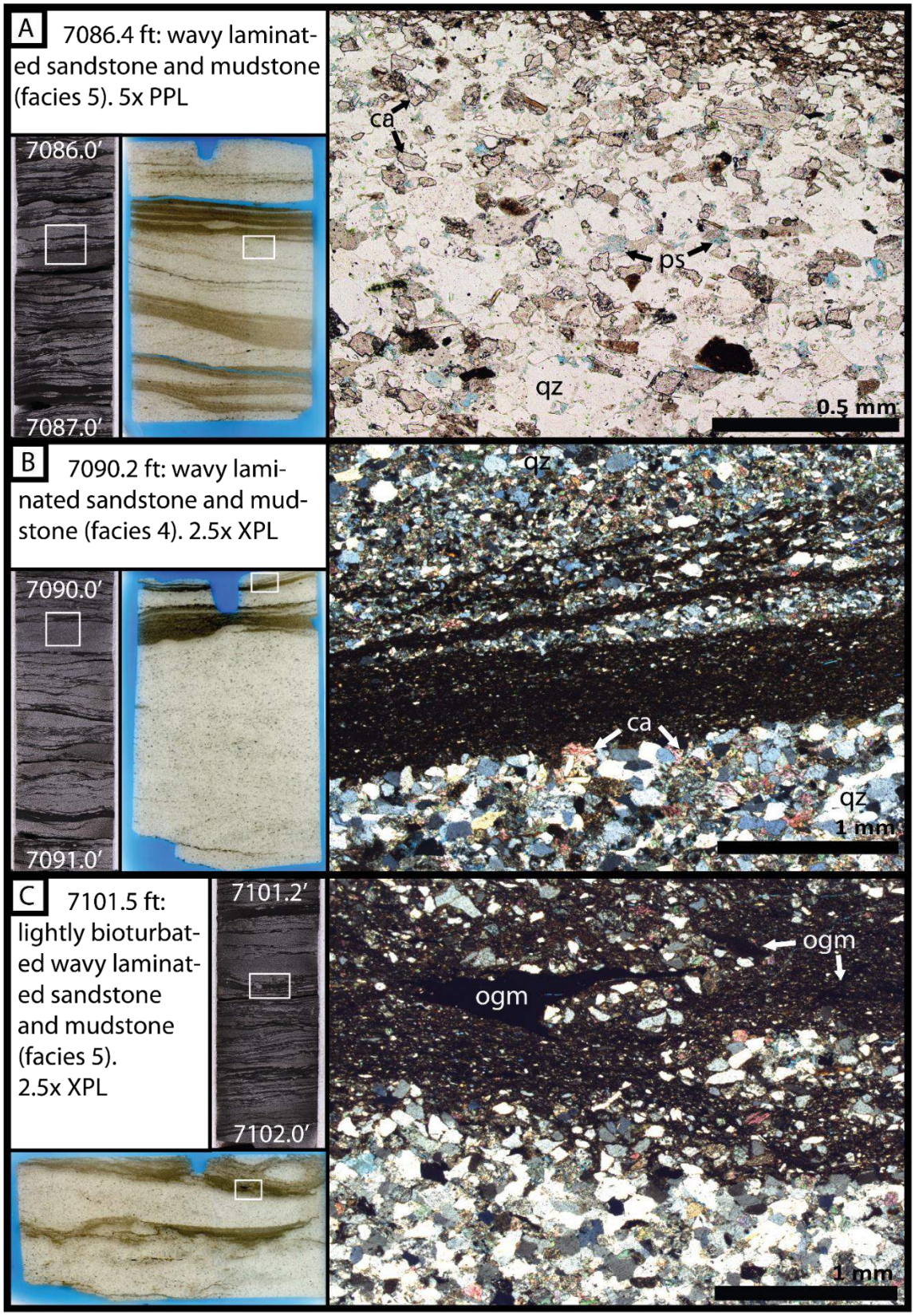

Figure 27. *Core images, thin section scans, and photomicrographs from the Boomer zone, Bonanza State 20-15H. All core photos are of 3-inch-wide core, and thin sections are 0.75 x 1.25 inches with blue epoxy impregnation. A) Very fine to fine-grained sandstone interlaminated with mudstone. Photomicrograph highlights interconnected pore space (blue) in fine sandstone. B) Interlaminated mudstone and ripple-laminated fine-grained sandstone. Photomicrograph shows sharp contacts between mudstone and sandstone and abundant calcite (high birefringence, red-green). Cross polarized light highlights angularity of quartz grains (white to dark gray). C) Lightly bioturbated sandstone and mudstone with mottled contacts. Note abundant dark brown-black organic matter captured within mudstone. PPL = plane polarized light, XPL = cross polarized light, ca = calcite, cl = clay, ogm = organic matter, ps = pore space, py = pyrite, qz = quartz.*

Authigenic Clay

The Mancos B contains abundant authigenic clays that result from the weathering and alteration of clastic minerals (figures 28, 29, 30e–f). Some authigenic clays, such as pore-filling illite and kaolinite are common in Mancos B sandstone, and can adversely impact reservoir quality by reducing porosity and permeability. As a general trend, there is more pore-filling illite and kaolinite in porous sandstone facies (facies 4–7) that contain ample pore space for clay minerals to precipitate.

Illite is the dominant clay mineral in all Mancos B lithofacies, making up to 11.5% of the bulk mudstone composition (figure 23). The majority of the illite is a result of in-situ transformation of detrital smectite to illite during burial diagenesis (Pollastro, 1990). This form of illite is preserved in the original depositional location and does not greatly impact the original reservoir quality. A relatively small illite fraction occurs as pore-filling authigenic illite (visually estimated <5% total illite) that reduces reservoir quality. Pore-filling illite was only observed in porous Mancos B sandstone lamina and beds (facies 4–7) and was not observed in mudstone-bound porosity.

Pore-filling illite occurs mainly as fibrous or "hairy" illite (figures 28f, 30d–f). This form of illite can be particularly problematic, as it is fragile and easily broken upon disturbance. Broken illite "hairs" are susceptible to migrating and potentially clogging small pore throats and thereby reduce reservoir permeability. Blocky and pore-bridging illite are less harmful to reservoir quality and are also observed (generally in lesser quantities than hairy illite) in the northeastern Uinta Basin (figures 28e, 29d, 30d).

SEM and EDS imaging from Bonanza State 20-15H illustrates that illite concentrations and morphology vary by stratigraphic zone: 1) the Bonanza zone contains minimal pore-filling illite (estimated <5% total sandstone pore space) in near equal proportions of hairy and blocky morphologies; 2) the Dirty Devil zone exhibits minimal illite development, related to an overall muddier zone; 3) the Boomer zone contains abundant pore-filling hairy illite (up to 10%–15% of total pore space, visual estimate). Weaver Ridge 13-16 exhibits slightly higher quantities of illite than Bonanza State 20-15H. These observations indicate that pore-filling illite varies not only within core stratigraphy, but also laterally over relatively short distances

Kaolinite is another common pore-filling authigenic clay that is a weathering product of feldspar minerals. It also occurs as pore-filling "booklets" that are loosely attached to detrital grains. Booklets of kaolinite are easily mobilized in a stimulated well and can block pore throats and reduce permeability. XRD data indicate that kaolinite is common at all core locations and stratigraphic intervals (figures 17–21, 23; appendix C). It is most abundant in the Weaver Ridge 13-16 core (~2.5%–4% total composition) and secondly in Bonanza State 20-15H (~0.5%–2%). The southeastern Uinta Basin core have relatively small fractions of kaolinite (0.5%–1%). Kaolinite most commonly occurs in sandstone and only rarely is observed filling pores in silty mudstone lamina.

Like illite, kaolinite also varies by stratigraphic location. In Bonanza State 20-15H, the highest concentration occurs in the Bonanza zone (1%–2%; figure 28b–d) and the lowest concentration in the Boomer zone (<1%). The Dirty Devil zone also exhibits a moderate amount of pore-filling kaolinite (1%–1.5%; figure 28a). SEM imaging in Weaver Ridge 13-16 and

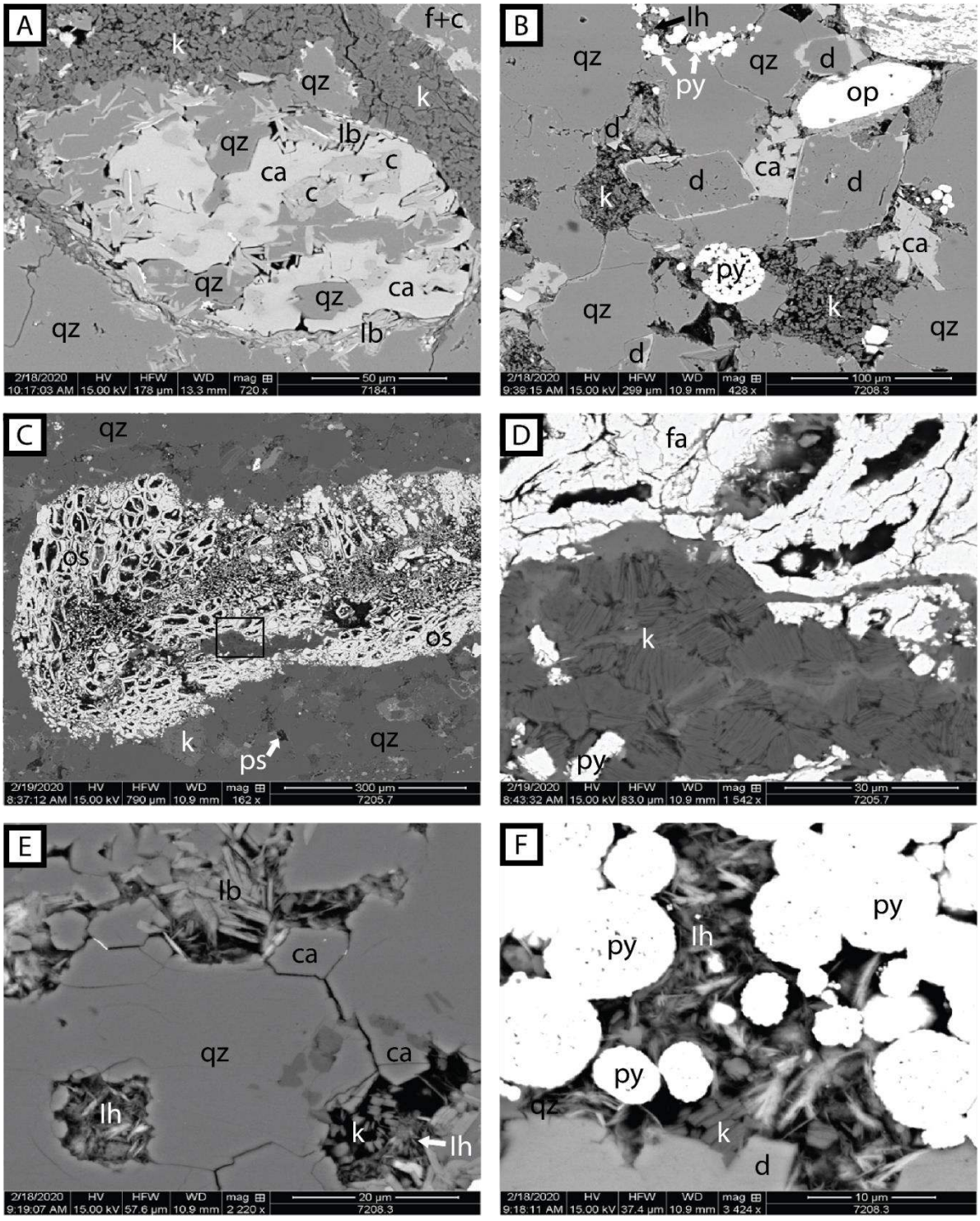
A
f+c
k
qz
k
qz
lb
c
ca
c
qz
qz
ca
qz
lb
2/18/2020 10:17:03 AM | HV 15.00 kV | HFW 178 µm | WD 13.3 mm | mag 720 x | 50 µm | 7184.1
B
lh
qz
py
qz
d
op
d
d
ca
d
k
ca
py
qz
k
qz
d
2/18/2020 9:39:15 AM | HV 15.00 kV | HFW 299 µm | WD 10.9 mm | mag 428 x | 100 µm | 7208.3
C
qz
os
os
k
ps
qz
2/19/2020 8:37:12 AM | HV 15.00 kV | HFW 790 µm | WD 10.9 mm | mag 162 x | 300 µm | 7205.7
D
fa
k
py
2/19/2020 8:43:32 AM | HV 15.00 kV | HFW 83.0 µm | WD 10.9 mm | mag 1 542 x | 30 µm | 7205.7
E
lb
ca
qz
ca
lh
k
lh
2/18/2020 9:19:07 AM | HV 15.00 kV | HFW 57.6 µm | WD 10.9 mm | mag 2 220 x | 20 µm | 7208.3
F
py
py
lh
py
qz
k
d
2/18/2020 9:18:11 AM | HV 15.00 kV | HFW 37.4 µm | WD 10.9 mm | mag 3 424 x | 10 µm | 7208.3

Figure 28. SEM images from the Dirty Devil and Bonanza zones. A) Heavily altered quartz grain surrounded by authigenic pore-filling kaolinite. B) Altered sandstone; note interlocking quartz grains (quartz overgrowth), diagenetic dolomite grains, calcite cement, feldspar-weathering-to-clay (upper right), and pore space containing authigenic kaolinite. C) Organic material composed of fluorapatite. D) Close up from C inset. E) Pore space with variable accumulation of authigenic hairy and block illite between altered quartz grains. F) Hairy illite and kaolinite near abundant pyrite framboids. ca = calcite, cl = detrital clay, c = clay (unidentified authigenic), d = dolomite, f = feldspar, fa = fluorapatite, Ib,= blocky illite, Ih = hairy illite, k = kaolinite, op = phosphorus-rich organic matter, os = sulphur-rich organic matter, ps = pore space, py = pyrite, qz = quartz.

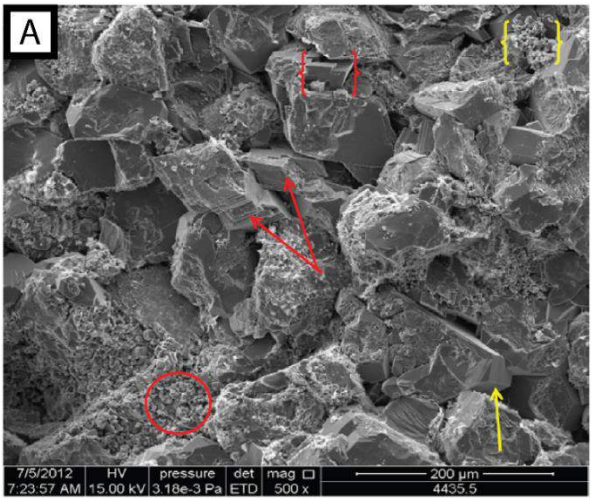
A
7/5/2012 7:23:57 AM
HV 15.00 kV
pressure 3.18e-3 Pa
det ETD
mag 500 x
200 µm
4435.5

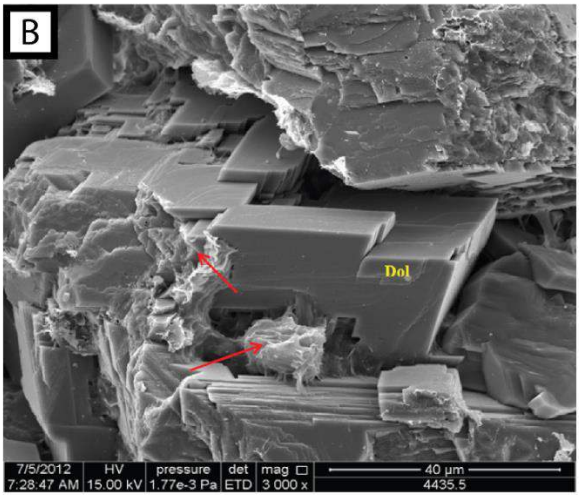
B
Dol
7/5/2012 7:28:47 AM
HV 15.00 kV
pressure 1.77e-3 Pa
det ETD
mag 3 000 x
40 µm
4435.5

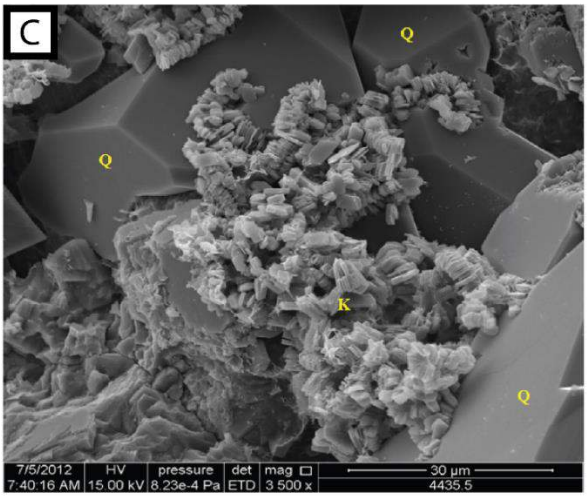
C
Q
Q
K
Q
7/5/2012 7:40:16 AM
HV 15.00 kV
pressure 8.23e-4 Pa
det ETD
mag 3 500 x
30 µm
4435.5

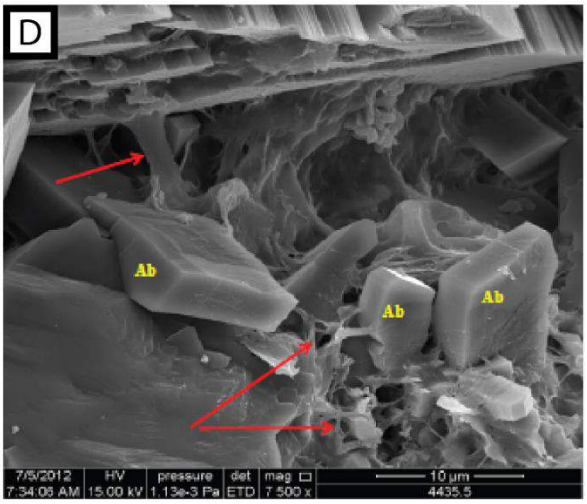
D
Ab
Ab
Ab
7/5/2012 7:34:06 AM
HV 15.00 kV
pressure 1.13e-3 Pa
det ETD
mag 7 500 x
10 µm
4435.5

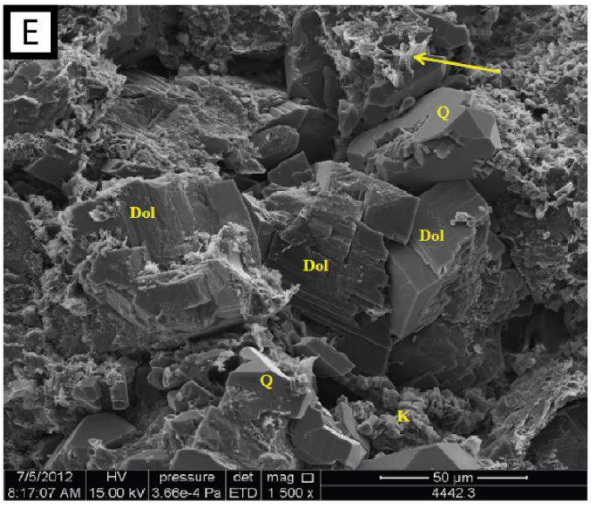
E
Q
Dol
Dol
Dol
Q
K
7/5/2012 8:17:07 AM
HV 15.00 kV
pressure 3.66e-4 Pa
det ETD
mag 1 500 x
50 µm
4442.3

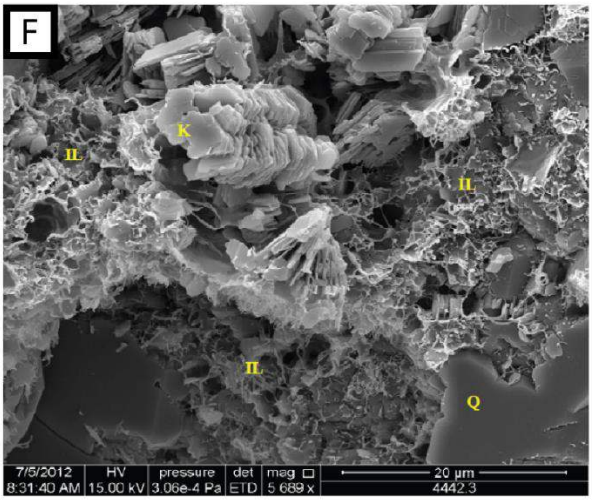
F
K
IL
IL
IL
Q
7/5/2012 8:31:40 AM
HV 15.00 kV
pressure 3.06e-4 Pa
det ETD
mag 5 689 x
20 µm
4442.3

Figure 29. *SEM images from Weaver Ridge 13-16 (Bonanza zone) and analyzed by CoreLabs. A) Quartz sandstone and authigenic dolomite (red arrows). Red brackets indicate area of (B) and yellow brackets indicate area of (C). B) Illite-smectite mixed layers (red arrows) around dolomite. Pore space is dominantly intergranular pores. C) Very fine to fine-grained sandstone exhibiting quartz overgrowth and pore-filling kaolinite. D) Authigenic albite and pore-bridging illite (red arrows). E) Very fine to fine-grained quartz sandstone with authigenic clay coating. F) Authigenic kaolinite, illite, and quartz overgrowth. Ab = albite, Dol – dolomite, K = kaolinite, Q = quartz overgrowth.*

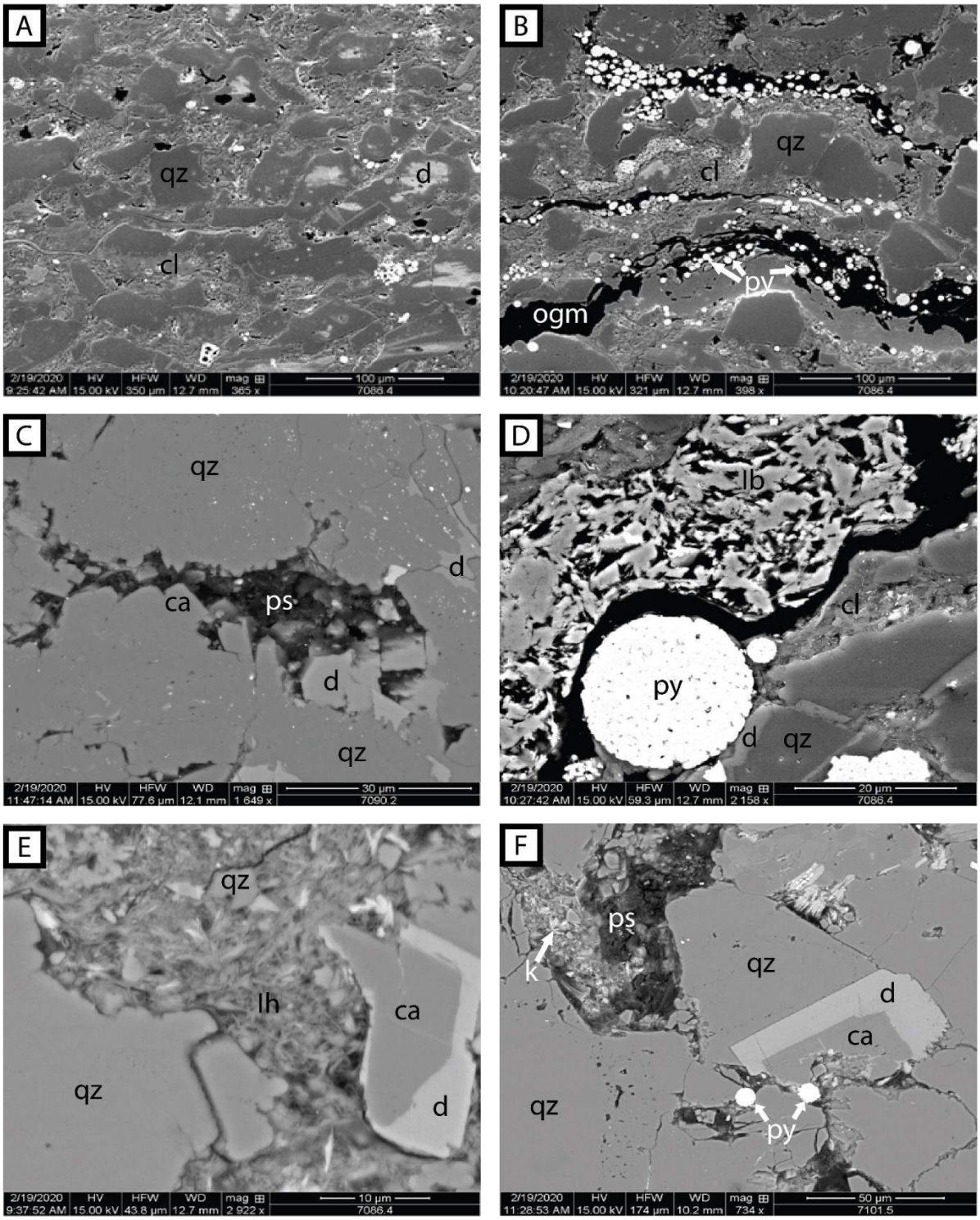
A
qz
d
cl
2/19/2020 9:25:42 AM HV 15.00 kV HFW 350 µm WD 12.7 mm mag 365 x 100 µm 7086.4
B
qz
cl
py
ogm
2/19/2020 10:20:47 AM HV 15.00 kV HFW 321 µm WD 12.7 mm mag 398 x 100 µm 7086.4
C
qz
d
ca
ps
d
qz
2/19/2020 11:47:14 AM HV 15.00 kV HFW 77.6 µm WD 12.1 mm mag 1 649 x 30 µm 7090.2
D
lb
cl
py
d
qz
2/19/2020 10:27:42 AM HV 15.00 kV HFW 59.3 µm WD 12.7 mm mag 2 158 x 20 µm 7086.4
E
qz
lh
ca
qz
d
2/19/2020 9:37:52 AM HV 15.00 kV HFW 43.8 µm WD 12.7 mm mag 2 922 x 10 µm 7086.4
F
ps
k
qz
d
ca
qz
py
2/19/2020 11:28:53 AM HV 15.00 kV HFW 174 µm WD 10.2 mm mag 734 x 50 µm 7101.5

Figure 30. *SEM images from the Boomer zone, Bonanza State 20-15H. A) Detrital clay with quartz silt grains and micro-porespace. B) Organic-rich lamina (black) with abundant pyrite framboids in silt and clay matrix. C) Open pore space amongst altered quartz grains. D) Blocky authigenic illite and pyrite framboids. Sinuous black line is presumed an induced fracture formed during sample preparation. E) Abundant authigenic hairy illite filling pore space. F) Pore space with kaolinite between heavily altered grains. ca = calcite, cl = detrital clay, c = clay (unidentified authigenic), d = dolomite, f = feldspar, fa = fluorapatite, Ib,= blocky illite, Ih = hairy illite, k = kaolinite, ogm = organic matter, ps = pore space, py = pyrite, qz = quartz.*

Bonanza State 20-15H confirm that kaolinite occurs primarily as pore-filling booklet morphologies and fills much of the available pore space (>40%) when present (figures 27 and 28).

Additional non-swelling clays are common weathering products of silt- and sand-sized clastic grains in the Mancos B (figure 28a). Chlorite is particularly common in Bonanza State 20-15H (~2.5%–5% total composition). All other cores generally contain <3% chlorite. Petrographic imaging of Bonanza State 20-15H illustrates that chlorite is largely from altered biotite (30%–90% degraded to chlorite; figure 24a) or is found amorphously filling pore space (figure 26c). Chlorite and other authigenic clays are less damaging to reservoir properties than illite and kaolinite, though still decrease available pore space.

Quartz Overgrowth and Cement

Quartz overgrowth results when quartz precipitates around a detrital grain and reduces reservoir quality by decreasing porosity. When overgrowths interlock, it acts as cement which reduces permeability and impacts hydraulic fracturing potential of a reservoir. Quartz overgrowth may explain some highly angular grains observed in thin section, and quartz cement is commonly observed in petrographic thin section and SEM by the presence of interlocking quartz grains (e.g., figures 25b, 26b, 29c). We observed that interlocking quartz is especially common in facies 5 and 6; however, we did not observe trends associated with specific locations or stratigraphic intervals and hypothesize that the impacts of quartz diagenesis are somewhat equal across the Uinta Basin.

Calcite Cement

Calcite cement reduces porosity and permeability and impacts the hydraulic fracture potential of reservoirs. Calcite cement is common in all sandstone facies, although it is highly variable in bulk abundance by lateral and stratigraphic location. At large, calcite cement correlates roughly with grain size. Coarser grained facies commonly contain abundant calcite cement and very fine grained mudstone facies tend to exhibit minimal calcite cement (figures 25 and 26). This is likely an artifact of more available pore space for calcite precipitation in sandstone facies and a higher original permeability that aided ion transport.

The northeastern Uinta Basin core locations show highly variable calcite cement development between the Bonanza Block and Banta Ridge. The Weaver Ridge 13-16 core, for example, generally has <1% total calcite concentration in the Bonanza zone, whereas the Bonanza zone in Bonanza State 20-15H has calcite concentrations ranging from 3% to over 30% in sandstone beds (appendix C). Massive medium-grained sandstone (facies 8) beds, which are found only in Bonanza State 20-15H, have lost all visible pore space to calcite cement and will likely act as local baffles to flow (figures 24a, 25b). Finer-grained sandstone facies exhibit less pervasive calcite development and preserve some visible pore space in the Bonanza State 20-15H Bonanza zone (figure 24b). The Dirty Devil and Boomer zones in Bonanza State 20-15H exhibit substantially less calcite development, visually estimated at <1% and 1–2% total sandstone composition (figures 26b, 27a).

XRD results show very low concentrations of calcite in the southeastern Uinta Basin though will require additional work to determine if the fractions are detrital or diagenetic in nature (see Future Work below). Given the large variation of calcite at local and regional scales, each prospective reservoir will benefit from a localized understanding of calcite abundance.

Dolomite Overprinting

Dolomite can reduce porosity and act as a baffle to flow, especially when it pervasively alters a laterally continuous bed or stratigraphic interval. High concentrations of dolomite (~5%–15%) and Fe-dolomite (1%–3%) are recorded by XRD analyses in all study cores and facies (figure 23). Higher dolomite concentrations (>20%) occur in thin <3-ft-thick zones at the base of some stratigraphic sequences (e.g., the contact with the Lower Blue Gate Member visible in Weaver Ridge 13-16 and Bonanza State 20-15H identified by low gamma and high resistivity on geophysical logs). Laterally continuous beds of ferroan dolomite are also observed in outcrop near Prairie Canyon, Colorado, which span distances greater than 1 kilometer before dipping into the subsurface (figure 7b). These observations indicate that dolomitization is commonly stratigraphically controlled in the Mancos B. In addition to pervasively dolomitized stratigraphic intervals, dolomite content is observed in variable proportions throughout the Mancos B.

SEM and EDS analyses of six samples from Bonanza State 20-15H suggest that much of the dolomite concentration occurs as dolomite overprinting of silt- and sand-sized grains (figures 28b, 29a–b and 30f). Additional dolomite populations consist of dolomite precipitation as cement from a quartz-hosted nucleation point (figure 30c) and dolomite overprinting calcite grains (figure 30e). It is estimated that dolomite development has a moderate impact on reservoir quality of the Mancos B where some sandstone beds in the Boomer and Bonanza zones have lost 5%–25% of their original pore space to dolomite precipitation.

Sulfide Precipitation

Sulfide precipitants can reduce pore space and decrease permeability, especially in mudstones. Sulfide precipitation is a common mineral in the Mancos B and occurs dominantly as framboidal pyrite in mudstone facies (figures 28f, 30b, 30d). Some quartz grains and plant fragments are also observed to be almost entirely replaced by pyrite, and pyrite-to-hematite pseudomorphs were observed in Bonanza State 20-15H (figures 24a, 25b).

Sulfide development does not vary significantly with stratigraphic interval but does vary greatly by facies and secondarily by region. Reservoir facies 5 and 6 in Weaver Ridge 13-16 and Bonanza State 20-15H generally contain <1.5% pyrite, whereas mudstone facies contain 2%–4% pyrite (appendix C). The southeastern Uinta Basin exhibits similar trends with <1.0% pyrite in sandstone-dominated facies and >1.0% in mudstone facies. From petrographic and SEM observations, we estimate that >95% of the sulfide minerals recorded by XRD occur as framboidal pyrite across the study region.

Reservoir Properties

Conventional core analyses from 187 core plugs show a wide range of porosity and permeability values, a result of the variable lithology and degree of diagenetic alteration (appendix D). Only samples from facies 1–6 were available for study, and the results highlight distinct variation by facies (figure 31). As expected, sandstone facies (in particular facies 5 and 6) exhibit the best reservoir potential with higher porosity and permeability values. Facies 1, 2, and 3 have very low porosity and permeability attributable to higher clay content. No data were available for sandstone facies 7 and only three samples were analyzed from sandstone facies 4. Based on grain-size similarities with facies 5 and 6, we speculate that facies 4 and 7 each have promising reservoir potential that would be shown with more data. Facies 8 also was not sampled; however, the abundant calcite cement in this facies greatly reduces its reservoir potential.

Porosity and permeability also vary by stratigraphic zone (figure 32). For example, samples from Bonanza State 20-15H (all facies 5 and 6) show distinct differences between Bonanza, Dirty Devil, and Boomer zones. The Bonanza zone has the highest permeability values, although Boomer has the highest porosity. The Bonanza zone also shows substantial variation between the northeastern Uinta Basin cores, where Weaver Ridge 13-16 facies 5 and 6 exhibit higher porosity and permeability averages than Bonanza State 20-15H facies 5 and 6. These stratigraphic and lateral variations reflect variable detrital clay content and the highly variable degree of diagenetic alteration observed in sandstone facies, specifically carbonate and authigenic clay content (see Diagenetic Features above). Even samples that appear the same at hand sample scale can exhibit highly different results at the micro- and nano-scale, which highlights the need for thin section analyses, detailed study of geophysical logs, and acquisition of quantitative data (e.g., porosity and permeability measurements) for prospective reservoirs.

CORE FACIES AND LOG TRENDS

The following section compares geophysical log observations with core-based facies interpretations in the northeastern and southeastern Uinta Basin. In general, higher gamma corresponds with a higher clay content (facies 1–3), whereas lower gamma corresponds with increased sandstone content (facies 4–8) as observed in core and log correlations (figure 33). Stratigraphic correlations were performed using the base of the Mancos B, identified by abrupt gamma and porosity kicks, because it is interpreted as a reliable chronostratigraphic marker (figures 16, 34–36). In contrast, log character of the top of the Mancos B (i.e., top reservoir) varies greatly across the eastern Uinta Basin, especially from the northeast to the southeast and is not interpreted as a chronostratigraphic marker.

Northeastern Uinta Basin

The Mancos B in the northeastern Uinta Basin exhibits architectural variation between the lower and upper Mancos B. The lower Mancos B contains thick stacked reservoir packages in the Bonanza, Dirty Devil, and Boomer zones, whereas the upper Mancos B is defined by high

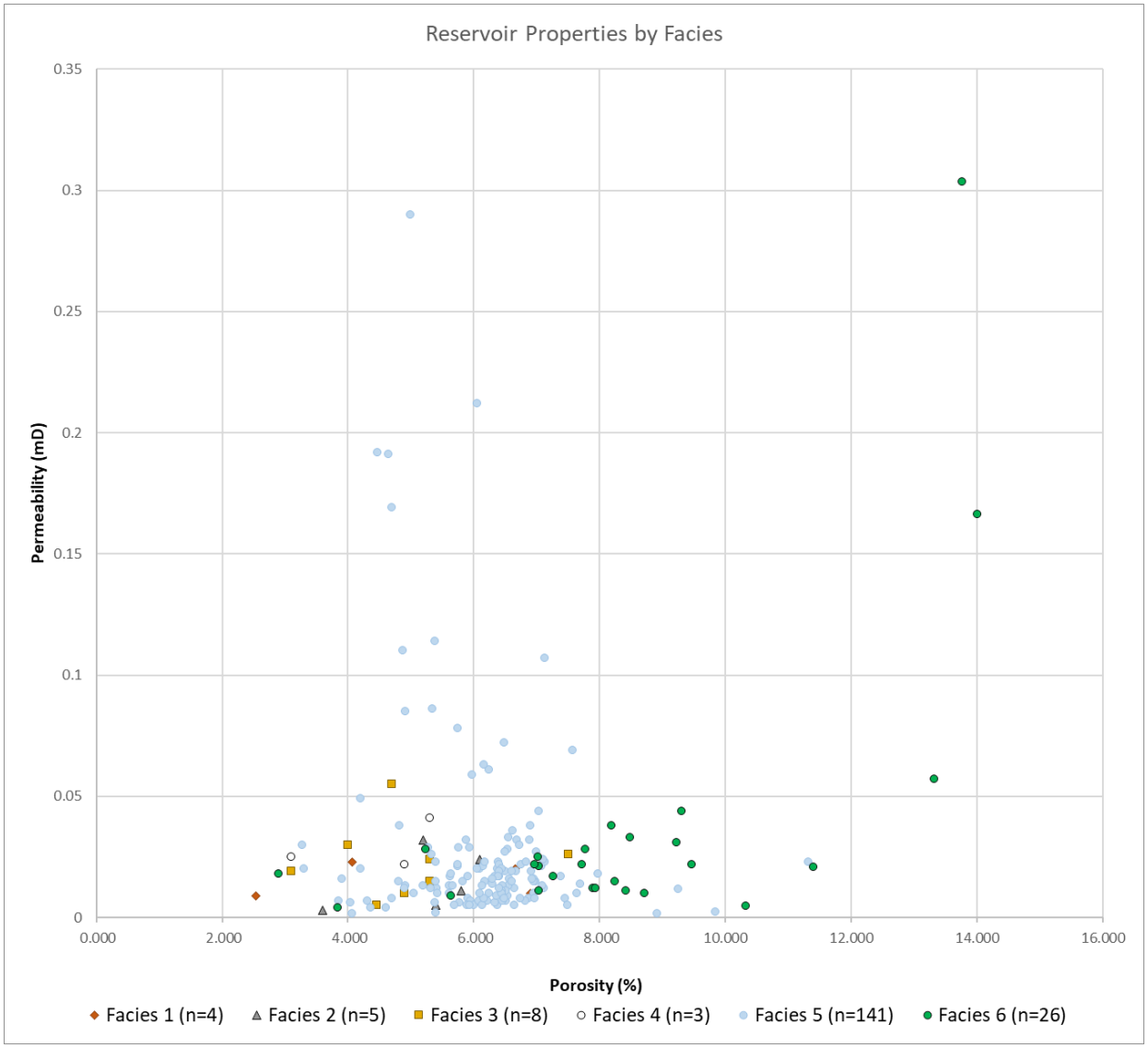

Figure 31. *Porosity and permeability from all cores, separated by facies.*

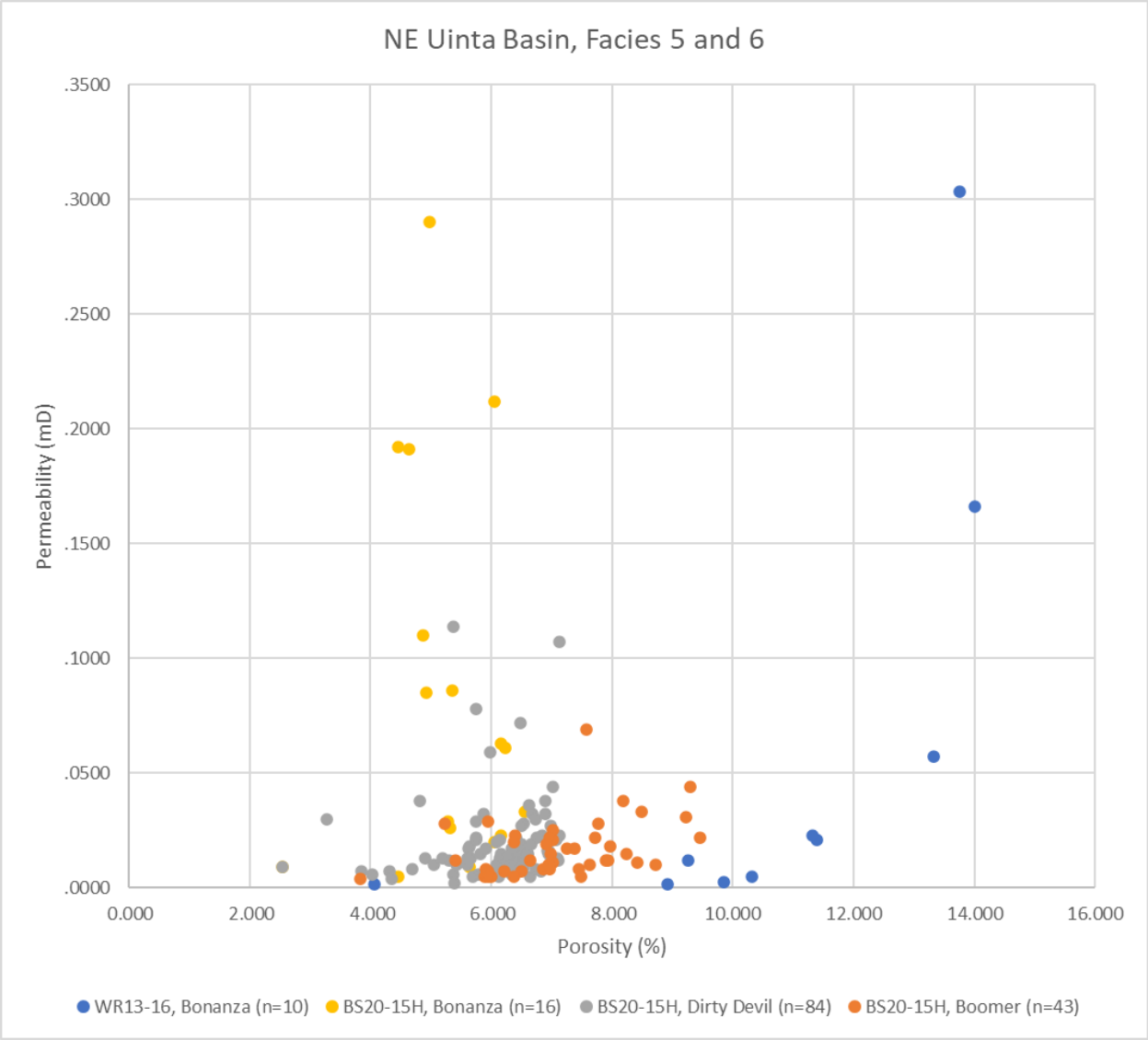

Figure 32. *Porosity and permeability from the NE Uinta Basin cores (Weaver Ridge 13-16 and Bonanza State 20-15H), separated by stratigraphic interval.*

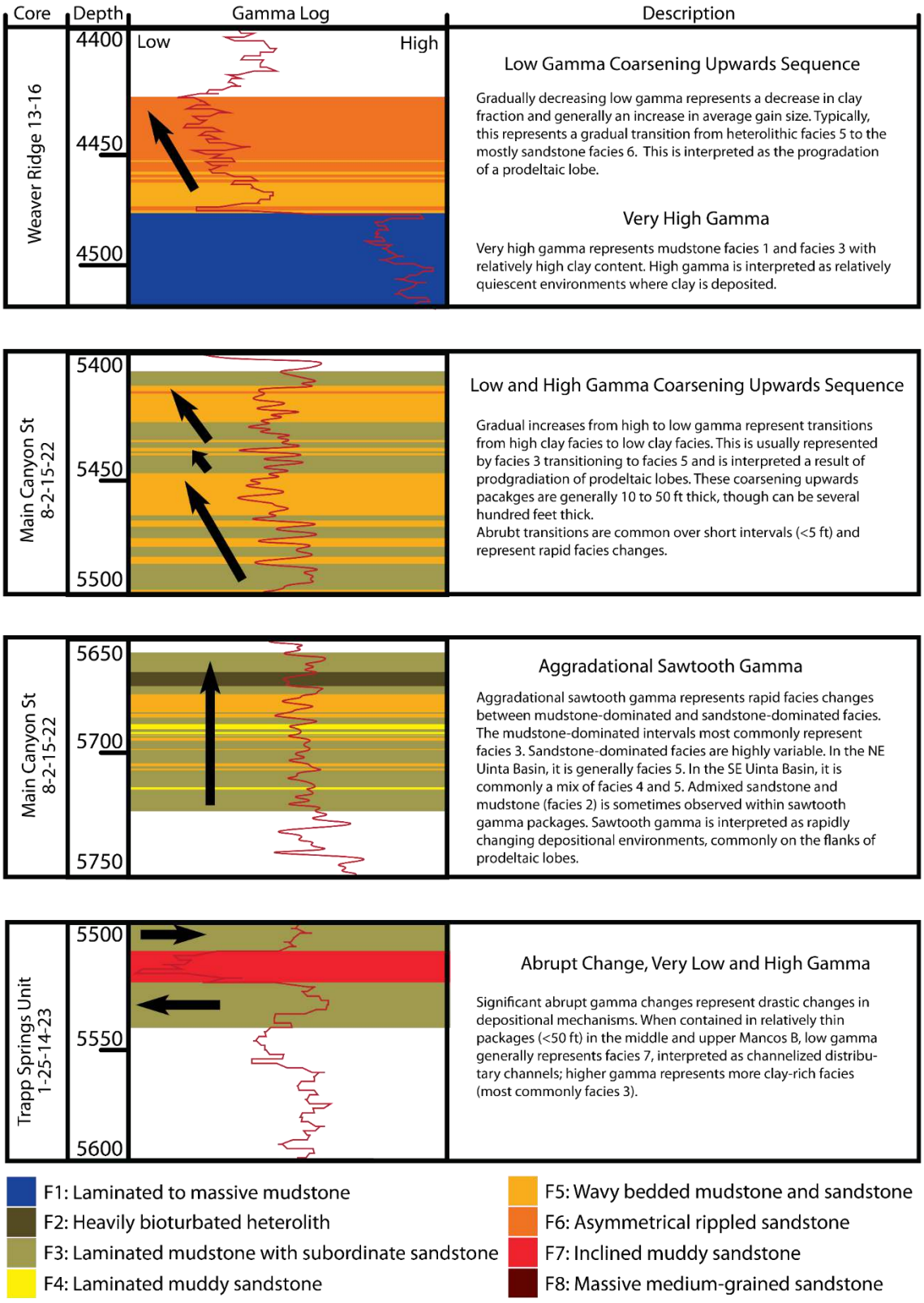

Figure 33. *Correlation between common gamma trends and core facies in the Mancos B in the eastern Uinta Basin.*

B - B′

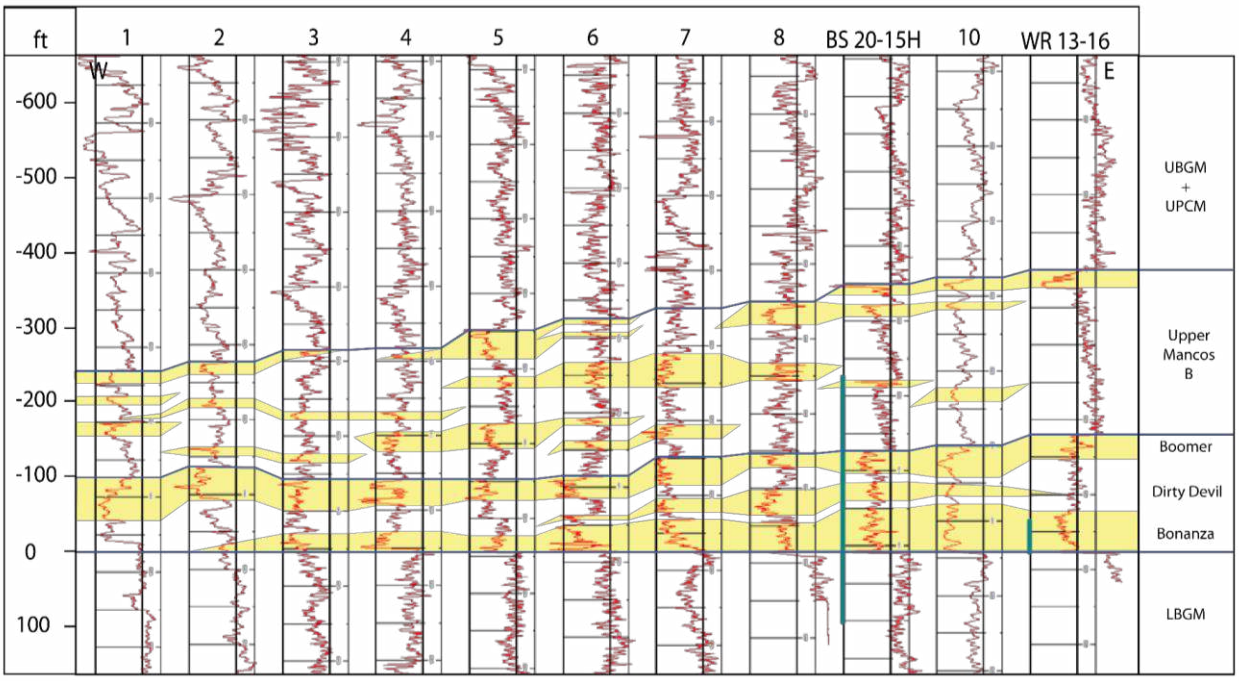

Figure 34. *Northwest-southeast cross section of the Mancos B. Datum is base of Mancos B. Vertical scale, depth in ft, is relative to datum. See figure 3 for location of B-B'. Interpreted bodies of genetically related, sandstone-rich facies highlighted with yellow. Green bars indicate cored intervals. UGBM=Upper Blue Gate Member; UPCM=Upper Prairie Canyon Member; LGBM: Lower Blue Gate Member. Wells: 1) Federal 21-19-9-19 (4304737621), 2) Bayless State 2-1 (4304734540), 3) Ouray 34-79 (4304733291), 4) Tribal 36-148 (4304734507), 5) White River Unit EIH 6DD-35-8-22, 7) NBE 5DD-10-9-23 (4304739346), 8) Dirty Devil 22x-27 (4304734825), 9) Bonanza State 20-15H (4304755745), 10) Watson 2 (4304710916), 11) Weaver Ridge 13-16 (0510311782).*

C - C′

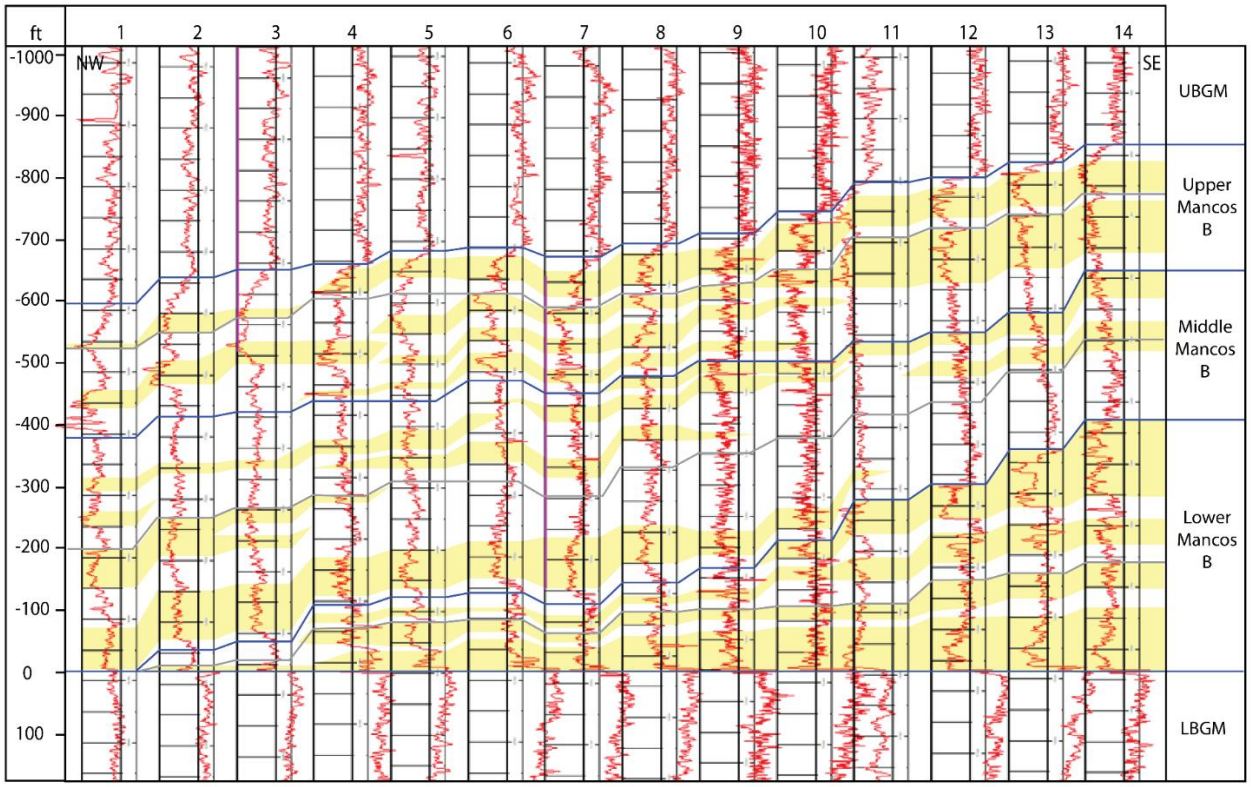

Figure 35. *Northwest-southeast cross section of the Mancos B. Datum is base of Mancos B. Vertical scale, depth in ft, is relative to datum. See figure 3 for location of C-C'. Interpreted bodies of genetically related, sandstone-rich facies highlighted with yellow. UGBM=Upper Blue Gate Member; LGBM: Lower Blue Gate Member. Wells: 1) Buck Camp 1 (4304730357); 2) Skyline Govt 1 (4304730165); 3) Seep Ridge 8 (4304730323); 4) 23 Crooked Canyon 13-17-14 (4304730619); 5) Crooked Canyon Unit 1 (4304730271); 6) Main Canyon 16-4-15-23 (4304731111); 7) Main Canyon 6-3-15-23 (4304731072); 8) Main Canyon Fed 11-10-15-23 (4304730639); 9) Lindisfarne 1-26 (4304735567); 10) Divide 1 (4301931413); 11) East Canyon Fed 2 (4301911011); 12) Lauck Federal 2 (4301931109); 13) Nicor Federal 2 (4301931020); 14) Valentine Fed 3 (4301931009).*

D - D′

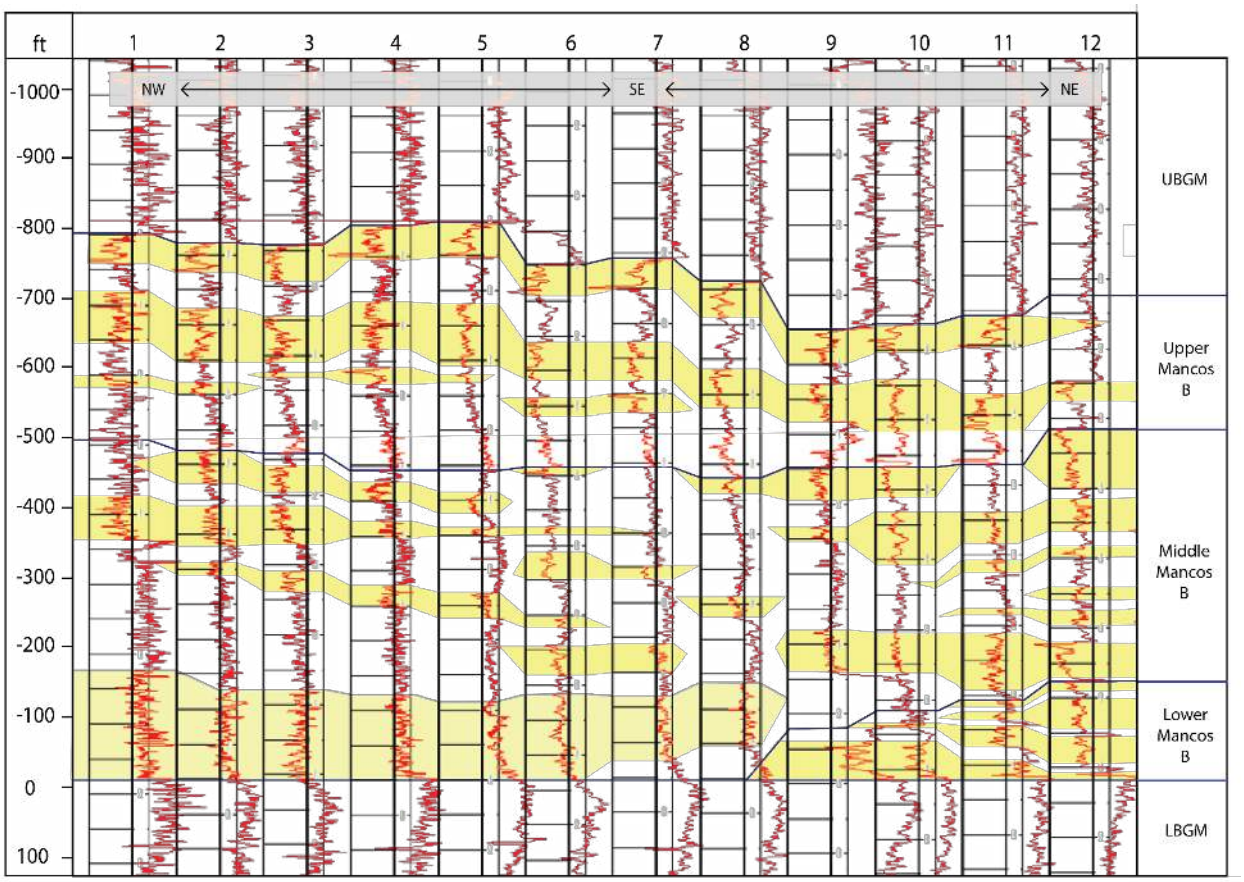

Figure 36. *Northwest-southeast-northeast cross section of the Mancos B. Datum is base of Mancos B. Vertical scale, depth in ft, is relative to datum. See figure 3 for location of D-D' and note directional shifts from NW-SE to -NE. Interpreted bodies of genetically related, sandstone-rich facies highlighted with yellow. UGBM=Upper Blue Gate Member; LGBM: Lower Blue Gate Member. Wells: 1) Hill Creek North 1-6-15-20 (4304735140); 2) Hill Creek North 10-10-15-20 (4304734830); 3) Hill Creek North 14-11-15-20 (4304734953); 4) Tumbleweed 18-9 (4304739299); 5) V Canyon 20-1 (4304738968); 6) Winter Ridge 1 (4304710018); 7) Federal 7-15-15-21 (4304731071); 8) Wolf Point Unit 1 (4304730355); 9) 22 Pine Springs 2X-16-14 (4304730621); 10) Pine Springs Unit 1 (4304730284); 11) 23 Crooked Canyon 13-17-14 (4304730619); 12) Crooked Canyon Unit 2 (4304730386).*

mudstone content and thin discontinuous reservoir facies (figure 34). Bonanza State 20-15H captures and exemplifies these distinct lithological differences between the upper Mancos B and the lower Mancos B (figure 18). Comparisons of the lower Mancos B between Weaver Ridge 13-16 and Bonanza State 20-15H illustrate lateral facies changes over short distances. The following discusses observations by stratigraphic zone in detail.

Lower Mancos B

Lower Mancos B reservoirs are 20–50 ft thick aggradational and coarsening upwards packages of sandstone facies 5 and 6 and are separated by thin intervals of facies 3 (figure 33). Both Bonanza State 20-15H and Weaver Ridge 13-16 captured sandstone-rich packages of the Bonanza zone. The Bonanza zone is characterized by a dolomitic sandstone base capped by a coarsening upwards package. Weaver Ridge 13-16 contains a dominantly sandstone-rich Bonanza zone, consisting almost entirely of facies 6. Facies 5 is only present at the base of the Weaver Ridge 13-16 succession. In contrast, Bonanza State 20-15H captures a muddier Bonanza zone and is dominated by facies 5 with thin and scattered intervals of facies 6. Bonanza State 20-15H is the only cored interval to contain medium-grained massive sandstone intervals (facies 8), which occur as thin beds (<0.2 ft) scattered across the Bonanza zone. The variability between cores exemplifies lateral facies changes that occur over relatively short distances in the Mancos B. Log mapping indicates a slight thickening of the Bonanza zone from northwest to southeast, roughly in line with depositional strike. This trend is further interpreted to correspond with an increase in reservoir quality (i.e., reservoir quality increases from northwest to southeast).

The Dirty Devil zone captured by Bonanza State 20-15H consists almost entirely of facies 5 with a relatively high bioturbation index (3–5). The zone also contains considerably higher amounts of glauconite and chlorite than typical of wavy bedded sandstone and mudstone (figure 26c). The Dirty Devil zone has a similar sawtooth gamma curve across the northeastern Uinta Basin, suggesting a similar facies assemblage (figure 33). The relatively high gamma (and interpreted relationship with high clay content) in the Dirty Devil across the northeastern study area makes it a poor reservoir and potential drilling hazard.

The 33.5-ft-thick Boomer zone is the most sandstone-rich and clay-lean portion of the Bonanza State 20-15H core. The basal half consists of a coarsening upwards package composed of facies 3, 5, and 6. The upper half is an aggradational sandstone-dominated package composed of facies 5 and 6. Weaver Ridge 13-16 exhibits similar gamma log trends, though considerably higher gamma counts, indicating a higher mudstone content.

Upper Mancos B

The upper Mancos B (“Mancos A” in some Colorado oil and gas fields) contains mudstone-dominated facies with a minor sandstone component in 25- to >200-ft-thick coarsening upwards packages that are relatively laterally isolated compared to the lower Mancos B (figures 33 and 34). In Bonanza State 20-15H, the upper Mancos B consists of three 25- to100-ft-thick coarsening upwards packages, which is correlative to one 215-ft-thick coarsening upwards package in Weaver Ridge 13-16. Facies 3 is the most common in the upper Mancos B, with minor thin intervals of facies 5 associated with low gamma. Log analysis indicates the non-

cored parts of the upper Mancos B in the northeastern Uinta Basin are similarly mudstone-dominated with thin and sparsely scattered sandstone reservoir components. The isolated and thin reservoir packages of the upper Mancos B do not make it as prospective as the lower Mancos B.

Southeastern Uinta Basin Facies

Because the cores from the three Coseka wells capture only thin, non-adjacent stratigraphic intervals, the extrapolation between core facies to geophysical logs in the southeastern Uinta Basin is possible but less certain (figures 16 and 33). Using the available core and log data, the following interpretations are made: 1) the lower Mancos B is broadly the most sandstone-rich with thick packages of facies 4 and 5; 2) the middle Mancos B is dominated by mudstone facies 3, although it contains several thick and laterally extensive reservoir packages interpreted as facies 4 and 5; and 3) the upper Mancos B contains mixed mudstone and sandstone facies and significant bioturbation that reduces reservoir quality (figures 35 and 36).

Lower Mancos B

Crooked Canyon 10-10-14-23 and Main Canyon State 2-8-15-22 contain portions of the upper part of the lower Mancos B, each with a unique facies assemblage. Crooked Canyon 10-10-1-23 exhibits facies 5 and 6, a ~35 ft coarsening upwards package, and a 25-ft-thick aggradational package of facies 4. Main Canyon 2-8-15-22 cored an approximately stratigraphically equivalent zone of the lower Mancos B as Crooked Canyon 10-10-1-23; however, it is dominated by mudstone facies 2 and 3. Main Canyon 2-8-15-22 also contains relatively thin (~0.2–6.0 ft) sections of facies 4 and 5 that correspond with gamma lows in the sawtooth gamma log (figures 16 and 21).

Akin to the core facies, geophysical logs exhibit significant vertical and lateral variation in the lower Mancos B across the southeastern Uinta Basin. Sequences present include 10- to 60-ft-thick coarsening and fining upwards packages, ~50-ft-thick aggradational low-gamma packages, and sawtooth gamma of varying gamma highs and lows are observable in any section of the lower Mancos B stratigraphy. Overall, the zone is interpreted to be a mix of sandstone and mudstone-dominated facies where the ratio of sandstone and mudstone depends on exact location. Thick coarsening upwards packages are likely dominated by facies 5 and 6, and aggradational packages interpreted as facies 3 and 4 (figure 33). Sawtooth gamma is largely interpreted to represent high-frequency interbedded sections of facies 3 and 5 in the lower Mancos B.

Middle Mancos B

The only well to core the middle Mancos B is Main Canyon State 2-8-15-22, which captured interbedded facies 3 and 5 in two ~25-ft-thick coarsening upwards packages (figures 16 and 21). Thin sections of facies 6 are also observed at the top of coarsening upwards sequences. Alteration of facies tends to occur on 1- to 9-ft-thick intervals and correspond with gamma changes.

On logs, similar 15- to 20-ft thick coarsening upwards packages and aggradation sawtooth gamma are observed in the middle Mancos B (figures 16, 35, and 36). The gamma trends are interpreted as alternating packages of facies 3 and 5 with a significant mudstone component (as observed in core). Low gamma peaks near the tops of the coarsening upwards sequences are interpreted as sandstone-rich lamina and beds of facies 5 and 6.

Reservoir packages identified on logs are 5 to 25 ft thick and can occur in any part of the >200-ft-thick middle Mancos B stratigraphy. Not all logs exhibit prospective reservoir packages. When reservoir packages are identified, they are not strongly correlatable (interpreted as lateral facies change), even at local scales. The highly variable vertical and lateral variation reservoir packages in the middle Mancos B will pose challenges for potential test wells.

Upper Mancos B

All three Coseka wells captured parts of the upper Mancos B (figure 16). All cores exhibit zones of very high bioturbation (facies 2) and thick sections of facies 3. Also, Trapp Springs 1-25-14-23 and Main Canyon State 2-8-15-22 each capture isolated 0.2- to 15-ft-thick sections of facies 5. Trapp Springs Unit 1-25-14-23 is the only core to capture facies 7 (inclined muddy sandstone), which occurs in a 12.5-ft-thick package in the middle of the upper Mancos B stratigraphy. A higher bioturbation index is present across all facies in the upper Mancos B cores relative to the middle and lower Mancos B. We interpret relatively high bioturbation indexes across the upper Mancos B facies (except facies 7) and potential reservoir impacts should be noted.

We interpret facies 7, a relatively clean sandstone facies, to be sporadically scattered across the upper Mancos B based on its unique log character defined by very low gamma with very sharp tops and bases (figure 33). Gamma logs contain numerous coarsening upward sequences on the scale of 20 to100 ft interpreted as facies 3 and 5; however, these packages are likely muddier than those that occur in the lower and middle Mancos B.

DEPOSITIONAL MODEL

A wide variety of depositional models have been proposed to describe the unique sandstone-rich Mancos B interval encased within the Mancos Shale (see Geologic Setting, Mancos B and the Prairie Canyon Member above). The outcrop, core, and log observations from this study provide additional evidence for a shallow marine, shoreline-detached prodeltaic lobe setting similar to the depositional model discussed in Buatois and others (2019). In this model, erosionally-based submarine channels delivered sediment from west to east (basinward) via turbidity and hyperpycnal flows, which ultimately was deposited in offshore prodelta lobes (table 7; figures 8 and 9). Paleocurrent data indicate delivery of sediment dominantly from the northwest-west to the southeast-east (Cole and Young, 1991; Cole and others, 1997; Hampson and others, 1999).

The recent cores from the northeastern Uinta Basin, Weaver Ridge 13-16 and Bonanza State 20-15H, provide additional insight into the depositional setting during the early Mancos B deposition. Each lower Mancos B core exhibits prominent oscillatory flow features that suggest

an environment well within fair weather wave base in a shallow marine setting. This is in stark contrast with the underlying Lower Blue Gate Member, which exhibits massive to parallel laminated mudstone depositions in more quiescent (deeper) oceanic conditions and less impacted by oscillatory currents (Birgenheier and others, 2017). This abrupt transition suggests that the onset of Mancos B deposition coincided with a prominent regression (e.g., Cole and Young, 1991; McCauley, 2013). With relative sea level fall, the combination of basinward progradation of deltas and a lower wave base likely remobilized sediment and deposited it in new locations farther from the shore (Cole and others, 1997). Similar oscillatory flow-influenced sedimentary structures are common but more interspersed in the middle Mancos B in the southeastern Uinta Basin. In the upper Mancos B, oscillatory flow structures are rarely observed. These observations suggest different depositional depths in time and space (relatively deeper in the southeastern Uinta Basin than the northeastern).

We observed a thickening of the Mancos B from northwest to southeast via subsurface mapping (figures 35 and 37). We also mapped variations in the depocenter locations of lower, middle, and upper Mancos B intervals. The lower Mancos B appears centered near the Utah-Colorado border, and pinches out northwestward and westward into the modern Uinta Basin (figure 36). The middle Mancos B has a greater depositional extent, thickens east to west and is mappable past the western extent of our study region. The upper Mancos B is observed over the same lateral extent as the middle Mancos B in the Uinta Basin, but exhibits more aggradational trends. These architectural observations are similar to those made by Kellogg (1977) and Johnson (2003), which supports an overall backstepping progradational pattern from south-southeast to north-northwest from lower to upper Mancos B. This interpretation is contrary to Cole and others (1997) and Hampson and others (1999) that interpreted an opposite southeastward-directed progradation of the Mancos B. However, those studies focused on outcrops of the middle and upper Mancos B, and did not include detailed study of the poorly exposed outcrops of the lower Mancos B integral to our north-northwest progradation interpretation.

Depositional dip directions vary within individual packages of the lower, middle, and upper Mancos B. For example, Coryell and McCarthy (2014) indicate dominantly west to east progradation of the lower Mancos B at Banta Ridge, whereas Longman and Koepsell (2005) observed a wide variety of dip directions and dominantly northwest on FMI logs from the 3-181 Pawwinnee well in the Natural Buttes field. While potentially peculiar, this variation of dip direction supports a prodeltaic lobe depositional model in which submarine flows splay semi-radially from a point source (figure 9).

The tectonic activity and role of the Douglas Creek Arch on Mancos B deposition remains controversial. Some research has suggested the Douglas Creek Arch may have been active during the time of Mancos B deposition (Cole and others, 1997; Bader and others, 2009). Cole and others (1997) further suggested this may have created an area of mud-winnowing and thereby resulted in the observed increase of sandstone content on the Douglas Creek Arch. However, Johnson (2003) and Kellogg (1977) mapped east-west thickening over the arch, which they have attributed to a potential topographic low and sediment trap that would imply the Douglas Creek Arch was not a topographic high during Mancos B deposition. While we did not observe firm evidence for Douglas Creek Arch activity in this study, it is plausible the arch was

active to some degree. In early Mancos B time, localized faulting near the arch may have created relatively minor and localized basin floor topography and adjusted localized accommodation that could explain local thickness variations in western Colorado near the axis of the Douglas Creek Arch. Given the architectural trends observed from lower to upper Mancos B in Utah, we hypothesize that uplift of the Douglas Creek Arch may have acted as a sill during middle and upper Mancos B time and aided northwest progradation of prodeltaic lobes.

Carbonate-rich beds that are mappable on local to regional scales were interpreted by Cole and others (1997) as representing periods of relative sea-level highstands in which carbonate precipitates accumulated in relatively deep locations farther from siliciclastic sediment sources. Our thin section analyses show abundant sub-millimeter-scale carbonate grains in mudstone facies (and less so in the clastic sandstone facies) supporting this hypothesis to some degree. However, petrographic and SEM images indicate that the majority of carbonate occurs as early diagenetic cement and secondary dolomite, not a result of primary deposition. Thus, we interpret major carbonate accumulation as a result of early diagenesis associated with relative lowstands that may mark flooding surfaces as observed within other strata of the Cretaceous Interior Seaway (e.g., Taylor and Gawthorpe, 2003, MacQuaker and others, 2007).

REGIONAL RESERVOIR DISTRIBUTION

The detailed stratigraphy and mapping of the Mancos B via well logs is complicated by abrupt lateral facies changes and complex vertical stacking of reservoir and non-reservoir facies observed in core and on logs (figure 16). The Mancos B commonly contains non-reservoir mudstone packages up to 100 ft thick that separate sandstone reservoir packages, thus the isopach (figure 37) herein does not reflect total reservoir body thickness but rather the total thickness of the Mancos B with potential reservoir packages.

The Mancos B ranges from 210 to 850 ft thick in the eastern Uinta Basin (figure 37). The highest sandstone-to-mudstone ratios, as observed on gamma logs correlated to core, occur within the lower Mancos B. In the lower Mancos B, Sandstone reservoir connectivity is relatively high and sandstone bodies are relatively laterally continuous. Reservoir distribution becomes increasingly complex in the middle and upper Mancos B. Sandstone reservoir bodies are less connected and more isolated. We interpret this to be a result of less coarse sediment input feeding thinner and more dispersed prodeltaic lobes, and to the presence of thin interbedded distributary turbidite channels in the middle and upper Mancos B.

The lower Mancos B exhibits the greatest variation in thickness, from ~400 ft thick in the southeast near Prairie Canyon and pinches out in the northern section of the SITLA Seep Ridge block (C-C′ in figures 3 and 36). The lower Mancos B also contains the highest ratio of sandstone-to-mudstone in the northeastern and southeastern study areas (figures 34–36). Further, the lower Mancos B is a proven liquid reservoir at Banta Ridge and the SITLA Bonanza Block in the northeastern Uinta Basin.

The middle Mancos B of the southeastern Uinta Basin is 100–400 ft thick and exhibits the lowest sandstone-to-mudstone ratio (figures 35 and 36). However, some sandstone-dominated packages up to 100 ft thick occur in the lower part of the middle Mancos B in the southeastern Uinta Basin, especially centered near the SITLA Seep Ridge block.

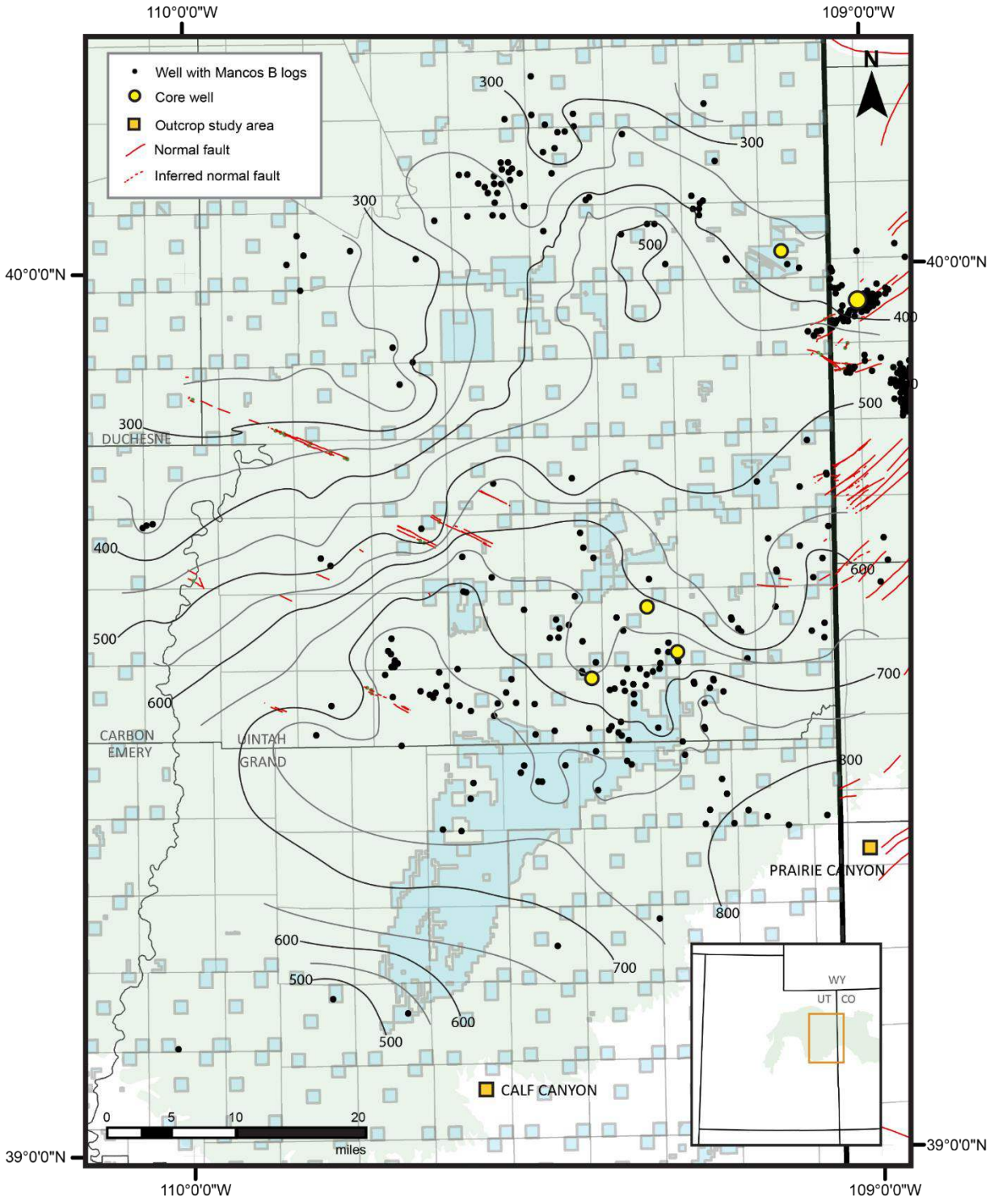

Figure 37. *Mancos B isopach in the eastern Uinta Basin.*

The 120- to 300-ft-thick upper Mancos B exhibits highly variable distribution of reservoir packages. In the northeastern Uinta Basin, the upper Mancos B contains mostly thin (<25 ft) packages of reservoir facies that are sparsely scattered (figure 34). In the southeastern Uinta Basin, the upper Mancos B contains more well-connected sandstone-rich packages up to 100 ft thick. In addition, the upper Mancos B contains thin packages of sandstone facies 7 interpreted as laterally limited turbidite distributary channels (figures 7d, 22; table 7). Outcrop observations indicate even the relatively uncommon multi-story bodies of these channels are less than 40 ft thick and less than 1 mile wide; most channelized bodies are much smaller (Hampson and others, 1999). Because of their limited depositional extent and channelized origin, these facies 7 reservoirs are difficult to map and hard to predict in the subsurface.

In addition to the sandstone-to-mudstone ratio related to depositional environment, reservoir quality also varies greatly based on the degree of diagenetic alteration. As observed in individual cores, the degree of diagenetic alteration varies greatly by lateral and stratigraphic location. In general, greater burial depths are associated with a greater degree of diagenetic alteration and increased fluid flow interactions. Therefore, areas of greater burial farther from the Douglas Creek Arch exhibit lower reservoir quality.

Structure

The depth of the Mancos B follows general Uinta Basin structural trends, with the deepest reservoir rock located nearer the central Uinta Basin (~13,500 ft in the SU Purdy 14M-30-7-22) and gradually shallows east towards the Douglas Creek Arch and to the south-southwest where the Mancos B is exposed at the surface along the southern margin of the Book Cliffs (figures 1 and 38).

Numerous normal faults have been previously mapped on the crest and flanks of the Douglas Creek Arch, a small number of which have been traced into easternmost Utah (Bader, 2009; Sprinkel, 2011; Coryell and McCarthy, 2014; figures 13 and 38). We expect that additional faults are present in the subsurface in the eastern Uinta Basin, especially near the Colorado border, but will require seismic data for detailed mapping. Fewer structures are observed in the southeastern Uinta Basin, as expected for the area which is distant from major compressional and extensional forces of the Laramide Orogeny. However, a number of small anticlines and synclines are mapped atop the Dakota Sandstone in the southeastern Uinta Basin (e.g., Roberts, 2003), in addition to a small number of surface faults near the Dry Burn and Agency Draw fields mapped by Sprinkel (2011) (figures 10, 37, and 38).

Because accurate fault mapping was so integral to operator success at Banta Ridge, detailed mapping of additional structures in the subsurface using 2D and 3D seismic data will improve potential success and reduce play risk in the Mancos B in Utah.

SOURCE ROCK

The main source rock for the Mancos B reservoir is likely not the Mancos B itself, but the underlying Niobrara-equivalent unit within the Lower Blue Gate Member of the Mancos Shale

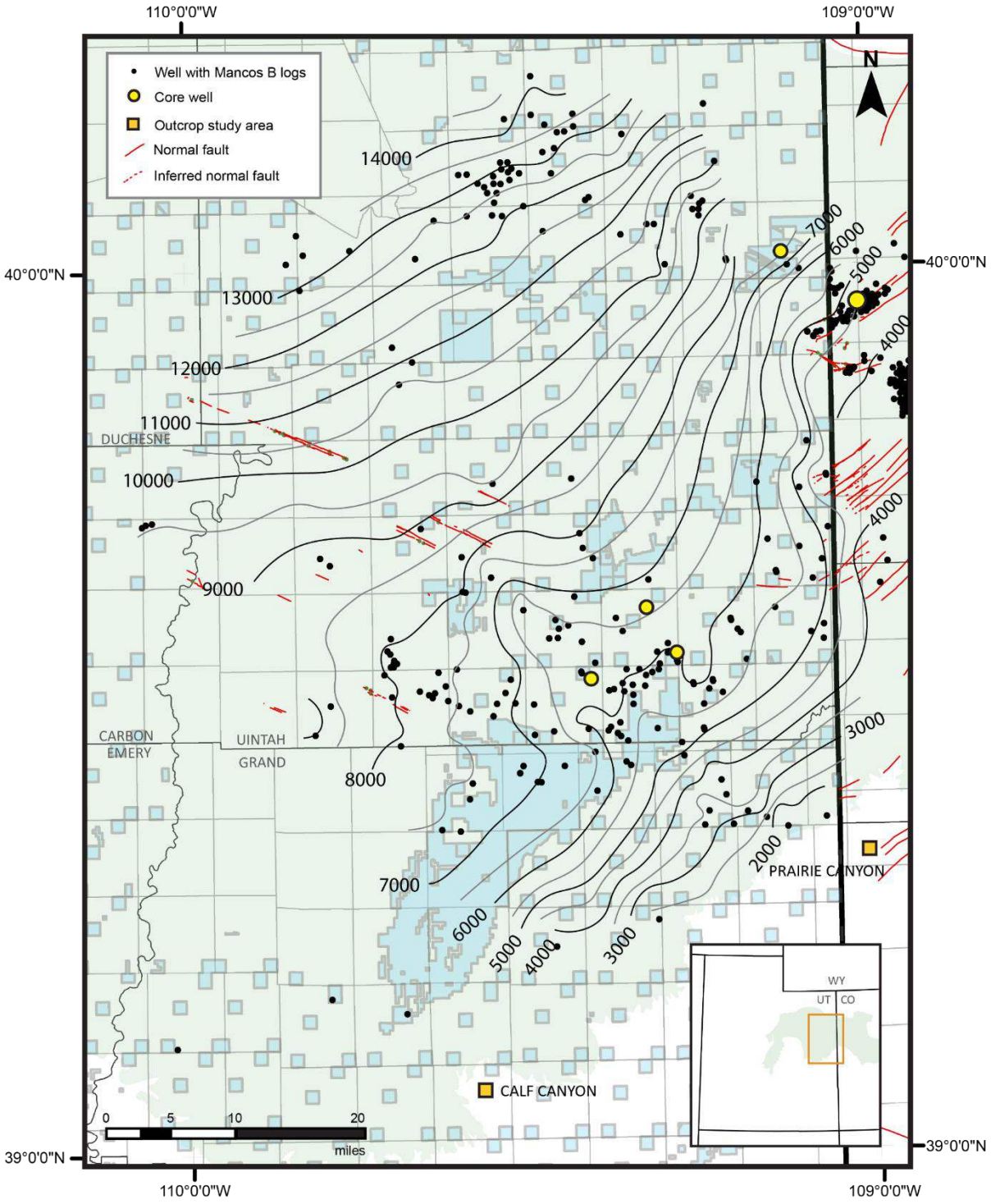

Figure 38. *Depth to base Mancos B (from surface) in the eastern Uinta Basin.*

(McCauley, 2013; Birgenheier and others, 2017). Source rock analyses from the Mancos B indicate total organic carbon (TOC) ranges from 0.2% to 1.5% (averages ~1.0%, n=26) and is generally Type III (gas prone) kerogen (figure 39; appendix E). Source rock analyses, burial modeling, and vitrinite reflectance data each indicate that the Mancos B organic matter reached the oil and gas window in the northeastern and southeastern Uinta Basin study areas (figure 40) (Kirschbaum, 2003; Hobbs and others, 2015). These factors indicate the Mancos B has potential for some locally sourced hydrocarbons; however, the relatively low TOC, kerogen type, and relatively thin section of organic-rich mudstones suggests that the Mancos B does not contain entirely self-sourced liquids. Rather, hydrocarbons most likely migrated into the Mancos B sandstone reservoirs from other members in the underlying and adjacent Mancos Formation (Lillis and others, 2003). Further, the exact source of the Mancos B hydrocarbons likely varies by location (e.g., Uinta vs. Piceance Basin) given the varied structure, burial history, and hydrocarbon generation within the Mancos Formation in the region (Nuccio and Roberts, 2003; Hobbs and others, 2015).

In the eastern Uinta Basin, on the Douglas Creek Arch and Piceance Basin, a probable source rock is the Niobrara-equivalent of the lower Mancos Formation, often referred to as the "Mancobrara." The Mancobrara is an especially organic-rich Mancos interval in western Colorado, with up to 3.36% TOC and within the oil and gas window within the Piceance Basin (Kirschbaum, 2003). Hydrocarbons generated in the Mancobrara have likely migrated to the Mancos B reservoirs on the Douglas Creek Arch (and surrounding area) via a fracture network related to Laramide deformation.

Within the Uinta Basin, Mancos Formation TOC values vary greatly (0.5%–4.0%) though are generally low (Hobbs and others, 2015). However, given the >1500-ft-thick section of Mancos Shale underlying the Mancos B, the lower Mancos Shale members are the most likely source rocks for charged reservoirs in the southeastern and northern (e.g., Natural Buttes and Wonsits Valley) Uinta Basin. Model predictions by Hobbs and others (2015) suggest ~1857 Bbbl oil and ~2887 Tscf gas has been generated by the Mancos Formation in the Uinta Basin, and that over 90% of the produced hydrocarbons have migrated. For the southeastern Uinta Basin study area, and the northern Uinta Basin (e.g., Natural Buttes and Wonsits Valley fields), oil is most likely supplied from the underlying Mancos section.

HYDROCARBON AND PRODUCTION CONTROLS

In the Mancos B play, the source rock is likely the Niobrara-equivalent interval of the lower Mancos Formation, the reservoir is the Mancos B sandstone facies, and the stratigraphic seal is the regionally extensive, mudstone-dominated Upper Blue Gate Member. Because the Mancos B reservoir is not self-sourcing, it is not a true resource play in the strict sense of the definition. And in some cases, particularly as seen at Banta Ridge, faults act as migration pathways and provide hydrocarbon seals or traps important to Mancos B well success in that area. The importance of fault-related oil migration and trapping is not typical for most resource plays.

As such, the most important factors for liquid hydrocarbon accumulation in the Mancos B are: 1) a porous sandstone reservoir facies (Facies 3–7); 2) a migration pathway such as a

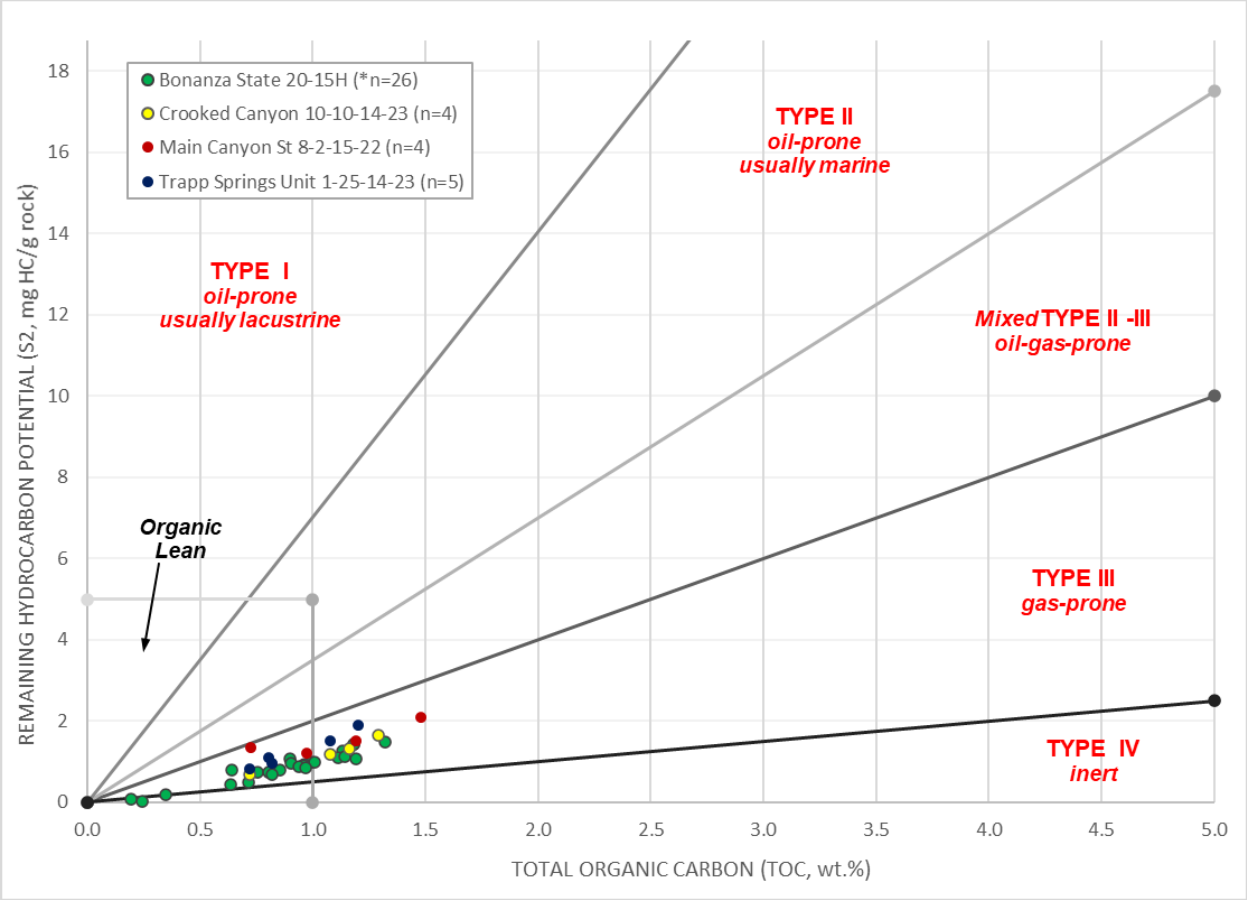

Figure 39. *Kerogen quality of Mancos B from SE and NE Uinta Basin cores. Note all samples have a relatively low TOC and are Type III gas-prone kerogen. Diagram adapted from Weatherford Labs analysis of Bonanza State 20-15H (Project CO-96022). *Bonanza State 20-15H core data contains 13 samples from uppermost Lower Blue Gate Member.*

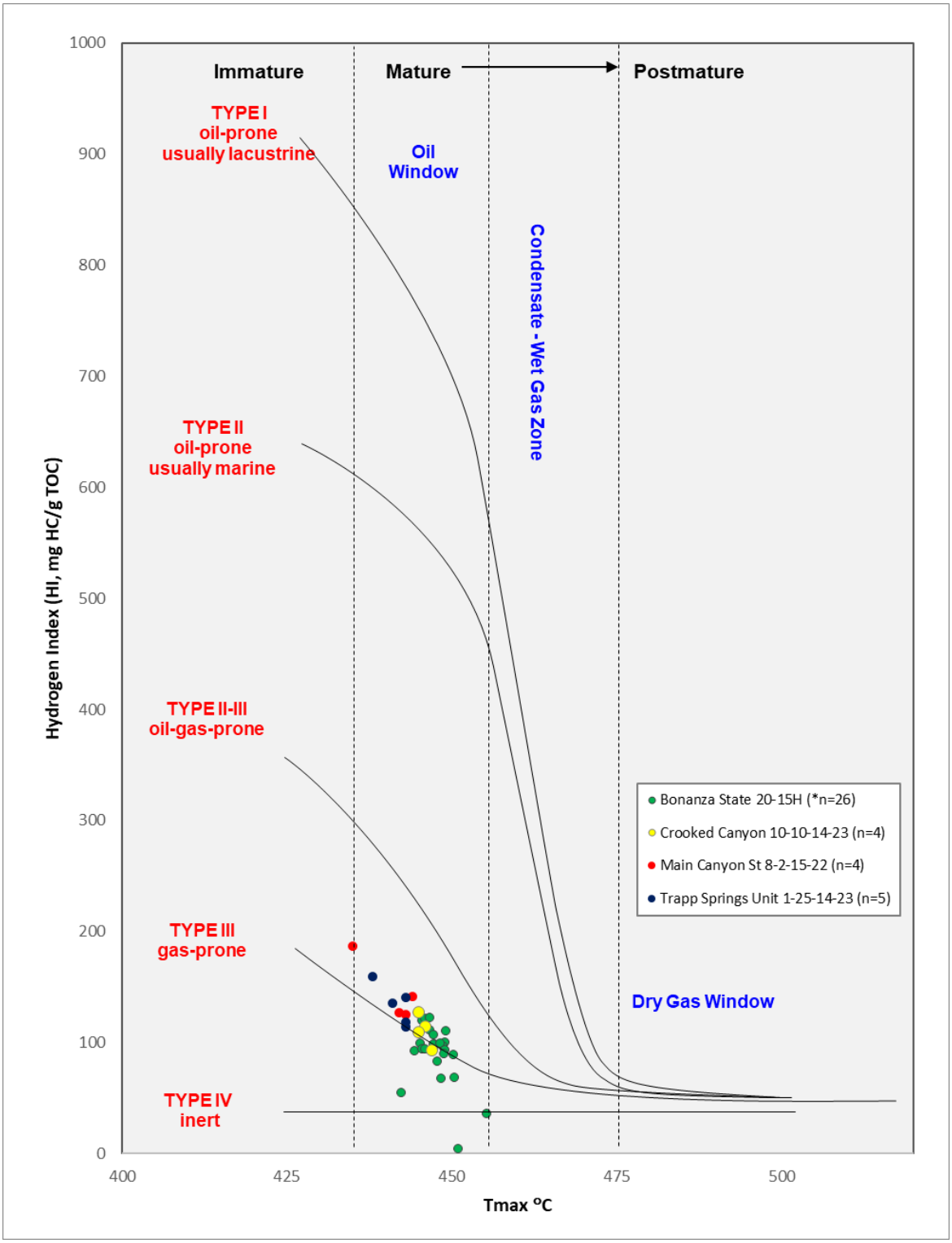

Figure 40. *Kerogen type and maturity from NE and SE Uinta Basin cores. Note most samples fall within the oil window. Diagram adapted from Weatherford Labs analysis of Bonanza State 20-15H (Project CO-96022). *Bonanza State 20-15H core data contains 13 samples from uppermost Lower Blue Gate Member.*

fracture network to charge the reservoir facies with hydrocarbons from an underlying source, likely the Niobrara-equivalent; and 3) a structural or stratigraphic trap and seal to hold liquids in place. Because reservoir facies are present throughout the Mancos B, we interpret migration pathways, seals, and traps to be especially important elements to identifying viable Mancos B plays.

Migration pathways of hydrocarbons typically rely on large fault networks and/or microfractures. In this study, we observed very few fractures in Mancos B facies at hand sample and thin section scales. This suggests large faults may be a primary control on hydrocarbon migration to Mancos B reservoirs. The most successful oil production field, Banta Ridge, exhibits a significant normal fault network that likely acted as migration pathways in the area. At Banta Ridge, faults may also play an integral role in laterally sealing hydrocarbons and compartmentalizing the reservoir. The Banta Ridge trend and similar fault networks extend from Colorado into Utah, although most areas in the Uinta Basin including the SITLA megablocks lack extensive and large fault networks. In these locations, the only trapping mechanism is the Upper Blue Gate Member stratigraphic seal. An improved understanding of subsurface faults and potential migration pathways that intersect the Mancos B in the eastern Uinta Basin will be integral to the potential success of this play.

Reservoir quality likely is related to the amount of water Mancos B wells produce in the Uinta Basin. In the Uinta Basin, relatively shallow burial depths of the Mancos B may not have generated enough pressure during hydrocarbon generation to expel formation water from tight mudstone facies. Wells drilled in reservoirs with substantial mudstone beds may therefore be high water producers as hydraulic fracturing will aid the release of clay-bound formation water. This is likely the case in the HCU 1-30F (4304740396) well that landed in the mudstone-dominated Lower Blue Gate Member and has produced substantial quantities of water. Mobile authigenic clays (illite and kaolinite) vary in proportion in the Mancos B stratigraphy and areal location, though can also impact production by potentially decreasing permeability.

Coryell and McCarthy (2014) have highlighted that no single attribute (i.e., geophysical logs) can predict the success of a Mancos B well in Banta Ridge. Rather, they note that structural position, reservoir quality, and GOR together play significant roles. For unconventional applications not targeting structurally trapped hydrocarbons like Banta Ridge, reservoir quality (clay content and diagenetic features) and GOR are important and will require detailed attention from operators planning and completing wells.

CONCLUSIONS

New and legacy core highlights the presence of potential reservoir packages within the 210–800-ft thick Mancos B interval in the eastern Uinta Basin of Utah. Reservoir packages are composed of interbedded and interlaminated sandstone and mudstone deposited offshore in the shallow Cretaceous Interior Seaway. Sediment was delivered from the west, likely via turbidity and hyperpycnal flows in bypass channels that deposited the sediment in prodeltaic lobes isolated from the time-equivalent shoreline sandstones of the Blackhawk Formation. These bypass channels (<40 ft thick) are observed in outcrop and core in the east-central Uinta Basin and are relatively thin and isolated within mudstone facies. Prodeltaic lobes occur in tabular

bodies that can be over 50 ft thick and are mappable at local scales. These lobes offer the best reservoir potential consisting of mostly sandstone facies. We interpret an overall northwest progradation (backstepping) of Mancos B prodeltaic lobes that can be split into three packages: lower, middle, and upper Mancos B. The lower Mancos B contains the most laterally extensive and thick sandstone packages and are especially prospective for development in the northeastern Uinta Basin. Further, the packages in the lower Mancos B exhibit evidence for continuous wave-reworking of sediment in the northeastern Uinta Basin that also improved reservoir quality by winnowing out mud. As a general observation, reservoir bodies become increasingly thinner and more isolated in the middle and upper Mancos B; however, thick reservoir units are observed in some locations both stratigraphic zones.

One of the challenges in Utah is understanding the hydrocarbon migration pathway and trapping mechanism. We interpret this to vary by region. In the easternmost Uinta Basin and near the Douglas Creek Arch, hydrocarbons are likely sourced from the underlying Mancos Shale (namely the Niobrara-equivalent of western Colorado), migrate via fault-fracture networks associated with Laramide deformation, and are contained in structural traps. In the southeastern Uinta Basin and other locales far from Laramide deformation, hydrocarbons are likely sourced from the thick section of underlying Mancos Shale in the Uinta Basin and are likely stratigraphically trapped by the clay-rich Upper Blue Gate Member. It is possible that small structural features play a role in hydrocarbon accumulation; however, if present, these features will require seismic data for detailed subsurface mapping.

The most successful oil wells to date are in the Banta Ridge area on the western flank of the Douglas Creek Arch in western Colorado. Banta Ridge, a northeast-southwest structural trend, extends into Utah and is a promising area for Mancos B development from the thick and relatively high-quality reservoir packages in the lower Mancos B. Similar northeast-southwest structural trends exist at the Utah-Colorado border north and south of Banta Ridge, marking additional prospective structural traps in Utah. The horizontal Bonanza State 20-15H also shows the potential for significant oil production from stratigraphically trapped hydrocarbons in the lower Mancos B in the SITLA Bonanza block. The southeastern Uinta Basin is less explored than the Utah-Colorado border, although promising reservoir packages exist from the lower to upper Mancos B (depending on location) and several wells from the early 2000s have proven the presence of liquids. The main future exploration task in the southeastern Uinta Basin will be determining the liquid charge of scattered reservoir packages in the region. These areas with few faults traps will likely benefit from an unconventional approach with horizontal wells targeting stratigraphically sealed Mancos B reservoirs.

We identify reservoir quality as a major factor that impacts well success. Mancos B reservoir quality is determined by two major factors: 1) sandstone-to-mudstone ratios tied to the primary depositional environment, and 2) secondary alteration tied to secondary burial and chemistry changes (diagenesis). The ratio of sandstone-to-mudstone is especially important in the eastern Uinta Basin, where relatively low burial depths may not have generated enough pressure to eject water from clay-bound formation water in mudstones. Thus, reservoirs with significant mudstone lamina may produce relatively high ratios of water-to-oil in the eastern Uinta Basin. Water is less likely to become trapped in sandstone facies of the Mancos B and provide more pore space for hydrocarbon accumulation.

Hydraulic fracturing can improve well success to help overcome the tight Mancos B reservoirs with diagenetic factors that reduce pore space, create flow baffles, and decrease permeability. We identify the major diagenetic factors as pore-filling authigenic clay and carbonate cement. These secondary features vary significantly both vertically and laterally at local and regional scales, a result of varied fluid flow and burial histories. Thus, detailed study of diagenetic features of potential reservoir targets in local and regional context will be integral to those designing well completion methods.

FUTURE WORK

The UGS has additional work scheduled that will be provided as an addendum to this report. This work includes biomarker and oil characterization from samples collected from Bonanza State 20-15H and State 28-13 and will be completed in collaboration with the U.S. Geological Survey in Denver, Colorado. Further, we will perform petrographic analyses of six samples from the three legacy Coseka wells in the southeastern Uinta Basin (Crooked Canyon 10-10-14-23, Main Canyon St 2-8-15-22, Trapp Springs Unit 1-25-14-23) in order to characterize the sandstone reservoir facies nearer the less-explored SITLA Seep Ridge and Holliday blocks.

Outside the scope of this study, operators will benefit from acquiring and interpreting 3D seismic in areas with potential structural traps. Further, we encourage operators to invest in reservoir engineering studies that will inform drilling and completion methods.

ACKNOWLEDGMENTS

In 2019, LaVonne Garrison, former Assistant Director of Oil and Gas for SITLA, commissioned the UGS to study the production potential of the Mancos B interval of the Mancos Shale in the eastern Uinta Basin, Utah. The project was completed by the UGS under a Memorandum of Understanding between the two agencies during the 2020 fiscal year. A subcontract was extended to Dr. Lauren Birgenheier at the University of Utah and the project benefited from her expertise on the Mancos Shale. Wes Adams, now Assistant Director of Oil and Gas for SITLA, was of great help via providing industry contacts that aided knowledge and data sharing between government and private agencies. Thank you is extended to KGH Operating Company and Robert L. Bayless, Producer LLC for providing the UGS with access to the Bonanza State 20-15H and Weaver Ridge 13-16 cores and for donating substantial core data to this project. Gratitude is extended to Andrew McCauley (Occidental Petroleum Corp.) who provided a basin-wide Mancos Shale database of digitized geophysical logs used in this report. Thank you to Robin Fults (University of Utah, now Dominion Energy) for her assistance analyzing and interpreting SEM and EDS data.

REFERENCES

Anderson, D.S., 2014, Rangely Field, *in* Rogers, J.P., Milne, J.J., Cumella, S.P., DuBois, D., Lillis, P.G., editors, Oil and gas fields of Colorado 2014: The Rocky Mountain Association of Geologists, p. 258–260.

Anderson, D., and Harris, N., 2006, Integrated sequence stratigraphic and geochemical resource characterization of the lower Mancos Shale, Uinta Basin, Utah: Utah Geological Survey Open-File Report 483, compact disk.

Bader, J.W., 2009. Structural and tectonic evolution of the Douglas Creek arch, the Douglas Creek fault zone, and environs, northwestern Colorado and northeastern Utah—Implications for petroleum accumulation in the Piceance and Uinta basins: Rocky Mountain Geology, vol. 44, no. 2, p. 121–145.

Bann, K.L., Tye, S.C., MacEachern, J.A., Fielding, CR., and Jones, B.G., 2008, Ichnological and sedimentologic signatures of mixed wave- and storm-dominated deltaic deposits: Examples from the Early Permian Sydney Basin, Australia, *in* Hampson, G., Steel, R., Burgess, P. and Dalrymple, R., editors, Recent Advances in Models of Siliciclastic Shallow-Marine Stratigraphy: SEPM Special Publication 10, p. 293–332.

Barnum, B.E., Scott, R.W., Jr., and Pantea, M.P., 1997, Geologic map of the Texas Mountain quadrangle, Rio Blanco County, Colorado: U.S. Geological Survey Miscellaneous Field Investigations Series Map MF-2321, 1:24,000, 1 sheet.

Birgenheier, L.P., Horton, B., McCauley, A.D., Johnson, C.L. and Kennedy, A., 2017, A depositional model for offshore deposits of the lower Blue Gate Member, Mancos Shale, Uinta Basin, Utah, USA. Sedimentology, v. 64, p. 1402–1438.

Blakey, R.C., 2014, Paleogeography and paleotectonics of the western interior seaway, Jurassic-Cretaceous of North America: American Association of Petroleum Geologists Search and Discovery 30392, v. 72.

Boden, T., and Tripp, B.T., 2012, Gilsonite veins of the Uinta Basin, Utah: Utah Geological Survey, Special Study 141, 50 p.

Buatois, L.A., Mángano, M.G., and Pattison, S.A., 2019, Ichnology of prodeltaic hyperpycnite–turbidite channel complexes and lobes from the Upper Cretaceous Prairie Canyon Member of the Mancos Shale, Book Cliffs, Utah, USA. Sedimentology, v. 66, no. 5, p. 1825–1860.

Cashion, W.B., 1967, Geology and fuel resources of the Green River Formation, southeastern Uinta basin, Utah and Colorado: U.S. Geological Survey Professional Paper 548, 48 p., 5 plates.

Chan, M.A., Newman, S.L., and May, F.E., 1991, Deltaic and shelf deposits in the Cretaceous Blackhawk Formation and Mancos Shale, Grand County, Utah: Utah Geological Survey, Miscellaneous Publication 91-6, 83 p.

Cole, R.D., and Young, R.G., 1991, Facies characterization and architecture of a muddy shelf-sandstone complex—"Mancos B" interval of Upper Cretaceous Mancos Shale, northwest Colorado-northeast Utah, *in* Miall, AD., and Tyler, Noel, editors, The three-dimensional facies architecture of terrigenous clastic sediments and its implications for hydrocarbon discovery and recovery: Society of Economic Paleontologists and Mineralogists, Concepts in Sedimentology and Paleontology, v. 3, p. 277–287.

Cole, R.D., Young, R.G. and Willis, G.C., 1997, The Prairie Canyon Member, a new unit of the Upper Cretaceous Mancos Shale, west-central Colorado and east-central Utah: Utah Geological Survey, Miscellaneous Publication 97-4, 26 p.

Coryell, G.F., and McCarthy, T.R., 2014, Banta Ridge Field, *in* Rogers, J.P., Milne, J.J., Cumella, S.P., DuBois, D., Lillis, P.G., editors, Oil and gas fields of Colorado 2014: The Rocky Mountain Association of Geologists, p. 24–30.

Cross, W., and Purington, C.W., 1899, Description of the telluride quadrangle, Colorado. U.S. Geol. Survey Geol. Atlas, v. 131, p. 14.

DeReuil, A.A., and Birgenheier, L.P., 2019, Sediment dispersal and organic carbon preservation in a dynamic mudstone-dominated system, Juana Lopez Member, Mancos Shale: Sedimentology, v. 66, no. 3, p. 1002–1041.

DeReuil, A.A., Birgenheier, L.P., & McLennan, J., 2019, Effects of anisotropy and saturation on geomechanical behavior of mudstone: Journal of Geophysical Research, Solid Earth, v. 124, no. 8, p. 8101–8126.

DeCelles, P.G., Lawton, T.F., and Mitra, G., 1995, Thrust timing, growth of structural culminations, and synorogenic sedimentation in the type Sevier orogenic belt, western United States: Geology, v. 23, no. 8, p. 699–702.

Dickinson, W.R., Klute, M.A., Hayes, M.J., Janecke, S.U., Lundin, E.R., Mckittrick, M.A., and Olivares, M.D., 1988, Paleogeographic and paleotectonic setting of Laramide sedimentary basins in the central Rocky Mountain region: Bulletin of the Geological Society of America, v. 100, no. 7, p. 1023–1039.

Dyman, T.S., Merewether, E.A., Molenaar, C.M., Cobban, W.A., Obradovich, J.D., Weimer, R.J., and Bryant, W.A., 1994, Stratigraphic transects for Cretaceous rocks, Rocky Mountains and Great Plains regions, *in* Caputo, M.V., Peterson, J.A., and Franczyk, K.J., editors, Mesozoic systems of the Rocky Mountain region, U.S.A.: Society for Sedimentary Geology, Rocky Mountain Section, p. 365–392.

Eide, C.H., Howell, J.A., and Buckley, S.J., 2015, Sedimentology and reservoir properties of tabular and erosive offshore transition deposits in wave-dominated shallow-marine strata: Book Cliffs, USA, Petroleum Geoscience, vol. 21, p. 55–73.

Fouch, T.D., Lawton, T.F., Nichols, D.J., Cashion, W.B. and Cobban, W.A., 1983, Patterns and timing of synorogenic sedimentation in Upper Cretaceous rocks of central and northeast Utah, *in* Reynolds, M.W., and Dolly, editors, Mesozoic paleogeography of west central United States, Rocky Mountain Section SEPM, p. 305–336.

Franczyk, K.J., Fouch, T.D., Johnson, Re., Molenaar, C.M., and Cobban, W.A., 1992, Cretaceous and Tertiary paleogeographic reconstructions for the Uinta-Piceance basin study area, Colorado and Utah: U.S. Geological Survey Bulletin 1787-Q, p. 1–37.

Hampson, G.J., 2010, Sediment dispersal and quantitative stratigraphic architecture across an ancient shelf. Sedimentology, v. 57, p. 96–141.

Hampson, G.J., 2016, Towards a sequence stratigraphic solution set for autogenic processes and allogenic controls—upper Cretaceous strata, Book Cliffs, Utah, USA: Journal of the Geological Society, v. 173, p. 817–836.

Hampson, G.J., Howell, J.A. and Flint, S.S., 1999, A sedimentological and sequence stratigraphic re-interpretation of the Upper Cretaceous Prairie Canyon Member ("Mancos B") and associated strata, Book Cliffs area, Utah, U.S.A.: Journal of Sedimentary Research, v. 69, p. 414–433.

Hampson, G.J., Burgess, P.M., and Howell, J.A., 2001, Shoreface tongue geometry constrains history of relative sea-level fall: examples from Late Cretaceous strata in the Book Cliffs area, Utah: Terra Nova, vol. 13, no. 3, p. 188–196.

Hancock, J.M., and Kauffman, E.G., 1979, The great transgressions of the Late Cretaceous. Journal of the Geological Society, v. 136, no. 2, p. 175–186.

Hettinger, R.D., and Kirschbaum, M.A., 2002, Stratigraphy of the Upper Cretaceous Mancos Shale (upper part) and Mesaverde Group in the southern part of the Uinta and Piceance basins, Utah and Colorado, Pamphlet to accompany Geologic Investigations Series I-2764, 24 p.

Hobbs, D.J., Birgenheier, L.P., Johnson, C.L., and Greb, M.D., 2015, Unconventional Petroleum System Analysis using a 3D Basin Model: Mancos Shale, Uinta Basin, Utah; *in* Vanden Berg, M.D., Ressetar, R., and Birgenheier, L.P., editors, Geology of Utah's Uinta Basin and Uinta Mountains: Utah Geological Association Publication 44, p. 219–255.

Johnson, R.C., and Finn, T.M., 1986, Cretaceous through Holocene history of the Douglas Creek arch, Colorado and Utah, *in* Stone, D.S., editors, New interpretations of northwest Colorado geology: Rocky Mountain Association of Geologists, p. 77–95.

Johnson, S.Y., 1992, Phanerozoic evolution of sedimentary basins in the Uinta-Piceance Basin region, northwestern Colorado and northeastern Utah, U.S. Geological Survey Bulletin, vol, 1878, 48 p.

Johnson, R.C., 2003, Depositional framework of the Upper Cretaceous Mancos Shale and the lower part of the Upper Cretaceous Mesaverde Group, Western Colorado and Eastern Utah: Petroleum Systems and Geologic Assessment of Oil and Gas in the Uinta-Piceance Province, Utah and Colorado., U.S. Geological Survey Digital Data Series DDS-69-B, 28 p.

Johnston, R.E., and Yin, A., 2001, Kinematics of the Uinta fault system (southern Wyoming and northern Utah) during the Laramide orogeny: *International Geology Review*, vol. *43*, no. 1, p. 52–68.

Jordan, T.E., 1981, Thrust loads and foreland basin evolution, Cretaceous, western United States. Bulletin of American Association of Petroleum Geologist, v. 65, p. 2506–2520.

Kellogg, H.E., 1977, Geology and petroleum of the Mancos B Formation Douglas Creek Arch area Colorado and Utah: Rocky Mountain Association of Geologists – 1977 Symposium, 13 p.

Kirschbaum, M.A., 2003, Geologic assessment of undiscovered oil and gas resources of the Mancos/ Mowry total petroleum system, Uinta-Piceance Province, Utah and Colorado: *in* USGS Uinta-Piceance Assessment Team, compilers, Petroleum systems and geologic assessment of oil and gas in the Uinta-Piceance Province, Utah and Colorado: U.S. Geological Survey Digital Data Series DDS–69–B, chapter 6, compact disk.

Kopper, P.K., 1962, Douglas Creek anticline and adjoining area, *in* Amuedo, C.L., and Mott, M.R., editors, Exploration for oil and gas in northwestern Colorado: Rocky Mountain Association of Geologists, p. 108–110.

Lillis, P.G., Warden, A., and King, J.D., 2003, Petroleum systems of the Uinta and Piceance Basins–geochemical characteristics of oil types. Petroleum systems and geologic assessment of oil and gas in the Uinta-Piceance province, Utah and Colorado: US Geological Survey Digital Data Series DDS-69-B, 25 p.

Livaccari, R.F., 1991, Role of crustal thickening and extensional collapse in the tectonic evolution of the Sevier-Laramide orogeny, Western United States: Geology, v. 19, p. 1104–1107.

Longman, M.W., and Koepsell, R.J., 2005, Defining and characterizing Mesaverde and Mancos sandstone reservoirs based on interpretation of image logs, eastern Uinta Basin: Utah Geological Survey, Open-File Report 458, 122 p.

Macquaker, J.H.S., Taylor, K.G., and Gawthorpe, R.L., 2007, High-resolution facies analyses of mudstones—implications for paleoenvironmental and sequence stratigraphic interpretations of offshore ancient mud-dominated successions: Journal of Sedimentary Research, v. 77, no. 4, p. 324–339, https://doi.org/10.2110/jsr.2007.029.

McCauley, A.D., 2013, Sequence stratigraphy, depositional history, and hydrocarbon potential of the Mancos Shale, Uinta Basin, Utah: Salt Lake City, University of Utah, M.S. thesis, 161 p.

McLennan, J.D., Roegiers, J.C., and Marx, W.P., 1983, The Mancos Formation: An evaluation of the interaction of geological conditions, treatment characteristics and production: Society of Petroleum Engineers—Department of Energy Low Permeability Gas Reservoir Symposium, SPE/DOE 11606, 10 p.

Mederos, S., Tikoff, B., and Bankey, V., 2005, Geometry, timing, and continuity of the Rock Springs uplift, Wyoming, and Douglas Creek arch, Colorado: Implications for uplift mechanisms in the Rocky Mountain foreland, USA: Rocky Mountain Geology, vol. 40, no. 2, p. 167-191.

Miall, A.D. and Arush, M., 2001, The Castlegate Sandstone of the Book Cliffs, Utah—sequence stratigraphy, paleogeography, and tectonic controls: Journal of Sedimentary Research, v. 71, p. 537–548.

Middlebrook, M.L., Branagan, P.T., Hill, R.E., Kukal, G.C., Peterson, R.E., McDonald, T.S., and Aslakson, J.K., 1993, Reservoir evaluation and completion results from a horizontal well in the Mancos B, Douglas Creek Arch, northwest Colorado: Society of Petroleum Engineers Low Permeability Reservoirs Symposium, SPE 25924, 14 p.

Molenaar, C.M., and Cobban, W.A., 1991, Middle Cretaceous stratigraphy on the south and east sides of the Uinta Basin, northeastern Utah and northwestern Colorado, *in* Evolution of sedimentary basins—Uinta and Piceance Basins: USGS Bulletin 1787, chapter P, 34 p.

Nadeau, P.H., and Reynolds, R.C., 1981, Burial and contact metamorphism in the Mancos Shale: Clays and Clay Minerals, vol. 29, no. 4, p. 249–259.

Narr, W., and Currie, J.B., 1982, Origin of fracture porosity—Example from Altamont field, Utah: American Association of Petroleum Geologists Bulletin, vol. 66, no. 9, p. 1231–1247.

Newman, S.L., 1985, Sedimentary and depositional history of shallow shelf deposits within the Cretaceous Blackhawk Formation and Mancos Shale, east-central Utah: Salt Lake City, University of Utah M.S. thesis, 158 p.

Noe, D.C., 1993, Mancos Marine Sandstones, *in* Hjellming, C.A., editor, Atlas of major Rocky Mountain gas reservoirs: New Mexico Bureau of Mines and Mineral Resources, Socorro, New Mexico, p. 99–100.

Nuccio, V.F., and Roberts, L.N., 2003, Thermal maturity and oil and gas generation history of petroleum systems in the Uinta-Piceance Province, Utah and Colorado, *in* USGS Uinta-Piceance Assessment Team, compilers, Petroleum systems and geologic assessment of oil and gas in the Uinta-Piceance Province, Utah and Colorado: U.S. Geological Survey Digital Data Series DDS–69–B, chapter 4, compact disk.

Pantea, M. P., and Schmitt, L.J., 1996, Geologic map of the Banta Ridge quadrangle, Rio Blanco County, Colorado: U.S. Geological Survey Miscellaneous Field Investigations Series Map MF-2308, 1:24,000, 1 sheet.

Pattison, S.A.J., 2005a, Isolated highstand shelf sandstone body of turbiditic origin, lower Kenilworth Member, Cretaceous Western Interior, Book Cliffs, Utah, USA: Sedimentary Geology, v. 177, p. 131–144.

Pattison, S.A.J., 2005b, Recognition and interpretation of isolated shelf turbidite bodies in the Cretaceous Western Interior, Book Cliffs, Utah, *in* Pederson, J., and Dehler, C.M., editors, Interior Western United States: Geological Society of America Field Guide, v. 6, p. 479–504.

Pattison, S.A.J., Ainsworth, B.R. and Hoffman, T.A., 2007, Evidence of across-shelf transport of fine-grained sediments—turbidite-filled shelf channels in the Campanian Aberdeen Member, Book Cliffs, Utah, USA: Sedimentology, v. 54, p. 1033–1064.

Pattison, S.A.J. and Hoffman, T.A., 2008, Sedimentology, architecture and origin of shelf turbidite bodies in the Upper Cretaceous Kenilworth Member, Book Cliffs, Utah, USA. In: Recent Advances in Models of Siliciclastic Shallow-Marine Stratigraphy (Eds G.J. Hampson, R.J. Steel, P.B. Burgess and R.W. Dalrymple), SEPM Spec. Publ., v. 90, p. 391–420.

Pollastro, R.M., 1990, The illite/smectite geothermometer—concepts, methodology, and application to basin history and hydrocarbon generation: Rocky Mountain Section (SEPM), 18 p.

Quick, J.C., and Ressetar, R., 2012, Thermal maturity of the Mancos Shale within the Uinta Basin, Utah and Colorado: American Association of Petroleum Geologists, Annual Convention and Exhibition, Long Beach, California, Search and Discovery article 50616, 5 p.

Ressetar, R., and Birgenheier, L.P., 2015, Cretaceous Mancos Shale Uinta Basin, Utah—Resource potential and best practices for an emerging shale gas play: UGS Final Report Subcontract No. 09122-07, 701 p.

Roberts, L.N.R., 2003, Structure contour map of the top of the Dakota Sandstone, Uinta-Piceance Province, Utah and Colorado, *in* USGS Uinta-Piceance Assessment Team, compilers, Petroleum systems and geologic assessment of oil and gas in the Uinta-Piceance Province, Utah and Colorado: U.S. Geological Survey Digital Data Series DDS–69–B, chapter 16, compact disk.

Schamel, S., 2006, Shale gas resources of Utah—Assessment of previously undeveloped gas discoveries: UGS Open-File Report 499, 83 p.

Schwans, P., 1995, Controls on sequence stacking and fluvial to shallow-marine architecture in a foreland basin, *in* Van Wagoner, J.C., and Bertram, G.T., editors, Sequence stratigraphy of foreland basin deposits—Outcrop and subsurface examples from the Cretaceous of North America: AAPG Memoir, v. 64, p. 103–136.

Sonnenberg, S.A., 2011, The Niobrara petroleum system— A new resource play in the Rocky Mountain Region, *in* Estes-Jackson, J.E., and Anderson, D.S., editors, Revisiting and revitalizing the Niobrara in the central Rockies: Rocky Mountain Association of Geologists, p. 13–32.

Sprinkel, D.A., 2011, Interim geologic map of the Seep Ridge 30′ x 60′ quadrangle, Uinta, Duchesne, and Carbon Counties, Utah and Rio Blanco and Garfield Counties, Colorado: UGS Open-File Report 549dm, 3 p.

Stoeser, D.B., Green, G.N., Morath, L.C., Heran, W.D., Wilson, A.B., Moore, D.W., Van Gosen, B.S., 2005, Colorado Faults, from the USGS Geologic Map Database: U.S. Geological Survey Open-File Report 2005–1351, shapefile data: http://pubs.usgs.gov/of/2005/1351/.

Stone, D.S., 1986, Seismic and borehole evidence for important pre-Laramide faulting along the Axial Arch in northwest Colorado: *in* Stone, D.E., editor, New Interpretations of Northwest Colorado Geology, Rocky Mountain Association of Geologists Guidebook, p. 19–36.

Swift, D.P., Hudelson, P.M., Brenner, R.M. and Thompson, P., 1987, Shelf construction in a foreland basin—storm beds, shelf sandbodies, and shelf-slope depositional sequences in the Upper Cretaceous Mesaverde Group, Book Cliffs, Utah: Sedimentology, v. 34, p. 423–457.

Taylor, D.R., and Lovell, R.W., 1995, High-frequency sequence stratigraphy and paleogeography of the Kenilworth member, Blackhawk Formation, Book Cliffs, Utah, USA *in* Van Wagoner, J.C., and Bertram, G.T., editors, Sequence Stratigraphy of Foreland Basin Deposits— Outcrop and Subsurface Examples from the Cretaceous of North America: American Association of Petroleum Geologists, Memoir 64, p. 257–275.

Taylor, K.G., and Gawthorpe, R.L., 2003, Basin-scale dolomite cementation of shoreface sandstones in response to sea-level fall: Geological Society of America Bulletin, v. 115, no. 10, p. 1218–1229.

Taylor, K.G., and Machent, P.G., 2010, Systematic sequence-scale controls on carbonate cementation in a siliciclastic sedimentary basin: Examples from Upper Cretaceous shallow marine deposits of Utah and Coloradao, USA: Marine and Petroleum Geology, vol. 27, no. 7, p. 1297–1310.

Taylor, K.G., and MacQuaker, J.H.S., 2014, Diagenetic alterations in a silt- and clay-rich mudstone succession: an example from the Upper Cretaceous Mancos Shale of Utah, USA: Clay Minerals, v. 49, p. 245–259.

Van Wagoner, J.C., Posamentier, H.W., Mitchum, R.M., Vail, P.R., Sarg, J.F., Loutit, T.S. and Hardenbol, J., 1988, An overview of the fundamentals of sequence stratigraphy and key definitions: SEPM Special publication, v. 42, p. 39–45.

White, T., Furlong, K. and Arthur, M., 2002, Forebulge migration in the Cretaceous Western Interior basin of the central United States: Basin Research, vol. 14, no. 1, p. 43–54.

Witherbee, L.J., Godfrey, R.D., and Dimelow, T.E., 1983, Predicting turbidite-contourite reservoir intervals in tight gas sands: a case study from the Mancos B sandstone: Society of Petroleum Engineers—Department of Energy Low Permeability Gas Reservoir Symposium, SPE/DOE 11609, 8 p.

Yoshida, S., 2000, Sequence and facies architecture of the Upper Blackhawk Formation and the Lower Castlegate Sandstone (Upper Cretaceous), Book Cliffs, Utah, USA: Sedimentary Geology, v. 136, p. 239–276.

Yoshida, S., Willis, A. and Miall, A.D., 1996, Tectonic control of nested sequence architecture in the Castlegate Sandstone (Upper Cretaceous), Book Cliffs, Utah: Journal of Sedimentary Research, v. 66, p. 737–748.

Zhang, Y., Gable, C.W., Zyvoloski, G.A., and Walter, L.M., 2009, Hydrogeochemistry and gas compositions of the Uinta Basin: A regional-scale overview. American Association of Petroleum Geologists Bulletin, vol. 93, no. 8, p. 1087–1118,